AD-A058 617 ENVIRONMENTAL RESEARCH INST OF MICHIGAN ANN ARBOR F/G 17/9
PROBLEMS OF IMAGING OCEAN WAVES WITH SYNTHETIC APERTURE RADAR.(U)
AUG 77 R A SHUCHMAN, P L JACKSON N00014-76-C-1048
UNCLASSIFIED ERIM-124300-1-T NL

1 OF 2
AD A058617

LEVEL II

(12)

(9) Interim Technical Report, Aug 76 - Aug 77

(6)

PROBLEMS OF IMAGING OCEAN WAVES WITH SYNTHETIC APERTURE RADAR

(10) R.A. SHUCHMAN, P.L. JACKSON, G.B. FELDKAMP
Radar and Optics Division

(11) AUG 77

(12) 118 p.

(14) ERIM-124300-1-T

Geography Branch
Office of Naval Research
Arlington, Virginia 22217
(15) Contract No. N00014-76-C-1048
Technical Monitor: Mr. Hans Dolezalek

ENVIRONMENTAL
RESEARCH INSTITUTE OF MICHIGAN
BOX 8618 • ANN ARBOR • MICHIGAN 48107

Unclassified

SECURITY CLASSIFICATION OF THIS PAGE *(When Data Entered)*

REPORT DOCUMENTATION PAGE		READ INSTRUCTIONS BEFORE COMPLETING FORM
1. REPORT NUMBER 124300-1-T	2. GOVT ACCESSION NO.	3. RECIPIENT'S CATALOG NUMBER
4. TITLE *(and Subtitle)* PROBLEMS OF IMAGING OCEAN WAVES WITH SYNTHETIC APERTURE RADAR		5. TYPE OF REPORT & PERIOD COVERED Interim Report August 1976 - August 1977
		6. PERFORMING ORG. REPORT NUMBER 124300-1-T
7. AUTHOR*(s)* R.A. Shuchman, P.L. Jackson, and G.B. Feldkamp		8. CONTRACT OR GRANT NUMBER*(s)* N00014-76-C-1048
9. PERFORMING ORGANIZATION NAME AND ADDRESS Environmental Research Institute of Michigan P.O. Box 8618, Ann Arbor, Michigan 48107		10. PROGRAM ELEMENT, PROJECT, TASK AREA & WORK UNIT NUMBERS
11. CONTROLLING OFFICE NAME AND ADDRESS Geography Branch, Office of Naval Research Arlington, Virginia 22217		12. REPORT DATE August 1977
		13. NUMBER OF PAGES vi + 111
14. MONITORING AGENCY NAME AND ADDRESS *(if different from Controlling Office)*		15. SECURITY CLASS *(of this report)* Unclassified
		15a. DECLASSIFICATION/DOWNGRADING SCHEDULE

16. DISTRIBUTION STATEMENT *(of this Report)*

Distribution of this document is unlimited

17. DISTRIBUTION STATEMENT *(of the abstract entered in Block 20, if different from Report)*

18. SUPPLEMENTARY NOTES

19. KEY WORDS *(Continue on reverse side if necessary and identify by block number)*

Ocean Waves	SAR Imagery	Fourier Transforms
Remote Sensing	L-Band	Digital Processing
Data Processing	X-Band	SAR Focusing
Multifrequency Synthetic Aperture Radar		

20. ABSTRACT *(Continue on reverse side if necessary and identify by block number)*

Progress is reported on three tasks designed to provide ~~the Navy with~~ information to evaluate the operational use of SAR, so that ultimately, meaningful ocean shallow-water wave spectra and coastal wave height information can be supplied to the Navy in real-time.

Under Task 1, a limited literature search was conducted to ascertain problems encountered in imaging sea states with SAR. The search indicated →

DD FORM 1 JAN 73 1473 EDITION OF 1 NOV 65 IS OBSOLETE

Unclassified

SECURITY CLASSIFICATION OF THIS PAGE *(When Data Entered)*

20. ABSTRACT (Continued)

four fundamental problem areas where basic research is needed, before SAR can become a useful tool for the Navy.

Under Task 2, solutions to SAR signal processing problems were explored and geometrical corrections of SAR wave imagery were considered.

A focusing algorithm (for use during the processing of SAR signal data) was developed. This algorithm compensated for the along track component of wave velocity, but not acceleration (as occurring in coastal regions), during SAR image processing.

A digital correction algorithm was also developed and tested under Task 2. This algorithm converts SAR slant range to ground range prior to spectra generation. The analysis on the digital algorithm showed that slant range geometry has two effects on waves.

An analysis of optical transform operations on SAR wave imagery was performed under Task 3. This analysis indicated the importance of geometrically correcting SAR data prior to exploitation. Results also indicated that two-dimensional transforms of SAR wave data contain information in a form which has potential for automatic spectra computation and that directional filtering operations do not appear to be practicable for coastal and deep water ocean wave analysis.

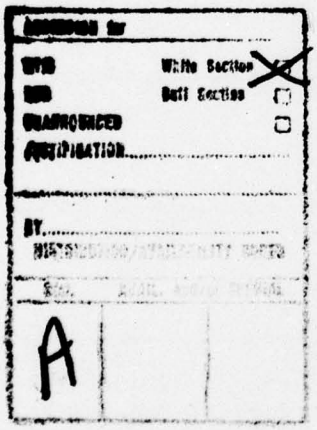

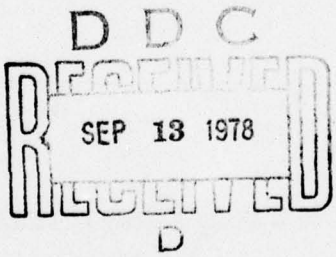

PREFACE

The work described in this report was conducted by the Radar and Optics Division of the Environmental Research Institute of Michigan (ERIM). The work was supported by the Office of Naval Research, Geography Branch under Contract No. N00014-76-C-1048. The Technical Monitor was Mr. Hans Dolezalek.

The Principal Investigator for this project was Mr. Robert A. Shuchman. Ms. Claudia Vandermade conducted the computer literature search (Appendix A). Dr. Philip L. Jackson performed the optical enhancement (Section 7) on the processed ocean wave radar data, while Mr. Gerald B. Feldkamp developed the necessary computer software and carried out the digital exploitation discussed in Section 6. Dr. Jerry Zelenka derived the focusing algorithm discussed in Section 4, and Mr. Charles Liskow contributed to Section 3 dealing with Synthetic Aperture Radar and moving targets.

The imagery presented in this report was processed at ERIM by Messrs. Alex Klooster and Jack A. Losee. Thanks are given to Messrs. Richard W. Larson, Charles Liskow, and Robert F. Rawson of ERIM for reviewing this report.

Parts of this report, notably the sections dealing with Synthetic Aperture Radar and Moving Targets, and the Processing of Ocean Wave Data from a Synthetic Aperture Radar were jointly developed under the Office of Naval Research Contract reported herein and a National Oceanic and Atmospheric Administration (NOAA), National Environmental Satellite Service (NESS) grant (No. 04-6-158-44078). The Technical Monitor on the NOAA/NESS grant was Dr. John W. Sherman III.

CONTENTS

PREFACE iii
LIST OF FIGURES v
1. INTRODUCTION AND SUMMARY 1
1.1 Description of Tasks 1
1.2 Summary of Results 2
1.3 Recommendations for Future Work 5
2. POTENTIAL USE OF ONR FUNDED DEVELOPMENTS IN OTHER PROGRAMS 7
3. BACKGROUND 9
3.1 Principles of the Synthetic Aperture Radar 10
3.2 Special Problems: SAR Imaging of Moving Targets 11
3.2.1 Velocity Effects 13
3.2.2 Acceleration Effects 15
4. LITERATURE SEARCH AND SAR WAVE IMAGING MODEL 22
4.1 Literature Search 22
4.2 SAR Mechanism for Imaging Ocean Waves 22
5. PROCESSING OF OCEAN WAVE DATA FROM A SYNTHETIC APERTURE RADAR 25
5.1 Introduction 25
5.2 Theory for Variable Azimuth Focus Algorithm 26
5.3 Experimental Observations 33
5.4 Other Considerations 39
5.5 Summary 41
6. SLANT-RANGE TO GROUND-RANGE CONVERSION OF SAR DATA 45
6.1 Introduction 45
6.2 Discussion 47
6.3 Results 54
6.4 Summary 60
7. OPTICAL FOURIER TRANSFORM OPERATIONS TO ANALYZE WAVE CHARACTERISTICS 61
7.1 Introduction 61
7.2 Background 62
7.3 Experiments 70
7.4 Discussion 76
APPENDIX A: LITERATURE SEARCH PERTAINING TO SYNTHETIC APERTURE RADAR IMAGING OF THE OCEANS 82
APPENDIX B: EFFECT OF MIXED INTEGRATION ON DEPTH OF FOCUS 100
REFERENCES 110

LIST OF FIGURES

1. Diagram Showing Airborne Radar Geometry and Image Presentation 4
2. Moving Train Displaced from Track. 14
3. Radar Image Displacement Caused by Target Velocity-Aircraft Case 16
4. Radar Image Displacement Caused by Target Velocity-SEASAT Case 17
5. Maximum Acceleration vs Radar Wavelength for Various Resolutions. 21
6. Velocity Corrections for Shallow-Water Waves, L-Band (HH), 3 x 3 Meter Resolution. 34
7. Velocity Correction for Deep-Water Waves, L-Band (HH), 3 x 3 Meter Resolution. 35
8. Focus as a Function of Wave-Train Direction, L-Band (HH), 3 x 3 Meter Resolution. 36
9. Focus as a Function of Wave-Train Direction, L-Band (HH), 8 x 6.25 Meter Resolution 37
10. Focus as a Function of Wave-Train Direction, L-Band (HH), 8 x 25 Meter Resolution 38
11. Graphical Demonstration of the Displacement or Defocusing of Waves as a Function of Motion in the Resulting Image. . . . 40
12. Wave Imagery as a Function of Multiple Looks (Mixed Integration Time) 42
13. Relationship Between Slant Range and Ground Range Coordinate Systems 46
14. Reconstruction Filter Magnitude Response: $f_c = 0.9375$. 51
15. Reconstruction Filter Phase Response: $f_c = 0.9375$. 52
16. Reconstruction of Slant Range Data 53
17. Slant Range Presentation of SAR Ocean Wave Imagery 55
18. Ground Range Equivalent of Outlined Region of Figure 17. 57
19. Spectrum of Outlined Region of Figure 17 58
20. Spectrum of Figure 18. 59

LIST OF FIGURES
(Concluded)

21. Fraunhofer Diffraction Setup to Obtain Two-Dimensional Fourier Transform of Photographic Image. Film Placed in Plane Wave of Monochromatic Light. 63

22. Fraunhofer Diffraction Setup to Obtain Two-Dimensional Fourier Transform of Photographic Image. Film Placed in a Diverging Beam of Monochromatic Light. 64

23. Diagrams of Linear Images and Corresponding Two-Dimensional Fourier Transforms. 66

24. Diagram of "Cylindrical" Distortion 68

25. Setup for Filtering in the Fourier Transform Plane. 69

26. Two-Dimensional Fourier Transform of a SAR Wave Image in a Rectangular Aperture 71

27. Two-Dimensional Fourier Transform of a SAR Wave Image with Diffraction from Aperture Blocked Out. 73

28. Two-Dimensional Fourier Transform of a SAR Wave Image with a Truncated Circular Aperture. 74

29. SAR Ocean Waves and a Directional Reference Function, Both Imaged with No Filter in the Optical System. 75

30. SAR Ocean Waves of Figure 29 Directionally Filtered with a Center at 60^{o} Azimuth. 77

31. LANDSAT Imagery and Directional Reference Function, Both Imaged with No Filter in the Optical System 78

32. LANDSAT Imagery and Directional Reference Function Imaged with Filter Centered at 60^{o} Azimuth. 79

B-1 A Fully Coherent Processor. 104

B-2 A Mixed-Integrator Processor. 107

1
INTRODUCTION AND SUMMARY

This interim report on Contract N00014-76-C-1048 summarizes work on three tasks comprising the first year's effort. The performance period for the work reported herein was August 1976 to August 1977.

This introduction contains a description of tasks and a discussion of their relevance to exploring the problems of imaging ocean waves with Synthetic Aperture Radar (SAR), a summary of progress to date on each task, and recommendations for the current year's effort (August 1977 to April 1978).

1.1 DESCRIPTION OF TASKS

Three tasks were performed in the first year's work. The overall goal of all three tasks of the ERIM ONR effort was to provide the Navy with information to evaluate the operational use of SAR, so that, ultimately, meaningful ocean wave spectra and wave height information can be supplied to the Navy in real-time. The first year study concentrated on fundamental questions pertaining to SAR imaging of the oceans that must be answered before meaningful real-time ocean wave spectra can be obtained.

Task 1 consisted of a limited exploration of current literature on the problems encountered in imaging sea states with SAR, including current SAR-wave interaction models.

Task 2 was a study aimed at finding solutions to some of the problems discovered in Task 1. Specifically, the question of processing SAR signal histories of moving ocean waves was addressed along with a careful study of distortions present in SAR wave imagery as a result of SAR's unique geometry.

Task 3 explored the use of optical Fourier transform operations on SAR wave imagery to analyze wave characteristics. Both the direct imaging of the Fourier transform, and spatial filtering in the Fourier transform plane were explored.

1.2 SUMMARY OF RESULTS

Under Task 1, a limited literature search was conducted to ascertain problems encountered in imaging sea states with SAR. The search indicated four fundamental problem areas where basic research is needed, before SAR can become a useful tool for the Navy. The problem areas are:

1. An imaging model needs to be developed to adequately explain the mechanism involved in imaging the sea with Synthetic Aperture Radar.
2. The conventional signal processing of SAR signal histories (i.e., assuming a stationary target) is inadequate when processing SAR images of moving ocean waves.
3. The slant-range presentation of SAR must be corrected prior to spectra generation.
4. The current methods (both optical and digital) used to extract meaningful wave spectra need further refinement and ultimately should be a real-time operation.

Under Task 2, solutions to SAR signal processing problems were explored and geometrical corrections of SAR wave imagery were considered.

A focusing algorithm (for use during the processing of SAR signal data) was developed. This algorithm compensated for the along track component of wave velocity, but not acceleration, during SAR image processing. The results of using this algorithm led to the following conclusions:

1. Given the same wave velocity, defocusing of wave imagery due to along track velocity components of waves is more pronounced at L-band than at X-band.

2. The 180° ambiguity of wave travel (for example, 90° or 270°) can be resolved by observing the direction of defocusing in the optical processor at L-band.

3. The 180° ambiguity should be marginally resolvable using a SEASAT radar with a proposed 8 m x 25 m resolution. Better results would be realized with an improved resolution of 8 m x 6.25 m.

4. Using the ERIM 1975 Marineland data to simulate the proposed SEASAT radar parameters, the effect of defocusing due to wave motion is only slightly discernible. However, with higher sea states and resulting higher wave velocities the defocusing should be more discernible.

5. The velocity correction necessary to focus ocean waves corresponds to the phase velocity of the waves rather than the orbital velocity.

A digital correction algorithm was also developed and tested under Task 2. This algorithm converts SAR slant range to ground range prior to spectra generation. The analysis on the digital algorithm showed that slant range geometry has two effects on waves. First, a compression of wave imagery will always occur, introducing an abnormally high range frequency component in the spectrum. Second, this compression is not constant; as shown in Figure 1, two adjacent wave crests at near range will appear closer together than two at far range. Slant range thereby produces an image showing continuously changing spacings of waves which are actually uniformly spaced. A Fourier transform of a large scene represented in slant range will falsely appear to include a wide range of frequency modulated wave components, whereas a Fourier transform of

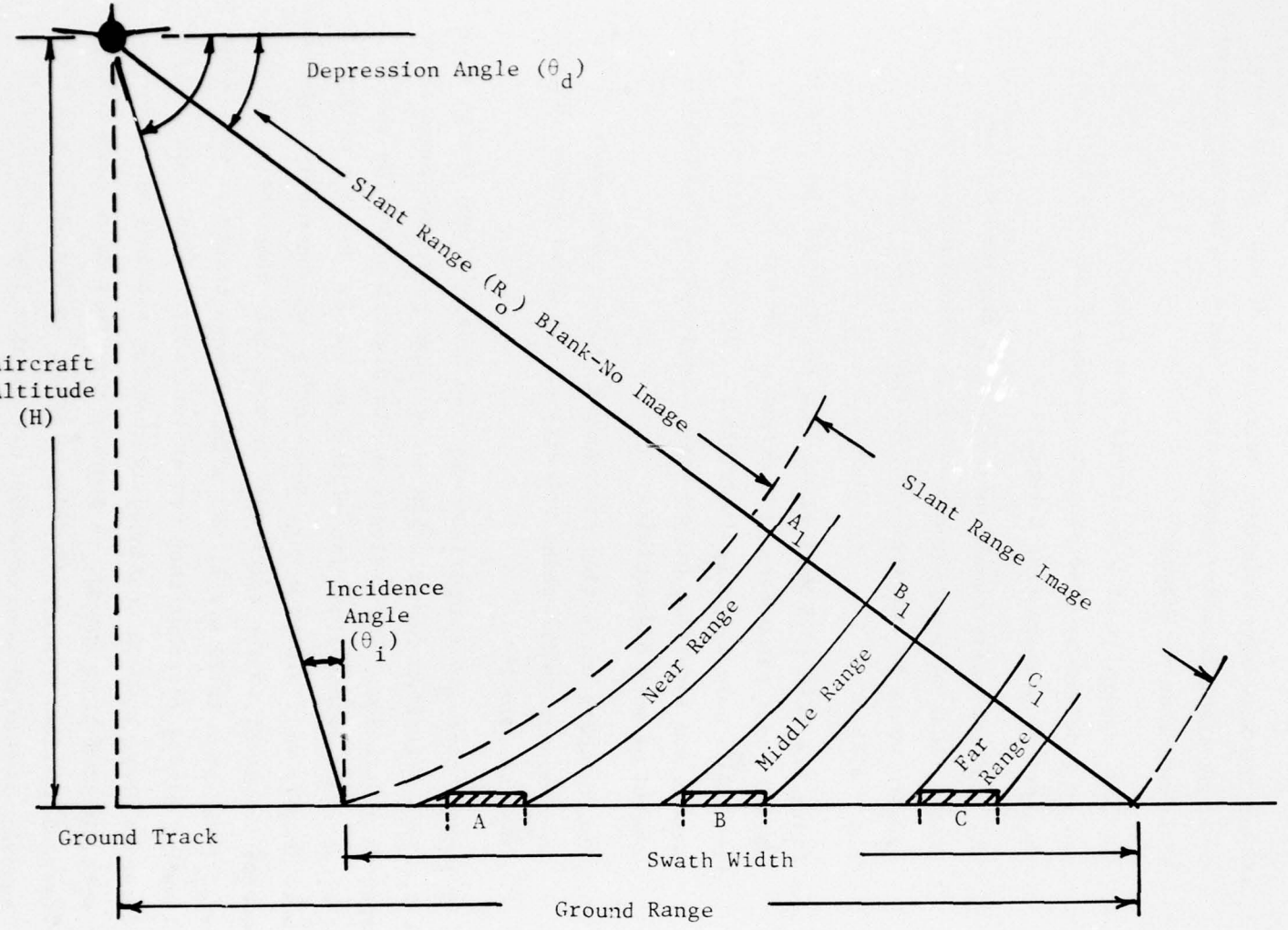

Figure 1. Diagram Showing Airborne Radar Geometry and Image Presentation

the proper ground range representation of uniformly spaced waves will produce a strong concentration of energy at a discrete frequency. Slant range representation results in a smearing of the spectrum which reduces the SNR. Slant-to-ground range conversion alleviates this problem.

The analysis of optical transform operations on SAR wave imagery indicated the importance of geometrically correcting SAR data prior to exploitation. Results also indicated that two-dimensional transforms of SAR wave data contain information in a form which has potential for automatic spectra computation and that directional filtering operations do not appear to be practicable for ocean wave analysis.

1.3 RECOMMENDATIONS FOR FUTURE WORK

The recommendations for future work are:

1. Continue exploitation of digital analysis of SAR ocean wave data. Included in this task are (1) removal of range-dependent antenna weighting, (2) use and evaluation of slant-to-ground range converted imagery, (3) investigation of the utility of averaging spectra from independent sections of SAR wave imagery and comparison with spectra obtained with multi-look imagery, (4) interpretation and development of algorithms to relate the distribution of spectral patterns to ocean wave refractions and other wave characteristics.

2. Explore the potential of wave spectra generation from SAR signal film with a single optical system. Included in this effort will be the exploration of methods to optically convert from slant-to-ground range, and to develop focusing algorithms for wave acceleration as well as velocity effects.

3. Continue to explore the mechanism of SAR imaging of ocean waves in terms of the extensive four-channel dual wavelength

experimental data we have gathered. A careful examination of current models will be undertaken, and the effects of wave motion considered.

2

POTENTIAL USE OF ONR FUNDED DEVELOPMENTS IN OTHER PROGRAMS

Although the present exploration of problems of imaging ocean waves with synthetic aperture radar is making important contributions to basic remote sensing, we wish to note that the developments which we are making are also potentially of use for proposed 6.2 programs of the U.S. Navy and in programs of other government agencies. Some of the anticipated or potential applications of these techniques are discussed below.

1. The presently developed ONR algorithms apply directly to processing SEASAT-A L-band SAR data. SEASAT-A is the NASA oceanographic satellite that is to be launched in the second quarter of 1978.

2. In addition to the proposed processing of NASA SEASAT-A data, the developed algorithms are being used in a joint ERIM-NOAA/SAIL program, Grant No. 04-6-158-44078, to further study the ERIM-Marineland data as well as ERIM-SAR data obtained over Lake Michigan.

3. Software developed at ERIM under the ONR will be used by NORDA to study ocean wave attenuation through ice. The SAR data used for this analysis comes from Project SAR 77: data collected near the coast of Labrador during February - March 1977.

4. Knowledge obtained from the ONR effort is available to design future SAR satellite sensors such as SEASAT-B and C and oceanographic shuttle missions that image ocean waves.

5. Upon development of a SAR wave height estimator algorithm, power density spectra can be obtained from the ocean SAR data, hopefully in near real-time. This data could greatly aid U.S. Navy oceanographers working on sea state prediction at Fleet

Numerical Weather Center. Civilian sea state prediction groups such as Ocean Routes, Inc. could also find this data very useful. USGS/CERC is also greatly interested in obtaining a power density spectrum in shallow water.

3
BACKGROUND

This section reviews briefly the principles of synthetic aperture radar (SAR) and discusses the special problems associated with imaging moving targets such as ocean waves with a synthetic aperture radar.

Radars exist in many different configurations, each designed to perform one or more specific functions. The type of radar which appears to offer a major long-term potential for reconnaissance and remote-sensing applications is the airborne imaging radar. Such a radar as shown in Figure 1 may be configured to generate a "microwave image" of a terrain or sea strip parallel to the flight path of the radar-bearing vehicle.

Such systems can be divided into two basic classes. One of these, known as real-aperture, side-looking airborne radar (SLAR), relies on a relatively large antenna; such an antenna achieves a narrow beamwidth which provides fine image resolution in the direction parallel to the flight path of the aircraft. The other class, known as synthetic aperture radar (SAR), consists of a coherent radar with a relatively small antenna (and hence a moderately broad antenna beam) which can be conveniently carried aloft by the vehicle. This system relies on data processing to effectively synthesize a large antenna, and thus achieve the effect of a sufficiently narrow beam to provide the required resolution.

Systems of both types exist today. The SLAR systems enjoy simplicity of design and do not require sophisticated data processing; however, when fine resolution is required, they are restricted to relatively short-range operation and the use of relatively short wavelengths (the latter approximately 3 cm or less). The SAR systems have fine resolution independent of range and wavelength.

3.1 PRINCIPLES OF THE SYNTHETIC APERTURE RADAR

Implementation of the synthetic aperture technique [1] requires the use of a coherent radar, a signal storage device, and a sophisticated data processor. By storing the received signal returns from a particular area for a period T and appropriately processing these data, the resolution in the along track (azimuth) direction can be reduced to

$$\rho_A = \frac{\lambda}{2\beta} \tag{1}$$

where λ is the radar wavelength and β is the along-track or azimuth angular width of the radar beam (beamwidth). This resolution is achieved by employing the rate of change in phase (i.e., Doppler frequencies which arise from the change in range as a target passes through the antenna beam) which is proportional to the angle β. If β is sufficiently small, so that $\beta \sim \sin \beta$, the Doppler frequency change is essentially linear. A linear swept Doppler frequency is thereby produced by the radar scan in the along track direction. This frequency modulated signal can be compressed using standard FM-pulse compression techniques. Because the Doppler bandwidth is only a function of the angle β, the resolution is independent of distance.

The angular width of the radar beam is

$$\beta \approx \sin \beta = \frac{\lambda}{d} \tag{2}$$

where d is the real antenna's effective aperture. If this entire beamwidth is included in the data processing, the resolution can be:

$$\rho_a = \frac{d}{2} \tag{3}$$

---

1. W. M. Brown and L. J. Porcello, "An Introduction to Synthetic Aperture Radar", IEEE Spectrum, Vol. 6, No. 9, September 1969, pp 52-66.

This relationship suggests that a relatively small antenna can be employed with SAR. Note that this fine resolution is achieved independently of the distance R_o from the vehicle to the terrain and independently of the wavelength of the transmitted radar energy. Thus, SAR provides a practical means to sense the earth with fine resolution from long range at frequencies distributed over useful portions of the microwave electromagnetic spectrum.

Fine range resolution ρ_R is achieved by transmitting an FM frequency modulated pulse. By use of pulse-compression techniques, the resolution in slant range direction can be reduced to

$$\rho_R = \frac{c}{2\alpha} \tag{4}$$

where c is the velocity of light and α is the radar modulation bandwidth.

From Figure 1, it can be observed that the range coordinate of radar imagery is related to propagation time and is inherently associated with a slant range display rather than horizontal or ground range display. A radar slant range display can be warped to resemble a ground range display. Radar range resolution remains constant in the slant range plane, and ground plane range resolution is dependent upon the line-of-sight depression angle. The effective ground range resolution is equal to the radar's range resolution divided by the cosine of the depression angle. This factor is of only secondary importance for small depression angles, but as the depression angle approaches 90° the effective ground range resolution becomes excessively large. This will be discussed in detail in Section 6.

3.2 SPECIAL PROBLEMS: SAR IMAGING OF MOVING TARGETS

Very interesting effects occur when a target moves during imaging. Constant velocity and constant acceleration generate different image effects in the range and azimuth directions, producing four separate cases.

1. Constant velocity in the azimuth direction changes the focal length of signals recorded on the signal film relative to the fixed targets in the azimuth direction.
2. Constant velocity in the range direction displaces the image in the azimuth direction.
3. Constant acceleration in the azimuth direction introduces defocusing but it is so small it is negligible for realistic acceleration values.
4. Constant acceleration in the range direction changes the focal length of the recorded signals in the azimuth direction and may deteriorate range resolution.

These effects are discussed in this section. The altered focal cases may be corrected by special processing which require refocusing.

The synthetic aperture technique as explained previously utilizes small differences in the slant range of stationary objects on the terrain relative to the moving radar antenna. These small range differences are detected by the radar as small phase changes of the radar echo signals and are used to discriminate between objects in the along track (azimuth) direction. The processor uses the Doppler frequency to locate the along-track position of a target and the time delay to locate the distance to the target. The Doppler frequency is generated by the relative motion of the aircraft with respect to the target.

Conventional operation of a synthetic aperture radar assumes that the sensor platform moves at a constant velocity and that objects to be imaged are stationary. However, ocean waves have both velocity and acceleration components in the azimuth, range, and elevation (vertical) directions. Information on the synthetic aperture imaging of moving targets is summarized in the open literature by Dr. R. K. Raney [2].

---

2. R. K. Raney, "Synthetic Aperture Imaging Radar and Moving Targets", IEEE Transactions on Aerospace and Electronic Systems, May 1971, Vol. AES-7, No. 3, pp. 499-505.

3.2.1 VELOCITY EFFECTS

Wave motion modifies the radar echoes so that conventional data processing results in defocused and displaced images. The defocusing effect is caused by the azimuth velocity component; this problem can be compensated in part by changing the azimuth focus control in the processor in direct proportion to the along-track velocity component. The azimuth focal length is a function of the rate of change of the Doppler frequency. It can be seen that wave velocity in the same direction as the radar vehicle's velocity will produce a reduced Doppler rate, while wave velocity in the opposite direction will produce an increased Doppler rate. The more detailed discussion of this process is provided in Section 5.

Since the synthetic aperture technique utilizes the small range rates of stationary reflecting objects to separate their images in the azimuth coordinate, targets moving in the range direction appear with altered azimuth positions in the processed image, but are still focused. A non-moving target will produce zero Doppler when it is on a line perpendicular to the aircraft track. However, if the reflecting object is moving toward the aircraft, zero Doppler will be produced after the aircraft has passed this perpendicular line, shifting the apparent position of the object in the same direction as the flight direction. Conversely, if the object is moving away from the aircraft, the apparent position will be shifted opposite the flight direction. To illustrate the displacement effects which can result from target motion in the range direction, observe Figure 2 which shows a SAR image of a moving railroad train displaced from its track. This displacement occurs because the radial component of its velocity produced radar echo phase rates that are different than the phase rate from the fixed targets. If the radial component of target velocity is large enough, the shifted Doppler frequency would exceed the bandpass of the radar data recorder and the intensity of the image of the moving object would be reduced and the resolution degraded.

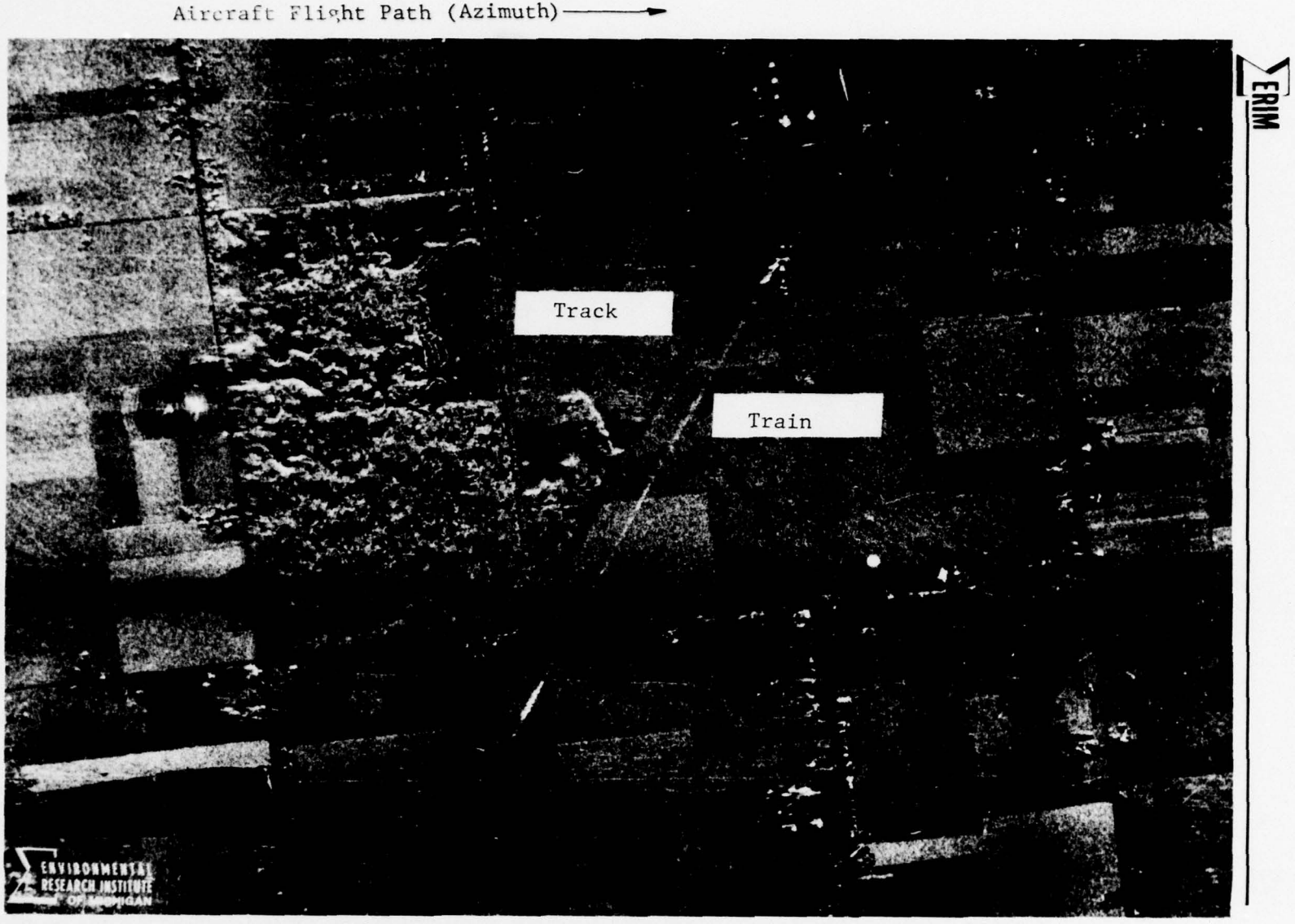

Figure 2. Moving Train Displaced from Track

The magnitude of the azimuth displacement can be expressed as:

$$\Delta X = \frac{V_R}{V_A} R_S \tag{5}$$

where ΔX = displacement

V_R = line-of-sight velocity component of reflecting object

V_A = velocity of the radar aircraft

R_S = radar range of the reflecting object

Note that image displacement is directly proportional to object radial velocity and radar range. It is inversely proportional to aircraft velocity and independent of radar wavelength. The magnitude of displacement can be minimized by using short radar range and high aircraft velocity. Examples of image displacement for several object velocities are shown in Figures 3 and 4. Figure 3 values were computed for aircraft altitudes and the nominal speed of the ERIM aircraft (C-46), of approximately 75 meters/sec. A 25 meter/sec wind could increase the aircraft ground speed to 100 meters/sec downwind or reduce it to 50 meters/sec upwind. This would make a two to one difference in the image displacement resulting from target object velocity. Figure 4 values were computed for satellite altitude and the nominal velocity of SEASAT of approximately 7.8 km/sec.

3.2.2 ACCELERATION EFFECTS

The effect of acceleration of ocean waves on X- and L-band SAR images should also be considered. This will be done relating the SAR resolution to integration time. It can be shown [3] that the theoretical Rayleigh resolution of SAR is

$$\rho = \frac{\lambda}{2L_s} \frac{H}{\cos \theta_i} = \frac{\lambda H}{2V_a T \cos \theta_i} \tag{6}$$

---

3. R. O. Harger, "Synthetic Aperture Radar Systems", Academic Press, New York, 1970.

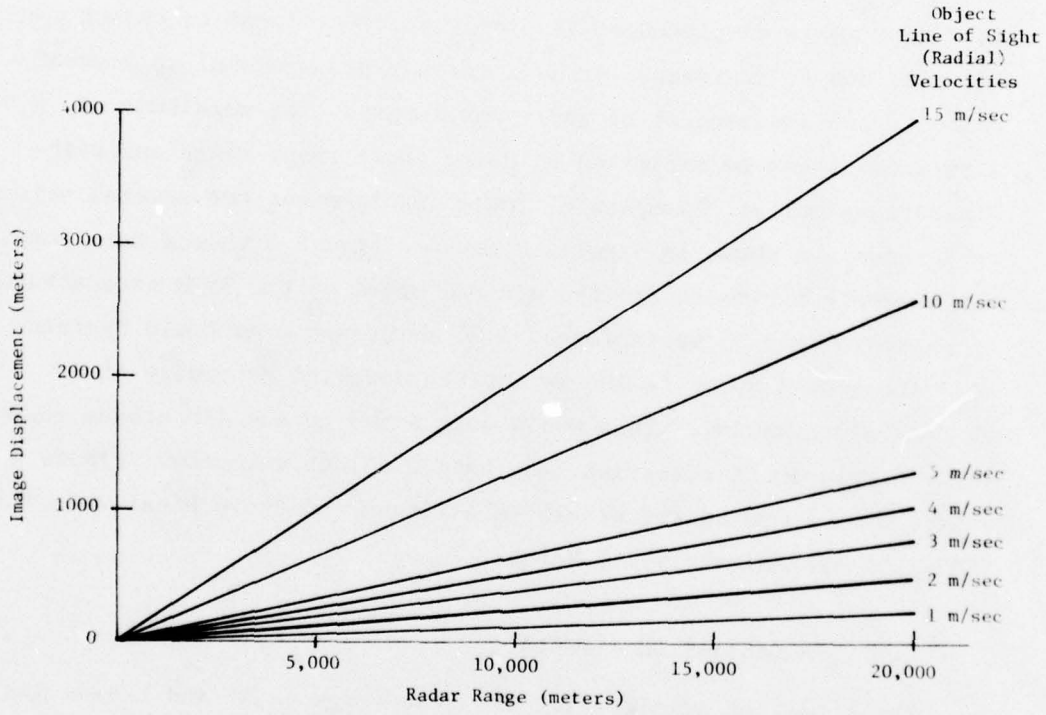

FIGURE 3. Radar Image Displacement Caused by Target Velocity-Aircraft Case (Aircraft Velocity 75 meters/second)

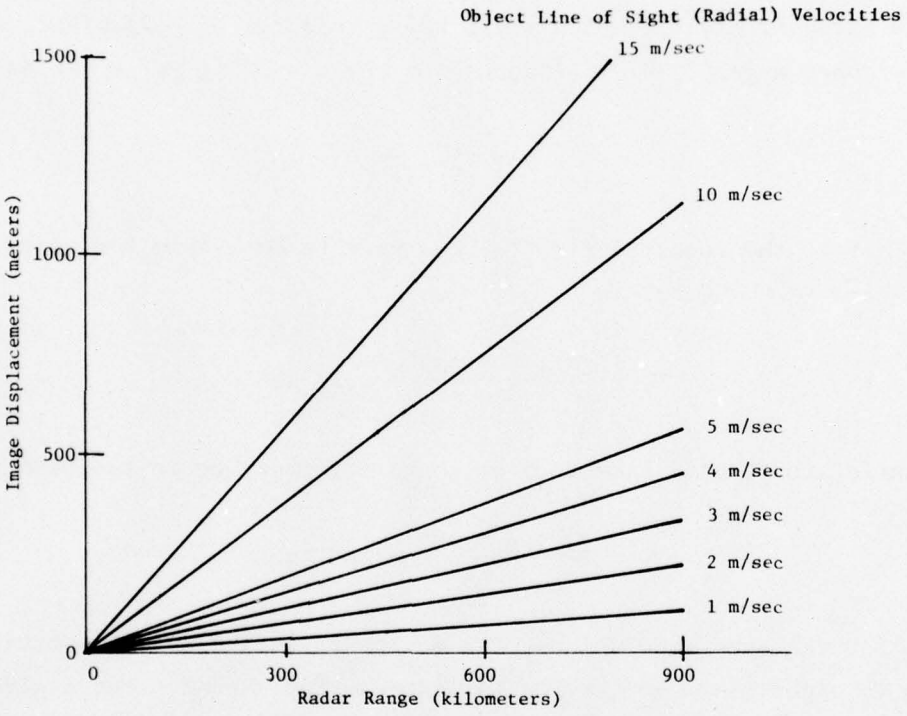

FIGURE 4. Radar Image Displacement Caused by Target Velocity - SEASAT Case (SEASAT Velocity 7.8 km/second)

where λ = radar wavelength

$L_s = V_a T$ = synthetic aperture length

V_a = velocity of aircraft

T = synthetic aperture time

H = altitude of radar

θ_i = incidence angle.

For an aircraft altitude of $H = 4.1$ km, a velocity $V_a = 75$ m/sec, and an incidence angle $\theta_i = 20°$ (depression angle = 70°), Eq. 6 yields

$$\rho = 29.1 \frac{\lambda}{T} \tag{7}$$

For $\rho = 5$ m, the required time for the wave to be within the radar beam for X-band ($\lambda = 3.2$ cm) is

$$T_X = \frac{29.1 \times 0.032}{5} = 0.19 \text{ sec} \tag{8}$$

Similarly, for L-band ($\lambda = 23.5$ cm), the wave must be in the beam for

$$T_L = \frac{29.1 \times 0.235}{5} = 1.37 \text{ sec} \tag{9}$$

Thus, for the same resolutions, the moving waves are in the aperture seven to eight times longer for L-band than for X-band. For a given resolution the required aperture times are proportional to the wavelengths, as is evident from Eq. 7.

The acceleration of a target in the along track direction affects the focus, but in a negligible way. The amount of such acceleration would have to be unrealistically high for the focus to be significantly affected.

However, acceleration of targets in the range direction causes significant degradation of the azimuth focal length. For a given resolution the maximum permissible acceleration A_R in the range

direction can be derived as a function of H, V_R, and T. The instantaneous range R to a target during the generation of a synthetic aperture is

$$R = R_0 + V_R t + \frac{1}{2} A_R t^2 \tag{10}$$

where R_0 = range at t = 0

V_R, A_R = components of target velocity (V_R is constant and only displaces the wave in the image) and acceleration (also a constant) in the range direction

t = time.

The error term ε which degrades azimuth resolution, by changing its focal length, is

$$\varepsilon = \frac{1}{2} A_R t^2 \tag{11}$$

The corresponding phase error ϕ_ε is given by

$$\phi_\varepsilon = \varepsilon \frac{4\pi}{\lambda} = \frac{2\pi}{\lambda} A_R t^2 \leq \frac{2\pi}{\lambda} A_R \left(\frac{T}{2}\right)^2 \tag{12}$$

where T is again the synthetic aperture time. The upper bound is realized at the start and the end of the SAR signal history*. The total time is T. Taking the correct phase as occurring at zero Doppler, then both the start and end of the signal history occur at a time interval $\frac{1}{2}T$ from zero Doppler time.

$$t = \frac{T}{2}$$

To obtain a properly-focused SAR image, the phase error should not exceed $\pi/2$. Thus

$$T \leq (\lambda/A_R)^{1/2} \tag{13}$$

---

* The "signal history" is the signal that is obtained during the time that a single scatterer is within the along-track beamwidth, i.e., the time that reflected energy is being received from the scatterer.

Using the previously presented values of H, V_a, and θ_i that follow Eq. 6, the maximum allowable acceleration is obtained by combining Eqs. 13 and 6

$$A_R \leq 4V_a^2 \cos^2\theta_i \, \rho^2/H^2\lambda \tag{14}$$

or

$$A_R \leq 1.18 \times 10^{-3} \, \rho^2/\lambda \tag{15}$$

Figure 5 graphs A_R (in m/sec^2) versus radar wavelength λ (in cm) for a SEASAT type satellite case; a family of such curves is plotted for various resolutions ρ (in meters). It should be noted that Figure 5 shows maximum allowable range acceleration assuming processor remains adjusted for stationary targets. The graph does not account for range smear due to A_R.

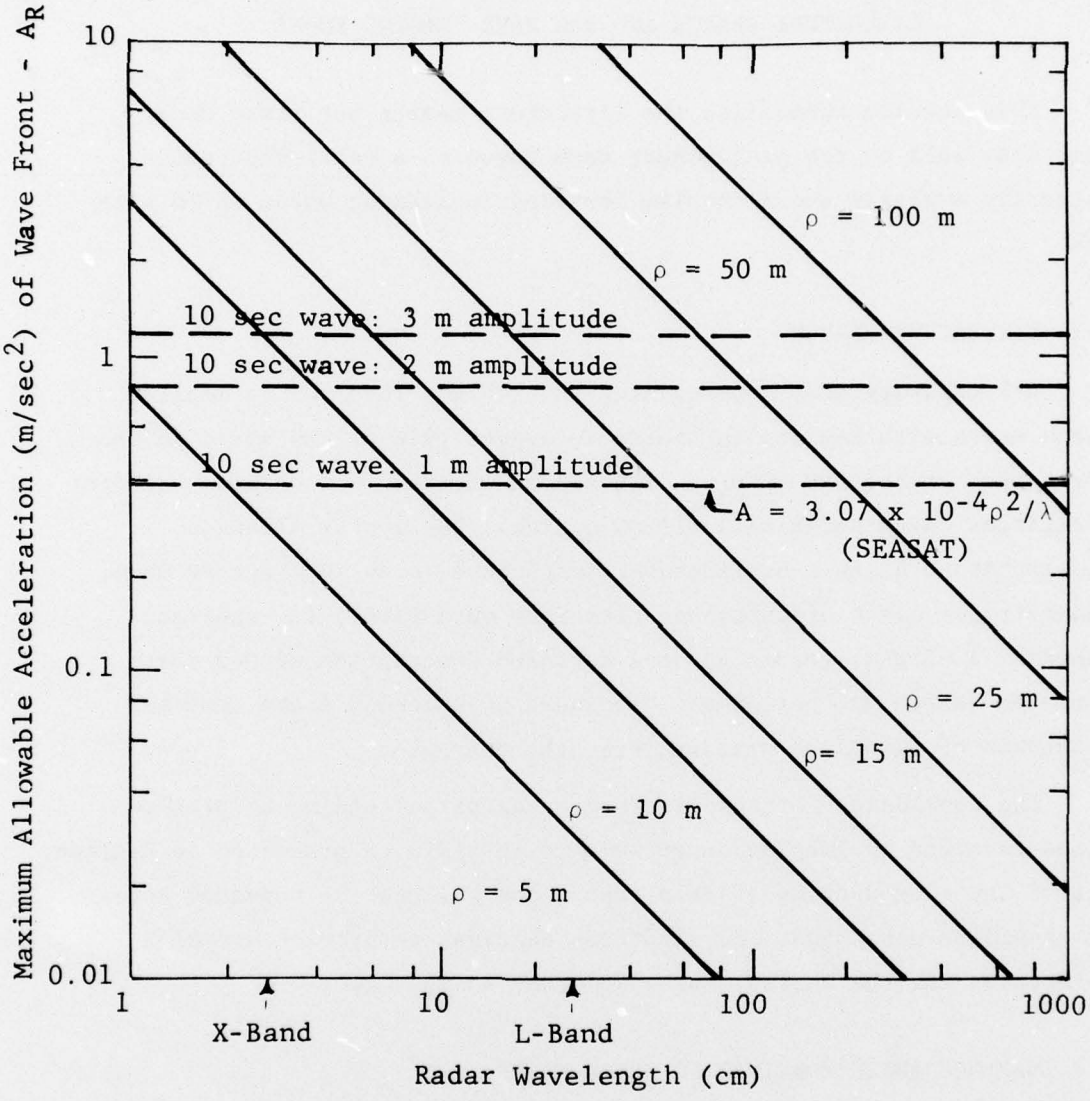

FIGURE 5. Maximum Acceleration vs Radar Wavelength for Various Resolutions

4
LITERATURE SEARCH AND SAR WAVE IMAGING MODEL

This section summarizes the literature search performed under Task 1 as well as the preliminary work begun on a model that satisfactorily explains the mechanism involved in imaging ocean waves with SAR.

4.1 LITERATURE SEARCH

A literature search pertaining to problems involved in imaging ocean waves with SAR was initiated in August 1976 at the start of the first year of the ONR effort. The search was done via on-line computer facilities using Lockheed's DIALOG system. The system allows a researcher to query a bibliographic data base in an interactive mode, and retrieve a set of pertinent citations on a particular subject. Appendix A of this report gives a detailed description of how the computer search was performed. Included in Appendix A are computer printouts of citations obtained from the search.

The conclusion of the literature search pertaining to problem areas involved in imaging ocean waves with SAR were presented in Section 1.2 of the introduction of this report and will not be repeated here. It should be noted that the citations continue to provide useful references for the current tasks underway in year two.

4.2 SAR MECHANISM FOR IMAGING OCEAN WAVES

A number of models which would explain ocean wave imagery taken with a synthetic aperture radar exist. The models considered correspond to three sources of radar backscatter modulation: tilt modulation, roughness variation, and the wave orbital velocity [4]. A careful

---

4. C. Elachi and W. E. Brown, "Models of Radar Imaging of the Ocean Surface Waves", IEEE Journal of Oceanic Engineering, Vol. OE-2, No. 1, January 1977.

examination of existing SAR wave data is necessary to find examples that support a radar backscatter model or combination of imaging models.

For example, the dependency of average σ_0 on radar look direction as well as the incidence angle sensitivity was measured on the Marineland data. The Marineland results support observations reported by Daley, Davis, and Mills [5] which indicate that, for low and moderate sea states, the L-band (HH)* σ_0 sensitivity to radar look direction (that is, up-wave, down-wave, and cross-wave) is negligible. At X-band, the data from 15 December 1975 indicate that, when the radar looks up-wave, a greater σ_0 results than when the radar looks cross-wave; the sea truth for 15 December indicates that the wind and waves were essentially in the same direction. The X-band data from 10 December 1975 confirm the observation made on the data from 15 December that σ_0 is significantly greater when the radar look direction is up-wave or down-wave as opposed to cross-wave.

A visual inspection of the ERIM four-channel Marineland data indicates that the X-band HH channel yields a strong return, but the X-band HV channel yields essentially no return from the sea other than at the breaker zone. In contrast, visual inspection also indicates that the return at L-band HV is as strong, if not stronger than the L-band HH channel. A wave imaging model would be required to explain these contrasting results.

As part of the task of explaining the SAR mechanism for imaging ocean waves ERIM contributed to a joint Marineland team (JPL, ERIM, NOAA/SAIL) paper entitled, "Comparison of In Situ and Remotely Sensed

---

* H = horizontal polarization; V = vertical polarization. The first letter represents the transmitting polarization, the second the receiving polarization.

5. J. C. Daley, W. T. Davis, and N. R. Mills, "Radar Sea Return in High Sea States", Report No. 7142, Naval Research Laboratory, Washington, D. C., September 1970.

Ocean Waves Off Marineland, Florida" [6]. The ERIM examination of the Marineland 4-channel SAR data indicated that better wave images can be generated from the X-band radar with parallel polarization than from the L-band radar. Simultaneously-obtained, identical-resolution X-band (HH) and L-band (HH) ocean wave images were compared. Both X- and L-band ERIM data have approximately the same signal-to-noise ratio (SNR). Scans of image photographic density in the direction perpendicular to the dominant crest direction indicate a higher crest-to-trough modulation for X-band than for L-band. Consequently, better definition is seen in wave-spectral peaks derived from X-band images than from L-band.

Further analysis of Marineland data indicates that optimum wave images result when the radar is looking essentially up-wave (waves propagating towards the aircraft in the range direction). This confirms the σ_0 measurements previously discussed. To explain the SAR mechanism of imaging ocean waves, proposed models should be consistent with all the above observed phenomena which include functions of frequency, look direction and incidence angle.

The literature search and the ERIM Marineland data indicate the major shortcoming of currently proposed SAR imaging mechanism models was insufficient SAR sea data to confirm their validity. The ERIM generated model will be based on dual polarization observations made at X-band (3 cm), L-band (24 cm) and K_a-band (0.89 cm).

The question of how the SAR images ocean waves is fundamental. It must be answered before a finalized focus algorithm can be developed. When this question is answered wave height determination from SAR should be possible as well as real time spectra generation.

---

6. O. Shemdin, W. E. Brown, F. G. Standhammer, R. A. Shuchman, R. F. Rawson, J. S. Zelenka, D. B. Ross, and R. A. Berles, "Comparison of In Situ and Remotely Sensed Ocean Waves off Marineland, Florida", Boundary Layer Meteorology (In Press).

5
PROCESSING OF OCEAN WAVE DATA FROM A SYNTHETIC APERTURE RADAR

This section discusses the focusing algorithm which accounts for the azimuthal velocity components of waves. The following discussion which is authored by R. A. Shuchman and J. S. Zelenka has been accepted for publication in a slightly different form in Boundary Layer Meteorology. ONR will receive copies of the reprint upon receipt.

5.1 INTRODUCTION

Synthetic aperture radar (SAR) is a coherent airborne radar that uses a moderately broad antenna beam. As discussed on page 9, the data collected by SAR are processed in such a way as to synthesize a very narrow beam, thus providing fine azimuth (along-track) resolution. Fine range resolution is achieved by transmitting either (1) very short pulses or (2) longer coded pulses which are compressed to equivalent short pulses by matched-filtering techniques. Usually, the coded pulse is linearly modulated in frequency. See Section 3.1 for a further discussion of some of the principles of synthetic aperture radar.

The SAR phase history of a scattering point in the scene is recorded on photographic film in the form of an anamorphic (astigmatic) Fresnel zone plate. The parameters of each such zone plate are determined (1) in the azimuth direction by the Doppler frequencies produced by the relative motion between the sensor and the point scatterer and (2) in the range direction by the structure of the transmitted pulses. The resulting signal film is a collection of superimposed zone plates representing all backscatterers in the scene. Placing this signal film at the input of a properly adjusted optical processor results in an optical image of the scene which had been illuminated by the radar [7].

---

7. A. Kozma, E. N. Leith, and N. G. Massey, "Tilted Plane Optical Processor", Applied Optics, Vol. 11, No. 8, August 1972, p. 1766.

The action of the optical processor is to focus the light passing through each anamorphic zone plate to a point of light representing the original microwave scatterer.

The problem of processing SAR data of ocean waves has been discussed in Section 3.2; this section will address the problem in more detail. An experimental investigation of the SAR wave imagery dependence on a number of processing parameters is discussed. In particular, the problem of forming sharp SAR images of moving ocean waves is considered.

Section 3.2 pointed out that azimuth defocusing can be compensated for by readjusting the azimuth focus by an amount proportional to the ocean wave phase velocity component in the azimuth direction. This technique is discussed in more detail here. In addition, the effects of changing (1) the range focus and (2) the number of superimposed coherent looks (i.e., the amount of noncoherent averaging) on SAR wave imagery are considered. The SAR data selected for these studies were collected on 15 December 1975 during a test conducted at Marineland, Florida using the ERIM X- and L-band dual-polarization system [8, 9].

5.2 THEORY FOR VARIABLE AZIMUTH FOCUS ALGORITHM

In this section, the amount of azimuth refocusing required to image specific ocean waves will be determined theoretically for both 3.2 cm (X-band) and 22.8 cm (L-band) SAR wavelengths, including the effects of radar system parameters and relative target velocity on depth of focus, f-number, and focal length of the processor. The resulting theoretical

---

8. F. L. Smith and R. F. Rawson, "Four-Channel Simultaneous X-L Imaging SLAR Radar", Proceedings of the Ninth International Symposium on Remote Sensing of the Environment, Ann Arbor, Michigan, 1974.

9. R. F. Rawson, F. L. Smith, and R. W. Larson, "The ERIM Simultaneous X- and L-Band Dual-Polarization Radar", Report of the IEEE 1975 International Radar Conference, New York City, p. 505.

relationships will then be applied to the ERIM X- and L-band radar with a nominal resolution of 3 meters as well as to the proposed SEASAT L-band radar with a resolution on the order of 25 meters.

Preliminary evaluations of the processed wave imagery (Section 5.3) support the theoretically determined relationships. Specifically, they indicate the following:

1. Given the same wave velocity, defocusing is more pronounced at L-band than at X-band.
2. The 180° ambiguity in direction of wave travel (for example 90° or 270°) can be resolved by observing the defocusing in the optical processor at L-band.
3. The 180° ambiguity should be marginally resolvable using a SEASAT radar with a proposed 8 m x 25 m resolution. Better results would be realized with an improved resolution of 8 m x 6.25 m.
4. Using the Marineland data to simulate the proposed SEASAT radar parameters, the effect of defocusing due to wave motion is only slightly discernible. However, higher sea states with resulting higher wave velocities should be more discernible.
5. The velocity correction necessary to focus ocean waves corresponds to the phase velocity of the waves rather than the orbital velocity.

First, the aximuth focal length dependence on azimuth target velocity will be determined. The azimuth focal length of a SAR target history is [10]

$$F = \frac{\lambda}{\lambda_\ell} \frac{R}{2} \frac{1}{(MP)^2} \tag{16}$$

10. J. W. Goodman, "Introduction to Fourier Optics", McGraw-Hill Book Co., New York, 1968, p. 192.

where R = slant range to the target

P = azimuthal packing factor defined below

M = azimuthal demagnification of the optical processor

while λ and λ_ℓ are the wavelengths at the radar and the optical processor respectively. The azimuth packing factor is

$$P = \frac{V}{v_f} \tag{17}$$

where V = relative along-track velocity between the radar transport and the moving wave, and

v_f = speed of the recording film.

Substituting Eq. 17 into Eq. 16 yields

$$F = \frac{R\lambda}{2M^2\lambda_\ell}\left(\frac{v_f}{V}\right)^2 \tag{18}$$

Now, let F_0 denote the along-track focal length of a stationary target. Then

$$F_0 = \frac{R\lambda}{2M^2\lambda_\ell}\left(\frac{v_f}{V_a}\right)^2 \tag{19}$$

where V_a = along-track speed of the radar.

For a moving target, the relative velocity becomes

$$V = V_a - v_T \tag{20}$$

where v_T = target speed in the along-track direction.

Combining Eqs. 18, 19, and 20, the shift in focal length produced by a moving target is

$$\delta F = F - F_0 = 2F_0\left(\frac{v_T}{V_a}\right)\frac{1 - \frac{1}{2}\frac{v_T}{V_a}}{\left[1 - \frac{v_T}{V_a}\right]^2} \tag{21}$$

If the target has an along-track speed which is much slower than that of the radar transport, Eq. 21 is approximated by

$$\delta F \sim 2F_0 \frac{v_T}{V_a} \tag{22}$$

The accuracy of this approximation is determined by direct comparison with Eq. 21. The resulting percent error is

$$\epsilon_{\delta F} = 150 \left| \frac{v_T}{V_a} \right| \frac{\left| 1 - \frac{2}{3} \frac{v_T}{V_a} \right|}{\left| 1 - \frac{1}{2} \frac{v_T}{V_a} \right|} \sim 150 \left| \frac{v_T}{V_a} \right| \tag{23}$$

The inverse of Eq. 21, that is, the dependence of focal length on target velocity is also of interest. Solving Eq. 21 for v_T yields

$$v_T = V_a \left(1 - \sqrt{1 - \frac{\delta F}{F_0 + \delta F}} \right) \tag{24}$$

Consider the ERIM SAR example:

$$V_a = 75 \text{ m/sec} \quad \text{and}$$

$$v_T = 12 \text{ m/sec}$$

where v_T = phase velocity of the wave.
Then, from Eq. 21, the shift in focal length introduced by the moving target in the along-track direction is

$$\delta F = 0.417 F_0 \tag{25}$$

if $v_T = 12$ m/sec; or

$$\delta F = -0.257 F_0 \tag{26}$$

if $v_T = -12$ m/sec.

Because F_0 in Eq. 19 is different for X- and L-band (see Table 1 of ERIM SAR parameters, next page), a 12 m/sec moving target introduces shifts in focal length of 0.579 mm for L-band and 1.264 mm for X-band. The -12 m/sec moving target introduces a focal-length shift of -0.357 mm for L-band and -0.779 mm for X-band.

The depth of focus DF for a SAR system is [10]

$$DF = \pm \frac{2}{\lambda_\ell} \left(\frac{v_f \rho}{M V_a} \right)^2 \quad * \tag{27}$$

where ρ denotes the azimuth resolution of the radar system (output image). For the ERIM system, the DFs are ± 0.0502 mm and ± 0.7804 mm for the 3 m resolution L- and X-band cases, respectively. Comparing the depth of focus at the output of the azimuth telescope with the focal length change introduced by a 12 m/sec wave, it is found that the X-band change is not detectable, because it is within the depth of focus. On the other hand, refocusing is required for the L-band case.

A simple expression for those wave velocities requiring processor compensation (i.e., refocusing) will now be derived. The resulting expression will then be applied to the SEASAT radar parameters. Setting $DF < |\delta F|$ in Eqs. 27 and 22,

$$\frac{2}{\lambda_\ell} \left(\frac{v_f \rho}{M V_a} \right)^2 < 2F_0 \frac{v_T}{V_a} \tag{28}$$

and recalling Eq. 21, one obtains

$$\frac{2}{\lambda_\ell} \left(\frac{v_f \rho}{M V_a} \right)^2 < \frac{2R\lambda}{2M^2 \lambda_\ell} \left(\frac{v_f}{V_a} \right)^2 \frac{v_T}{V_a} \quad . \tag{29}$$

Solving the above expression for v_T yields

---

* The depth of focus has been arbitrarily defined to be the total displacement from the optimal focal plane for which the resolution is degraded by a factor of two over the diffraction limit.

TABLE 1. ERIM SAR PARAMETERS

	L-Band	X-Band
R	4370 m	4370 m
λ	0.228 m	0.032 m
λ_ℓ	0.6328×10^{-6} m	0.6328×10^{-6} m
M	18.67	13.11
v_f	0.00186 m/sec	0.00515 m/sec
ρ	3 m	3 m
V_{AC}	75 m/sec	75 m/sec
F_0	1.3891×10^{-3} m	3.0313×10^{-3} (for V_a = 75 m/sec)

$$v_T > \frac{2\rho^2 V_a}{\lambda R} \tag{30}$$

The question arises as to whether imagery obtained from SEASAT is sensitive to wave motion. The SEASAT-A parameters are:

V_a = 7,868 m/sec

R = 845 km

λ = 0.235 meters

When used in Eq. 30 these give

$$v_T > \frac{(2)(7,868)(6.25)}{0.235(845,000)}$$

$$v_T > 3.10 \text{ m/sec}$$

for a resolution of 6.25 m. If the resolution is 25 m for one-look (fully coherent),

$$v_T > 49.53 \text{ m/sec}$$

If SEASAT uses mixed integration during data processing (i.e., use of four non-coherently averaged images to produce a four-look 25 meter image), a smaller minimum v_T is required than for the fully coherent case:

$$v_T > 12.38 \text{ m/sec}$$

This smaller minimum is required because the depth of focus for a mixed-integration processor is equal to the geometric mean of the depth of focus corresponding to the full aperture and depth of focus for the partial aperture (i.e., 6.25 and 25 meters). Appendix B of this report entitled "The Effects of Mixed Integration on Depth of Focus" discusses this statement in detail.

Thus if SEASAT-A uses either a resolution of 6.25 m or employs four-look mixed integration processing, refocusing to compensate for the azimuth component of the wave velocity will be necessary.

5.3 EXPERIMENTAL OBSERVATIONS

Figure 6 shows L-band, parallel-polarized data of near-shore, shallow-water waves, which was gathered on 15 December 1975. The upper image corresponds to normal processing (assuming a stationary target). The lower image was focused in the processor to observe a wave traveling at 14 m/sec in a direction opposite to that of the aircraft.

Figure 7 is an L-band, parallel-polarization image of a deep-water wave obtained on 15 December 1975, where the velocity of the waves was 14-15 m/sec. The upper image was again normally processed. Again, the lower image was corrected for the defocusing effects caused by the moving waves.

Figure 8 demonstrates the ability to detect the direction of wave propagation by observing the effect of defocusing in the image. The upper, L-band, parallel-polarization image was processed under the assumption that a 14 m/sec wave was traveling in a direction opposite to the radar flight path; the waves are clearly discernible. The lower image was processed under the assumption that a 14 m/sec wave was traveling with the aircraft; in this case, the assumption of the wrong direction of wave propagation caused such severe defocusing of the waves that they are no longer visible in the image.

Figures 9 and 10 demonstrate the same detection ability with SEASAT type resolution. The L-band, parallel-polarization, 8 x 6 m resolution, single-look image (Figure 9) shows focusing corrections for a wave train propagating in the along-track direction with the same and opposite directions as the aircraft velocity. The upper image is the correction necessary for waves traveling in the same direction as the aircraft while the lower image is corrected for wave motion in the opposite direction.

Figure 10 is the same as the Figure 9 L-band case, except that the resolution is degraded to 8 x 25 m with four images noncoherently

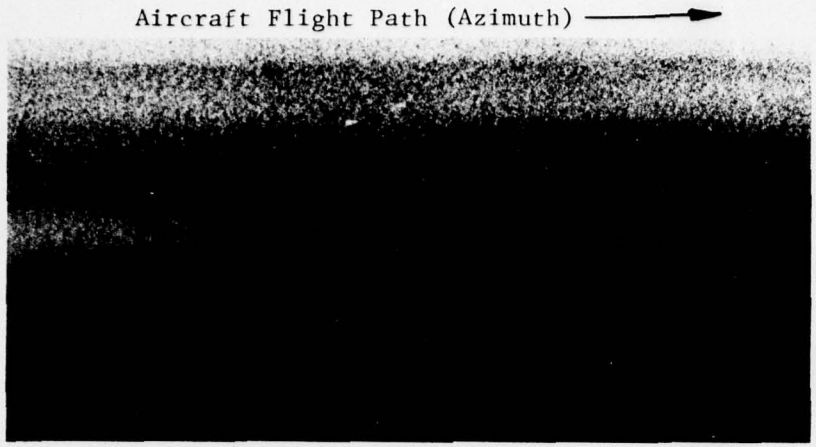

(a) Stationary-Target Focus

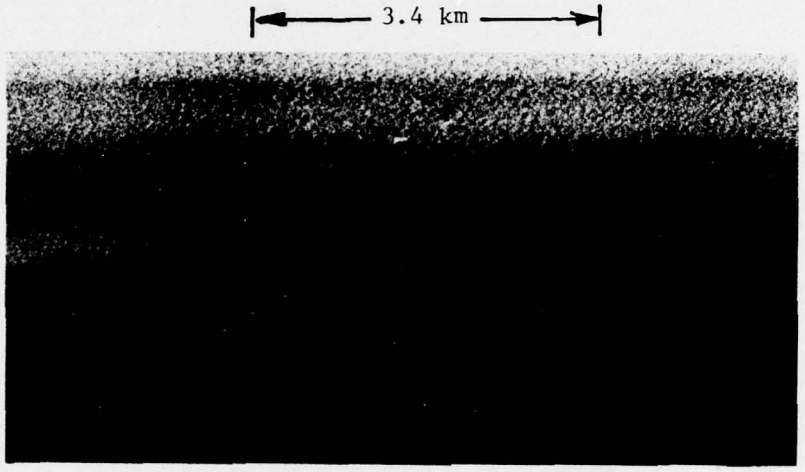

(b) Optimum Focus (Corrected for Wave Motion)

Figure 6. Velocity Corrections for Shallow Water Waves, L-Band (HH), 3 x 3 Meter Resolution

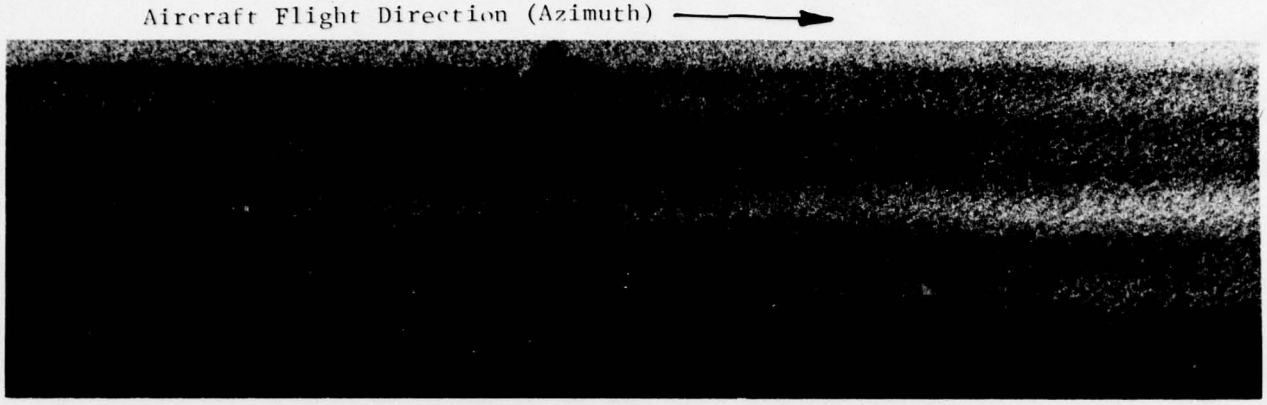

(a) Stationary-Target Focus

4 km

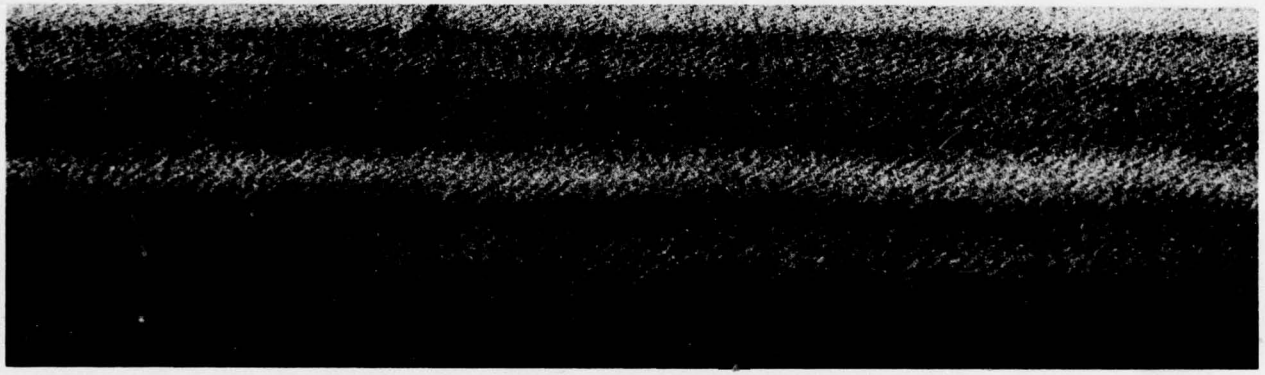

(b) Optimum Focus (Corrected for Wave Motion)

Figure 7. Velocity Correction for Deep-Water Waves, L-Band (HH), 3 x 3 Meter Resolution

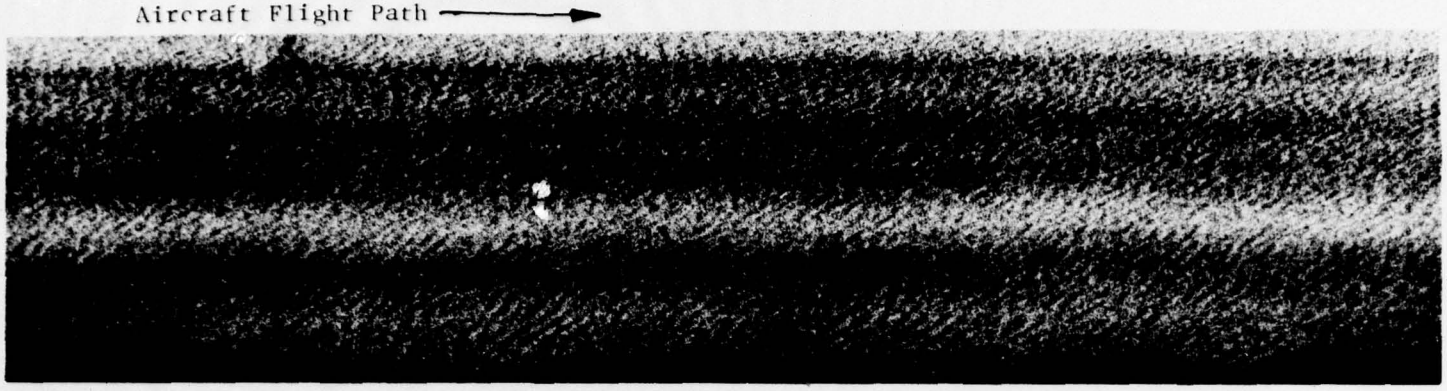

(a) Correction for 14 Meter/Sec Waves Traveling Toward Aircraft

3.7 km

Direction of Wave Travel

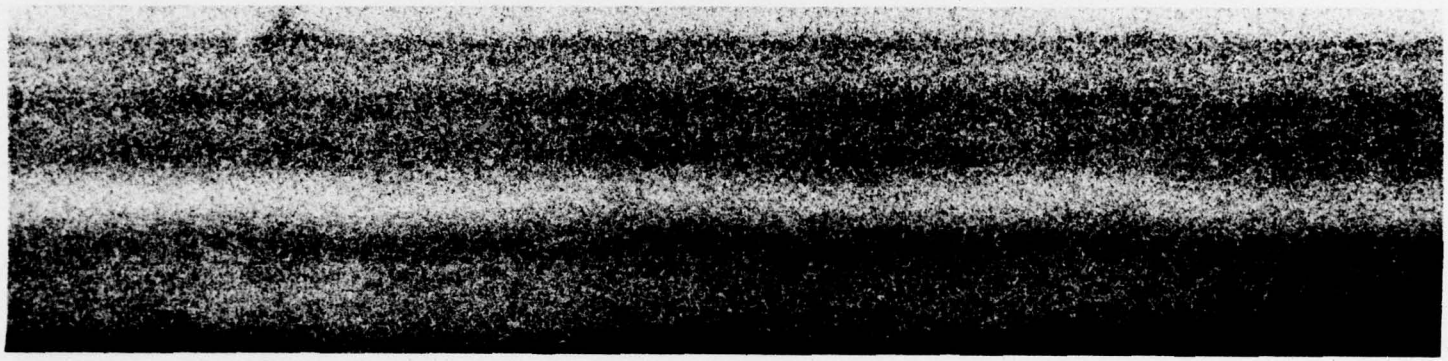

(b) Correction for 14 Meter/Sec Waves Traveling with Aircraft

Direction of Wave Travel

Figure 8. Focus as a Function of Wave-Train Direction, L-Band (HH), 3 x 3 Meter Resolution

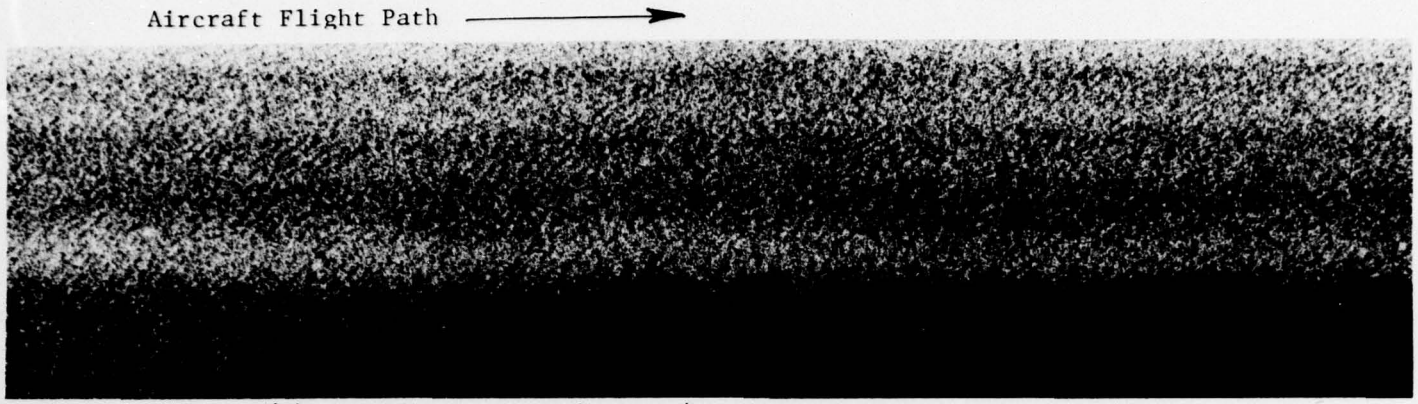

(a) Correction for 14 Meter/Sec Wave Traveling Toward Aircraft

3.3 km

Direction of Wave Travel

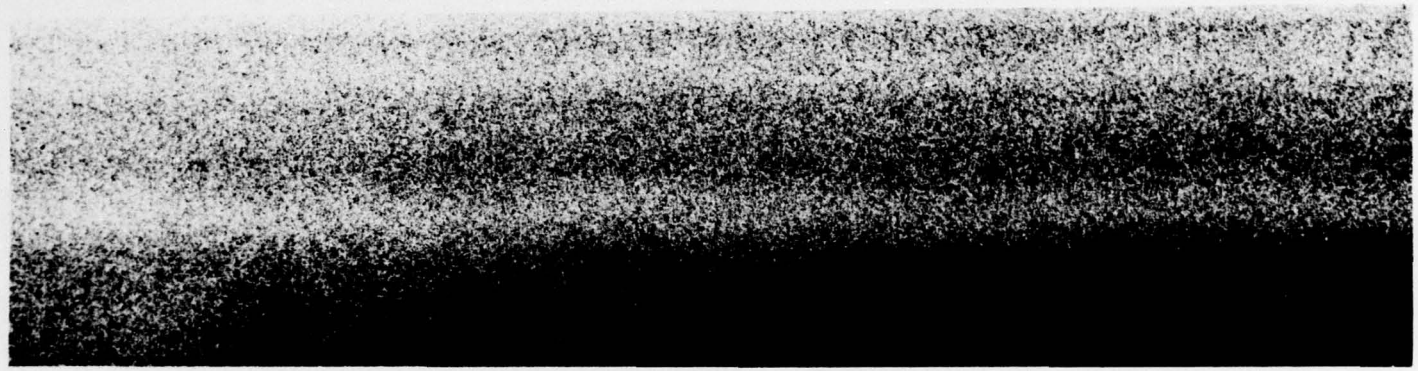

(b) Correction for 14 Meter/Sec Wave Traveling With Aircraft

Direction of Wave Travel

Figure 9. Focus as a Function of Wave-Train Direction, L-Band (HH), 8 x 6.25 Meter Resolution

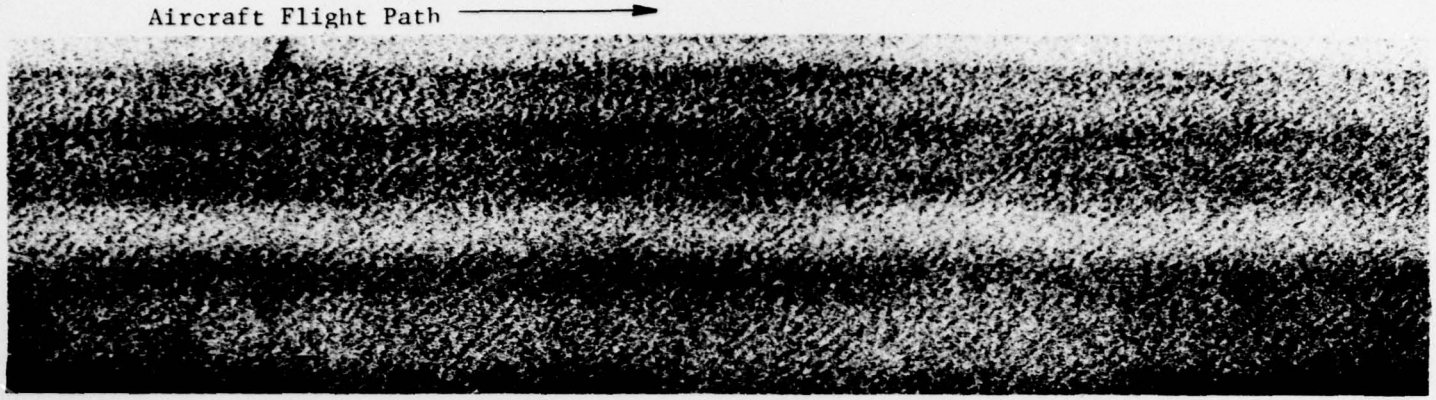

(a) Correction for 14 Meter/Sec Wave Traveling Toward Aircraft

3.7 km

Direction of Wave Travel

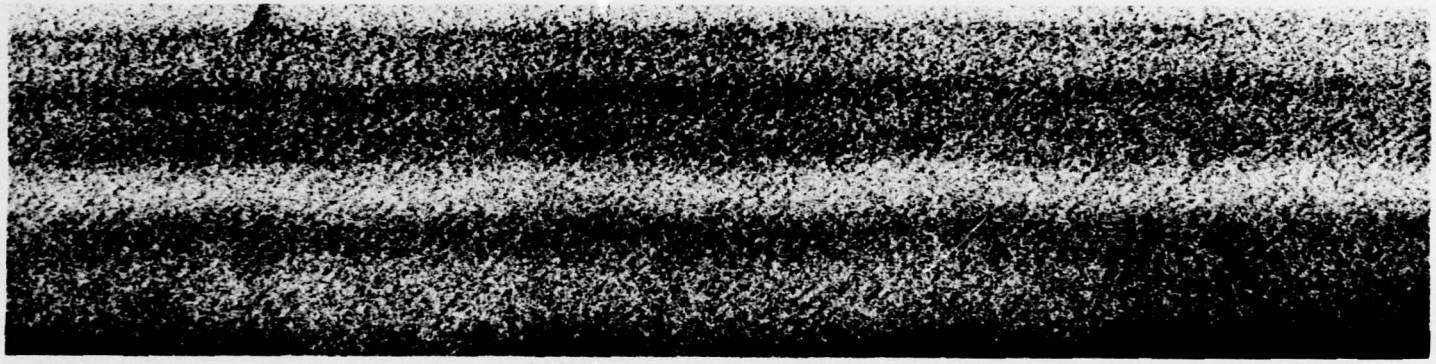

(b) Correction for 14 Meter/Sec Wave Traveling With Aircraft

Direction of Wave Travel

Figure 10. Focus as a Function of Wave-Train Direction, L-Band (HH), 8 x 25 Meter Resolution

averaged to produce the figure. The changes in focus with SEASAT resolutions are admittedly subtle; however, both Figures 9 and 10 show that wave direction is obtainable from SEASAT imagery by analysis of defocusing effects in the processor. It was also observed that, if the azimuth telescope is moved toward and away from the plane of focus for a stationary target by an amount larger than that necessary to correct for wave train motion, more obvious defocusing effects occur.

5.4 OTHER CONSIDERATIONS

A spectrum sampling was performed to evaluate the effect of using low, zero, and high Doppler information in processing wave data. The low, zero, and high Doppler correspond to varying squints of -4°, 0°, and +4°, respectively, at L-band. Experimental results indicate that little information is gained or lost as a result of selecting different portions of the Doppler spectrum.

Range focus was also varied in the processor. From this test, it was discerned that waves traveling in the range direction appear much less likely to produce azimuth defocusing. The explanation for this is that waves moving in the range direction introduce a constant Doppler shift. Since the radar achieves fine azimuth resolution by estimating when each scatterer has a zero Doppler shift, this type of movement merely displaces the image in the along-track dimension rather than causing a defocusing effect. This along-track displacement of waves should not be visible in the imagery except at boundaries such as shorelines. Figure 11 graphically demonstrates the displacement or defocusing of waves in the resulting image as a function of radial motion. This figure indicates that the range resolution controls the quality of the imagery.

A single coherent image was compared with one of equal resolution produced from four such images averaged together. The number of independent looks is a measure of the statistical image-intensity

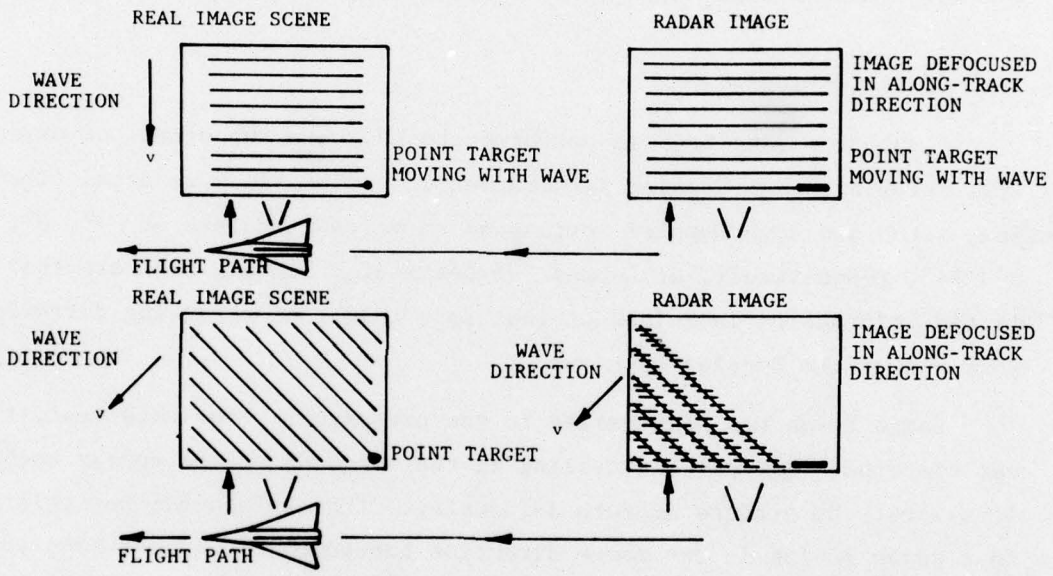

Figure 11. Graphical Demonstration of the Displacement or Defocusing of Waves as a Function of Motion in the Resulting Image

fluctuations of homogeneous diffuse targets. If the individual resolution cells of a coherent imaging system are distinguishable, then diffuse objects will show a very pronounced speckle pattern with independent intensity variations around the corresponding mean intensity. By averaging independent images, these statistical fluctuations are smoothed.

The results, as exhibited in Figure 12, indicate that the currently planned set of four multiple looks of mixed integration for SEASAT-A radar data sufficiently enhances the wave data. A probable explanation for this indication is the following. If wave crests are considered specular targets, the signal-to-noise ratio (SNR) improvement is proportional to $\sqrt{N}$, where N is the number of independent coherent looks [11]. Thus, the four-look imagery has an SNR improvement of a factor of two. Figure 12 is also interesting because it represents imagery with a resolution that simulates that proposed for SEASAT-A. Recall that, at 20° incidence angle, 8 m slant range resolution is the equivalent of 25 m ground range resolution. The mixed-integration equivalent to four multiple looks was achieved by limiting the input along-track aperture of the optical processor while exposing the output (image) film through a slit several resolution elements wide.

5.5 SUMMARY

Variation of the azimuth focus and the range focus indicates the rather high sensitivity of the images of wave components traveling in the along-track direction to azimuth focus and the rather low sensitivity to range focus of wave components traveling in the cross-track direction. Images of waves traveling in the azimuth direction can be effectively suppressed by defocusing to enhance the images of waves traveling in the

---

11. L. J. Porcello, N. G. Massey, R. B. Innes, and J. M. Marks, "Speckle Reduction in Synthetic Aperture Radars", J. of the Opt. Soc. of America, Vol. 66, No. 11, p. 1305.

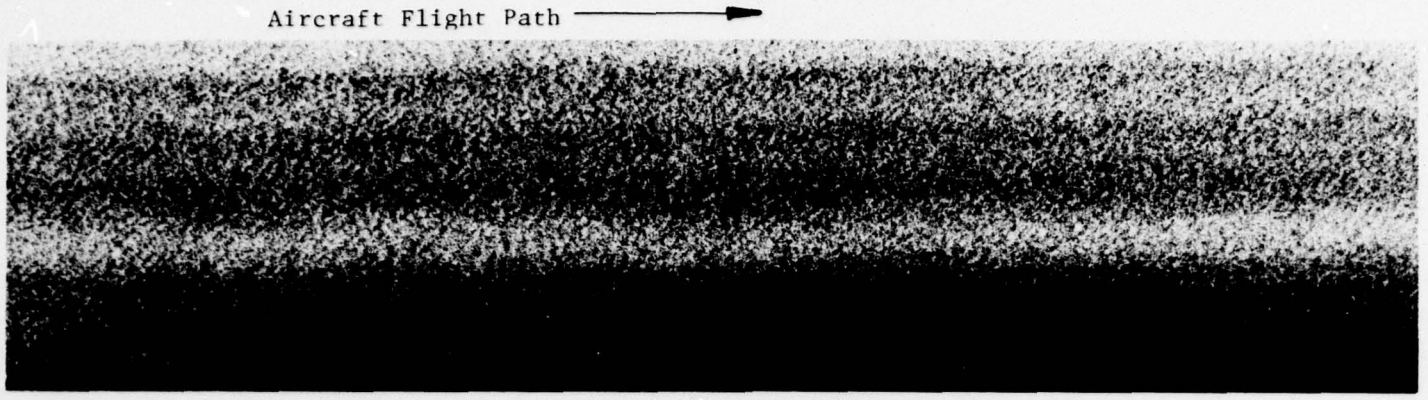

(a) Single Look (Fully Coherent), 8 x 6.25 Meter Resolution

3.3 km

Direction of Wave Travel

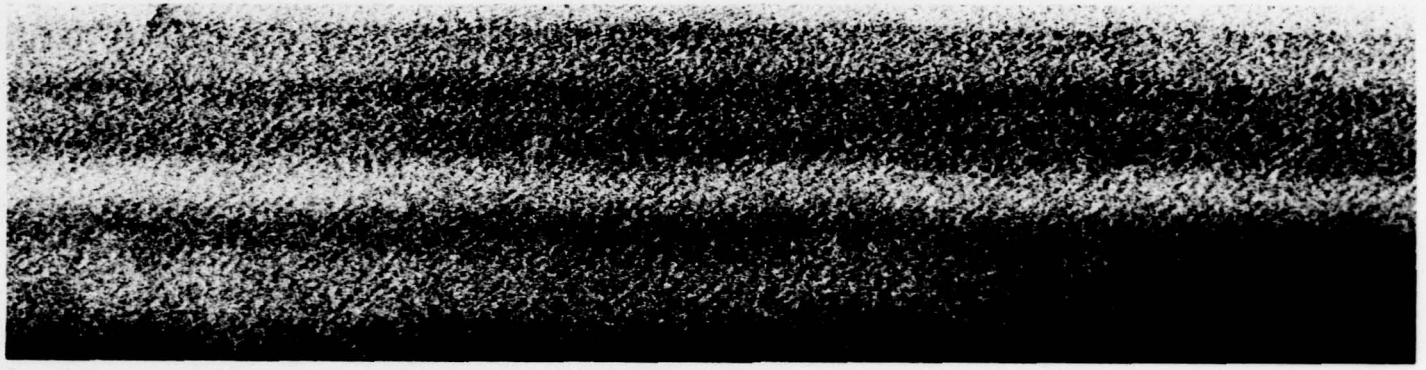

(b) Four Looks, 8 x 25 Meter Resolution

Direction of Wave Travel

Figure 12. Wave Imagery as a Function of Multiple Looks (Mixed-Integration Time)

range direction. This enhancement technique was successfully employed on both Jet Propulsion Laboratory (JPL) L-band and ERIM X-band L-band SAR wave data [12].

Ultimately, defocusing could be used as an enhancement tool for generating ocean-wave spectra. Separate Fourier transforms (FTs) generated for waves traveling in the range direction may be combined with the FTs of focused azimuth waves to obtain a clearer FT representation of sea state.

The azimuth defocusing caused by wave motion should not pose a serious problem for SEASAT imagery of sea states similar to those present at Marineland (that is, light to moderate seas). However, data from higher sea states are apt to require refocusing. The importance of the defocusing effect due to wave motion is twofold. First, this effect can be used to determine the direction of ocean-wave propagation. Second, it can be used as a rough estimator of the phase velocity associated with these waves. Wave-height information may also be learned from measurements of depth of focus along the radar line of sight [13].

Currently, focusing studies are underway at both ERIM and JPL. Hurricane and West Coast SAR wave imagery collected by the JPL L-band system shows the same focusing sensitivity discussed in this section. JPL has reported [14] significant improvement in the ability to see azimuth traveling waves when focusing is performed.

---

12. R. A. Shuchman, R. F. Rawson, and E. S. Kasischke, "Analysis of Synthetic Aperture Radar Ocean Wave Data Collected at Marineland and Georges Bank", ERIM Final Report 123000-11-F, Ann Arbor, Mich.
13. T. R. Larson, L. I. Moskowitz, and J. W. Wright, "A Note on SAR Imagery of the Oceans", IEEE Trans. on Antennas and Propagation, Vol. AP-24, No. 3, 1976, pp. 393-394.
14. O. Shemdin, Jet Propulsion Laboratory, Personal Communication.

In this section we have not considered the defocusing effects caused by wave acceleration (see Section 3.2), but consideration has been restricted to defocusing or Doppler shift caused by the constant-velocity component of wave motion.

6
SLANT-RANGE TO GROUND-RANGE CONVERSION OF SAR DATA

The following section discusses slant-range to ground-range conversion of SAR stripmap data. As this section will describe and Figure 13 indicates, SAR geometry is unique. One dimension of the SAR image is proportional to the "slant-range" distance from the aircraft to the point on the earth which is being imaged, rather than distance along the earth as in a conventional map. Thus previously developed scanner or map rectification algorithms do not apply to the SAR case. The distortion caused by the SAR slant-range representation is a relative compression of objects closest to the aircraft ("near range"). This slant-range distortion is usually moderate enough for the eye to accept, so SAR images are processed with the distortion. However, the distortion is too severe to perform machine computation on ocean waves because the slant-range image shows the waves unnaturally bent unless the waves are precisely perpendicular or parallel to the flight line. This bending distorts the two-dimensional Fourier transform, the computation which gives the wave direction and wavelength.

6.1 INTRODUCTION

In the digital exploitation of SAR ocean wave imagery, a reasonable first step is to remove the geometric distortion introduced by imaging the waves in slant range. In an ideal case of the ground range data being perfectly sinusoidal, the slant range image will appear as a frequency-modulated wave. Any frequency decomposition technique applied to such data will yield a spectrum with a smeared peak at, near, or possibly a significant distance from the sharp peak produced by a frequency analysis of the corresponding ground range image.

In realistic data it is probably unreasonable to expect that even the ground range image will ever yield a sharp peak in its spectral

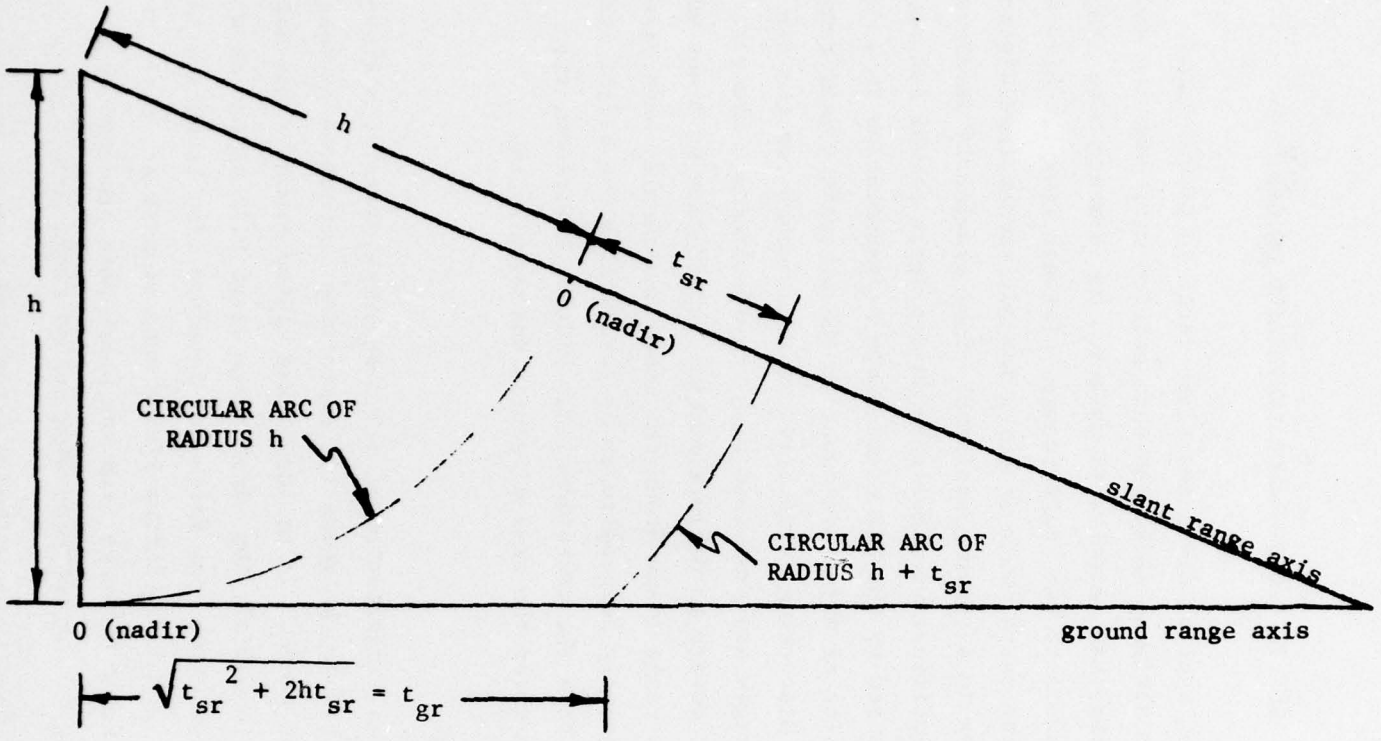

FIGURE 13. Relationship Between Slant Range and Ground Range Coordinate Systems

decomposition; however, the geometric distortion caused by the slant range presentation continues to be bothersome. The remainder of this section describes the slant-range to ground-range conversion algorithm developed at ERIM for use in digital exploitation of SAR ocean wave imagery. Examples of the effect of the conversion on wave spectra are included.

The SAR data made available for digital exploitation is digitized by ERIM's Image Dissector and Digitization (IDD) facility [15]. The optical processor's slant-range output imagery is sampled at an appropriate rate and recorded on a computer-compatible digital tape. This is the data which acts as input to subsequent digital post-processing steps.

6.2 DISCUSSION

One of these post-processing steps is a conversion of the digital slant-range data to ground-range. The relationship between these coordinate systems is suggested by Figure 13. It is convenient to consider both systems as being defined on $(0, \infty)$, where a coordinate value of 0 corresponds to a point at nadir*. In Figure 13, h is the aircraft altitude; also, t_{sr} is a general distance in slant-range, and t_{gr} is the corresponding distance in ground-range. Hence,

$$t_{gr} = \sqrt{(h + t_{sr})^2 - h^2} = \sqrt{t_{sr}^2 + 2ht_{sr}} \tag{31a}$$

* An extension to $(-\infty, +\infty)$ is straight forward, but serves no useful purpose here.

15. D. A. Ausherman, W. D. Hall, J. N. Latta, and J. S. Zelenka, 1976, "Radar Data Processing and Exploitation Facility", Proceedings IEEE International Radar Conference, Washington, D. C.

alternatively, one may write

$$t_{sr} = \sqrt{t_{gr}^2 + h^2} - h \qquad (31b)$$

Equation 31 shows that for a given increment Δt_{sr} in slant range, Δt_{gr} is always larger. Practically, this means that if the slant range data is frequency bandlimited, then the corresponding ground range data is bandlimited, at most, to the same frequency. An intuitive feel for this can be obtained by considering the effect of the coordinate change on a sinusoid in slant range. Everywhere the coordinate change is a stretching of the t_{sr} axis, so that a sine wave of a given frequency in slant range becomes a signal of lower instantaneous frequency in ground range. In the digitization procedure, the slant range image is lowpass filtered prior to sampling time, so that it is indeed bandlimited. Because the actual sampling rate exceeds (greatly, in fact) the Nyquist rate*, it is possible (in principle) to reconstruct the analog slant range signal. Further, the same sampling rate must be sufficient for the ground range data.

We intend to take fast Fourier transforms of the SAR wave data, in an effort to determine wave direction and wavelength. Since FFTs assume

---

* In its simplest form the Shannon Sampling Theorem states [16]:

> Given a signal, s(t), which is frequency bandlimited to (-W, +W), then sampling of s(t) at any rate, f_s, greater than 2W samples per second will permit exact reconstruction of the continuous-time signal s(t) from the sample values.

The "Nyquist rate" is the lower bound rate of 2W. Sampling at rate $f_s \leq$ Nyquist rate will cause terms of s(t) with frequencies $\geq f_s/2$ to be reconstructed as sinusoids of frequency less than $f_s/2$. This phenomenon is referred to as "aliasing" or "spectral foldover".

16. J. M. Wozencraft and I. M. Jacobs, "Principles of Communication Engineering", John Wiley & Sons, Inc., New York, 1967.

input data is uniformly sampled it is desirable that a slant range to ground range conversion program produce equally spaced points in ground range from equally spaced points in slant range. Due to the geometric distortion, the objective can be restated as one of reconstructing unequally spaced slant range samples from given equally spaced points in the same system.

This reconstruction can be accomplished by filtering the slant range data with a finite-duration digital filter, whose frequency response is comparable (over one period) to that of the ideal analog low-pass reconstruction filter, which imparts constant gain and zero phase change over the passband. Then reconstructing slant range data involves weighting the existing samples by certain filter values and summing over the duration of the filter (i.e., implement a discrete convolution of the digitized data with a reconstruction filter).

The reconstruction filter used is commonly referred to as a "raised cosine-weighted sinc"[†]. Specifically, the selected digital filter $h(t_k)$ is given as

$$h(t_k) = \left(0.54 + 0.46 \cos \frac{4\pi t_k}{2N}\right) \frac{\sin 2\pi f_c t_k}{2\pi f_c t_k} \tag{32}$$

where

$$t_k = \frac{N - 1}{4} + \frac{k}{2}, \quad k = 0, 1, \ldots, N - 1,$$

for N equal to the number of filter terms. The parameter f_c is interpreted as the filter's "cutoff frequency"; varying f_c in Eq. 32 varies the number of zero crossings of $H(t_k)$*. (Note also that a sampling interval of T = 1/2 has been selected. This presents no problem; we

---

[†] $\text{sinc } x \triangleq \frac{\sin \pi x}{\pi x}$

* The number of zero crossings is given as Nf_c.

can choose to think of the units of the slant range axis in any convenient way.)

To evaluate the frequency response of $h(t_k)$, a z-transform is computed and evaluated at $z = e^{j2\pi fT}$ for many choices of f. In Figures 14 and 15 the magnitude and phase responses are shown for N = 16 and $f_c = 0.9375$, respectively. The sampling rate of 2 Hz (T = 1/2) forces the spectrum to have a period of 2 Hz; one period ($f \in [-1, +1]$) is shown in Figures 14 and 15. The choice of $f_c = 0.9375$ places the cut-off frequency very nearly equal to the one-sided bandwidth of 1; this accounts for the 0 dB gain and the 0 radian phase change across most of the band. Use of this filter, then, will not artificially emphasize any wave components in the data; the conversion can proceed without any preconceived notions of the signal content.

In implementing this filter, one soon sees that the above explanation does not tell the entire story. In producing an output sample from a set of input samples, the operations suggested by Figure 16 are used. An output position, t_{out}, is first fixed. Conceptually, a continuous-time (still finite duration) version of $h(t_k)$ is then centered at t_{out}, and N samples of this continuous version are generated at positions t_k, equal to the given input sample positions. Since the scaling of the slant axis is arbitrary, let the k'th sample in slant range for k = 1, 2,..., be assigned a position $t_k = (k-1)/2$. Let $h_c(t)$ be the continuous version of $h(t_k)$, i.e., define

$$h_c(t) \begin{cases} \left(0.54 + 0.46 \cos \frac{2\pi t}{N}\right) \frac{\sin 2\pi f_c t}{2\pi f_c t}, & t \in \left(-\frac{N}{4}, \frac{N}{4}\right) \\ 0 & \text{otherwise} \end{cases} \tag{33}$$

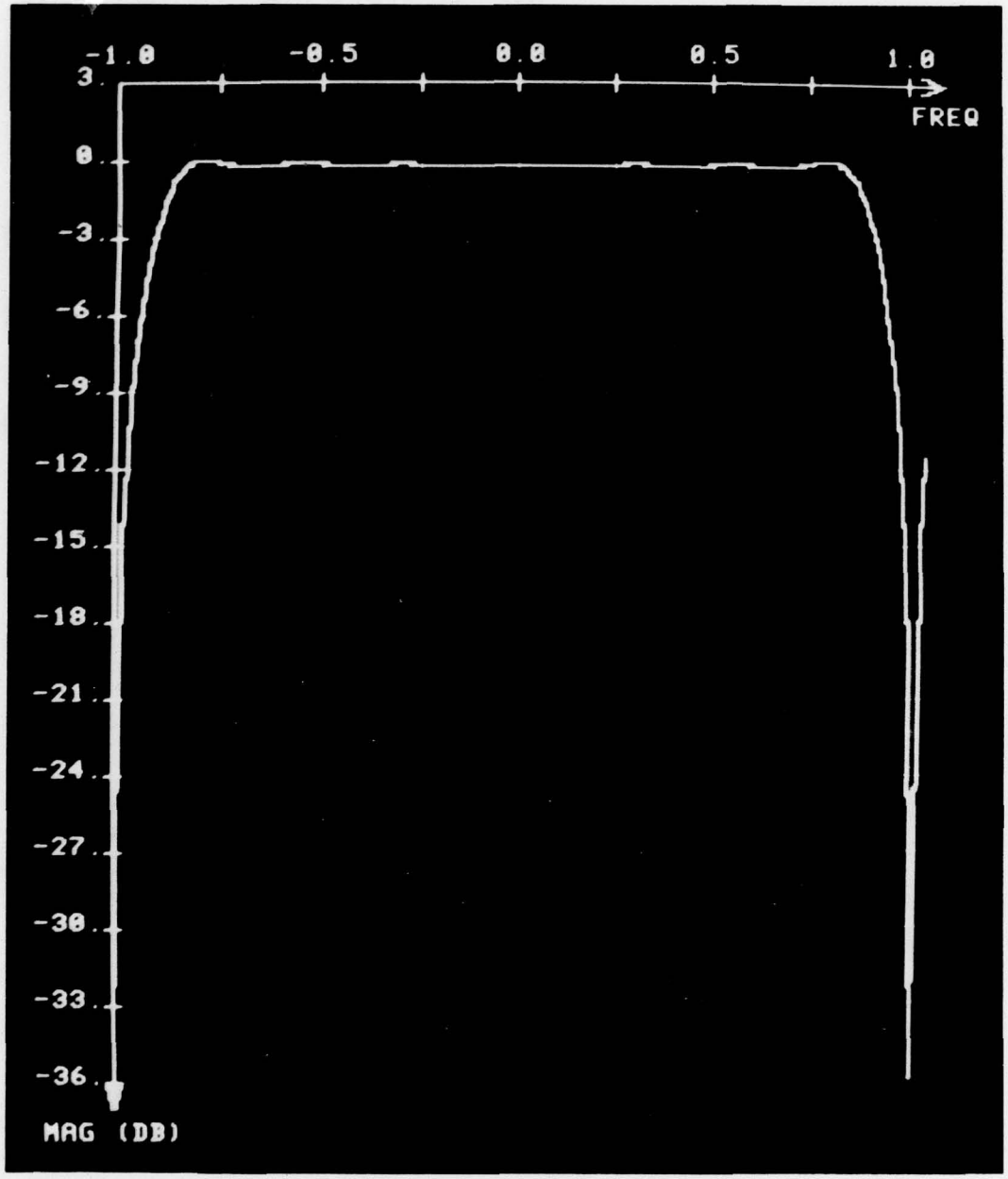

FIGURE 14. Reconstruction Filter Magnitude Response: $f_c = 0.9375$

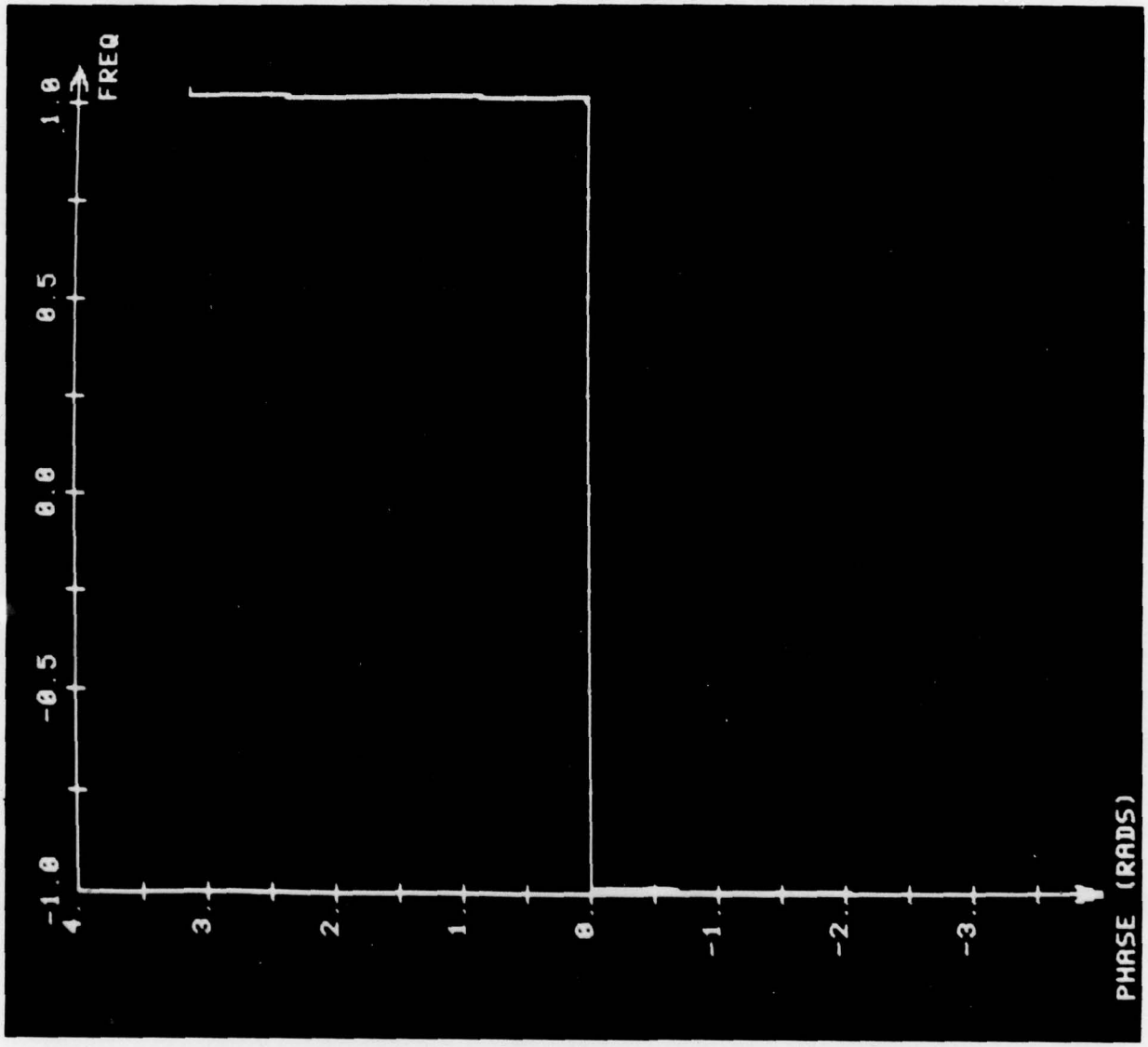

FIGURE 15. Reconstruction Filter Phase Response: $f_c = 0.9375$

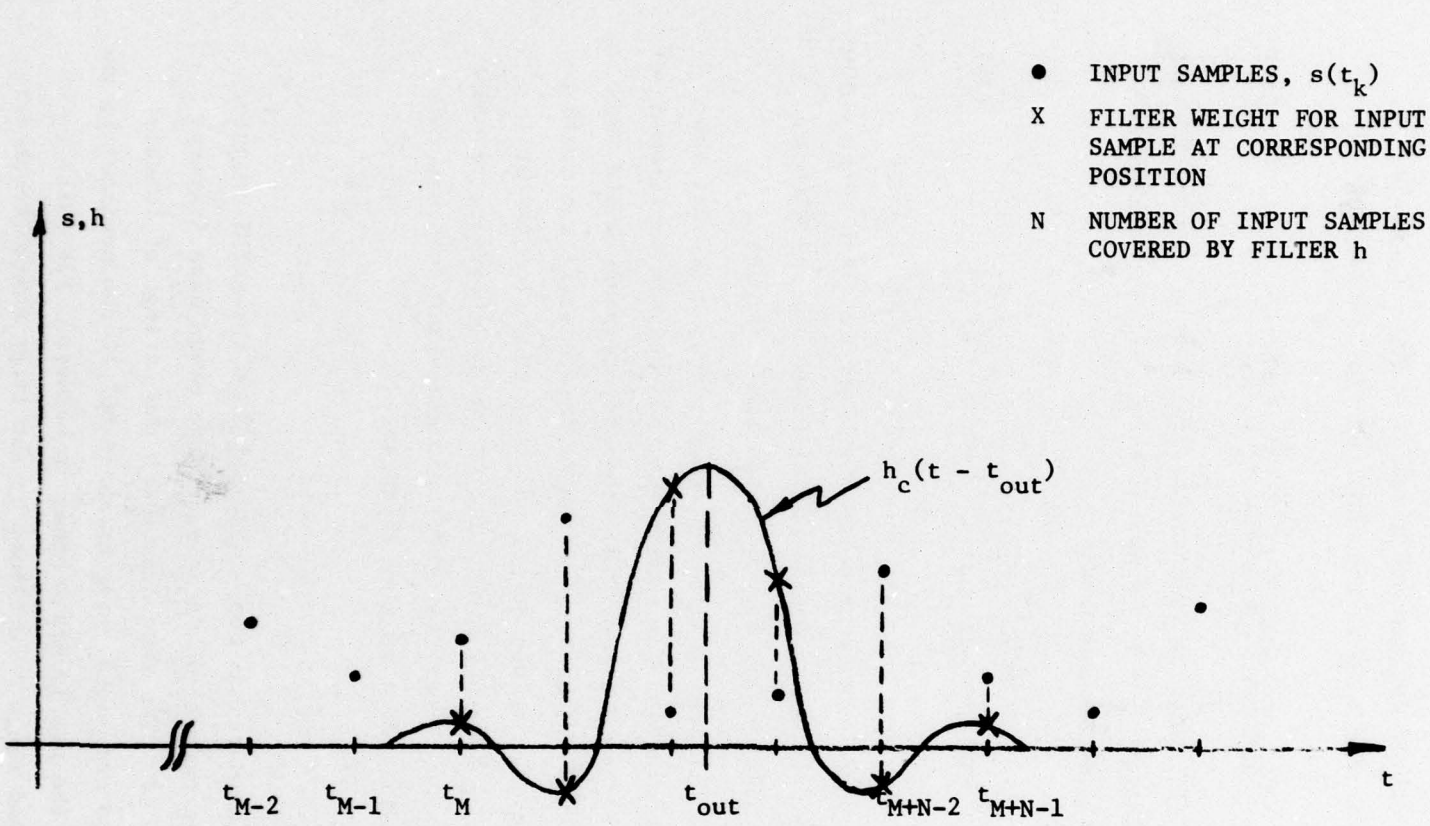

FIGURE 16. Reconstruction of Slant Range Data

Then the required filter weights are given as $h_c(t_k - t_{out})$, $k = M, M + 1,\ldots,M + N - 1$, where t_M is the sampling time satisfying

$$t_{out} - \frac{N}{4} \leq t_M < t_{out} - \frac{N}{4} + 1/2 \qquad (34)$$

Since $t_M = (M - 1)/2$, Ineq. 34 is satisfied for M equal to the integer on the interval $\left[2t_{out} - \frac{N}{2} + 1,\ 2t_{out} - \frac{N}{2} + 2\right]$. Thus, the required output sample, $v(t_{out})$, is computed as

$$v(t_{out}) = \sum_{k=M}^{M+N-1} h_c(t_k - t_{out})\ s(t_k) \quad . \qquad (35)$$

An entire slant range scan is converted to ground range by iteratively applying Eq. 35 after selecting a set of slant range output positions, $\left\{t_{out_j}\right\}$, which are consistent with Eq. 31b and with the desire to end up with equally spaced ground range samples.

The potential difficulty with the above approach is that the filter weights are time-varying, due to the non-uniform positioning of t_{out} between input sample times. The frequency response would then depend upon time, and the quality of the data reconstruction would be in doubt. Fortunately, it has been found that this time jitter associated with t_{out} has only minor effects on the frequency response of the reconstruction filter, so that for engineering purposes, the filter may be considered to be time-invariant.

6.3 RESULTS

The above procedure has been implemented on the ARIES computer facility [14]. An example of SAR slant range ocean wave imagery appears in Figure 17. The wave crests are the strings of loosely connected white to gray dots lying at about 60° to the horizontal; the wave troughs are the nearly black bands in between. The patch to be converted to ground range is outlined by the large white rectangle.

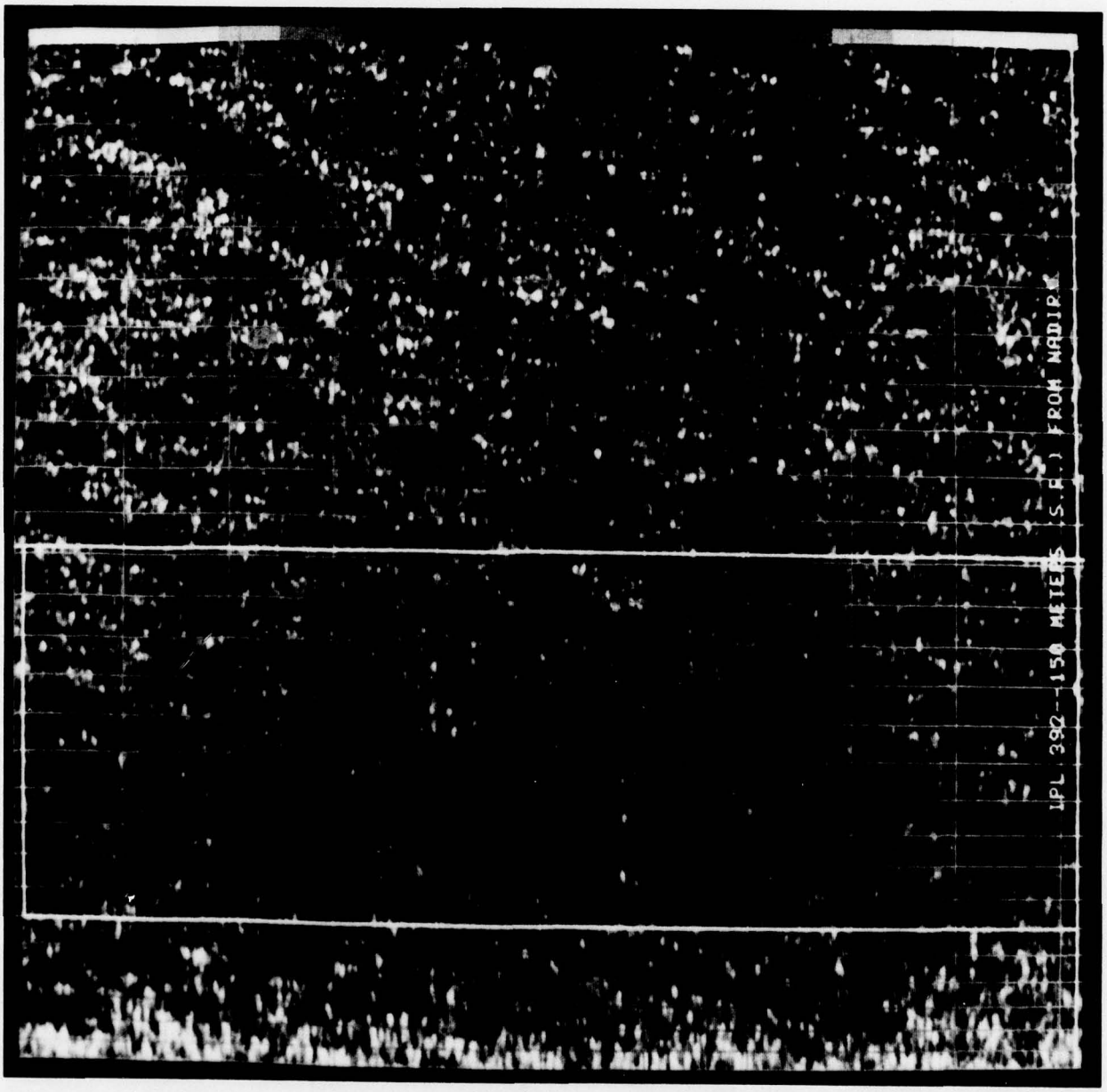

FIGURE 17. Slant Range Presentation of SAR Ocean Wave Imagery

This particular section was selected because of its proximity to nadir: severe bending of the 45° waves is noted. Figure 18 is the ground range version of the outlined region of Figure 17, the geometric distortion introduced by the slant range presentation has been removed, and the waves now assume their proper orientation. It should be emphasized that relative to their respective coordinate systems, both slant range data and ground range data are sampled every 1.5 m; from earlier remarks we know that this sampling rate is adequate for the converted data. The number of samples generated in ground range for a given outlined region in slant range thus depends solely on how close to nadir we request a conversion be made; we need not, for example, rely on an engineering judgement that twice as many ground range samples as slant range samples are needed.

The "smeared" nature of the range dimension of Figure 18 is to be expected. Since the signal is originally digitized in slant range to 3 m resolution, the stretching encountered in the coordinate system change forces ground range resolution to be worse than 3 m. For regions near to nadir, the resolution gets very poor indeed.

An idea of the severity of the slant range distortion can be obtained from Figures 19 and 20. Fourier transforms of the outlined region of Figure 17 and of Figure 18 were computed, and are displayed in Figures 19 and 20, respectively. Note that in these displays the range frequency dimension is the vertical dimension. The faulty slant range geometry has two effects. First, a compression of the waves will always occur, and will be significant near nadir. This introduces an abnormally high range frequency component in the spectrum. Second, the compression effect is monotonically decreasing with increasing slant range, so that a transform of a large patch of data will belie the presence of a frequency-modulated wave component. This would appear in the spectrum as a smearing of the transform in the vicinity of the abnormally high range frequency component mentioned above. The selected patch is too small for this effect to be noticeable.

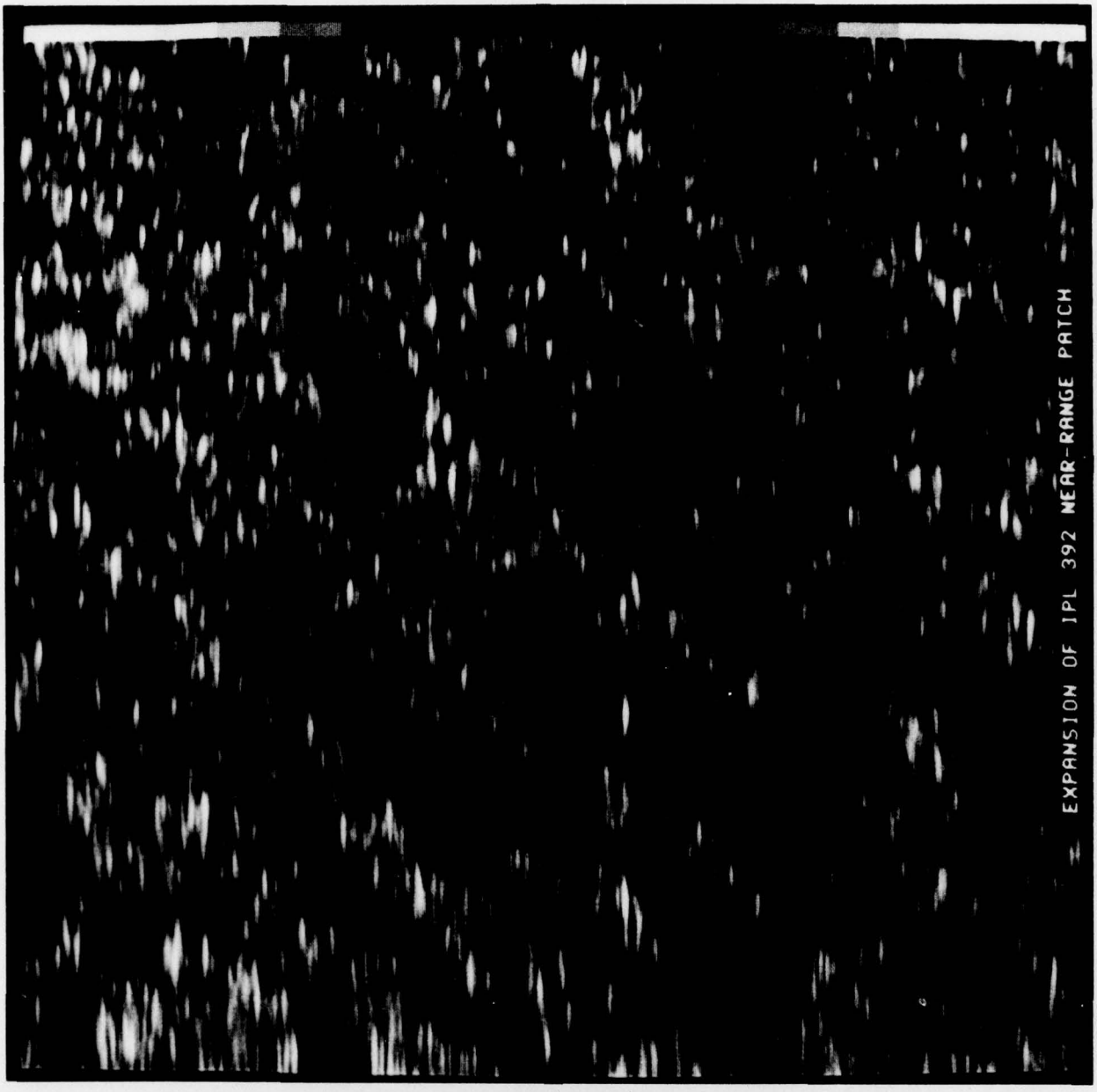

FIGURE 18. Ground Range Equivalent of Outlined Region of Figure 17

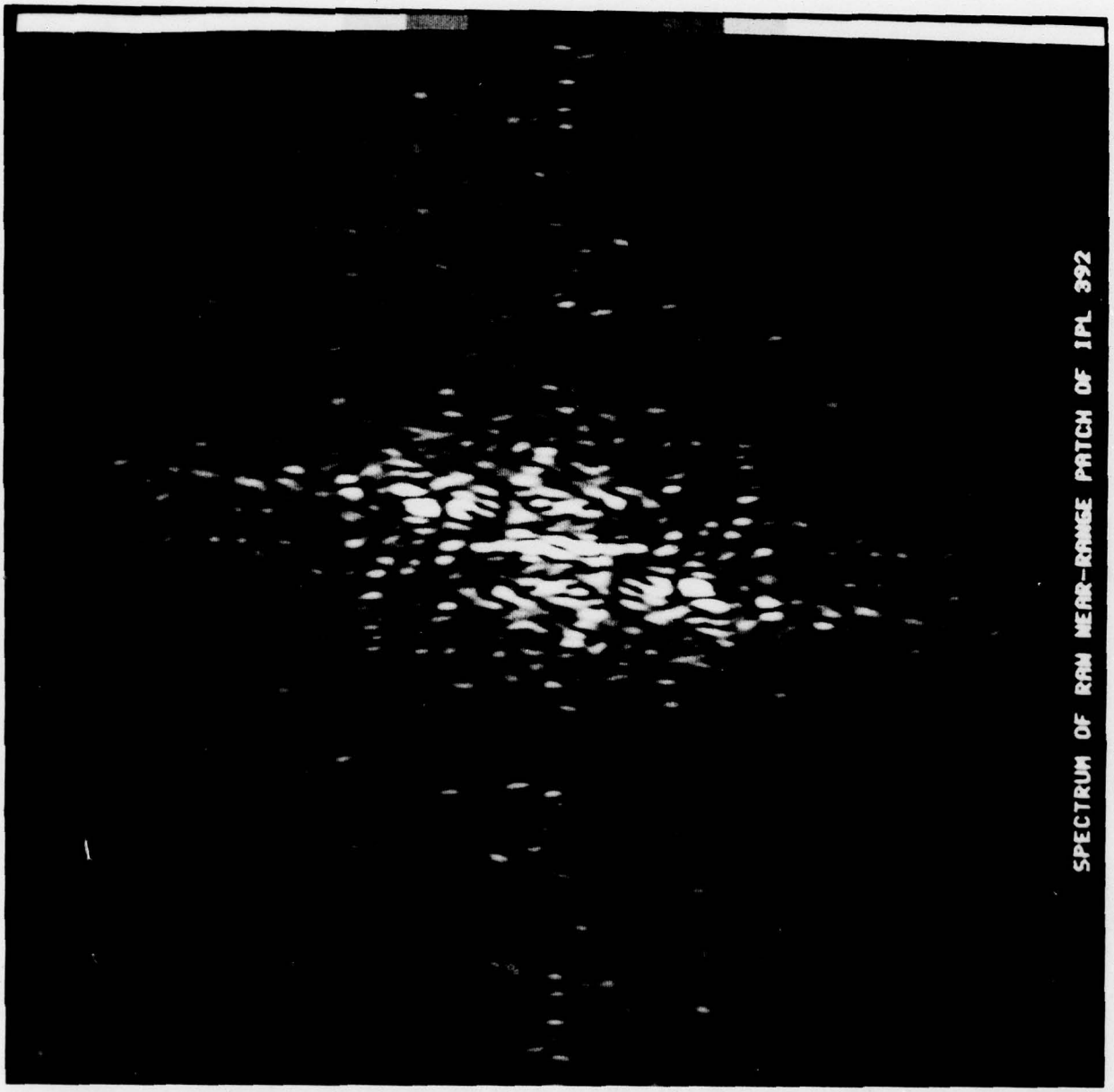

FIGURE 19. Spectrum of Outlined Region of Figure 17

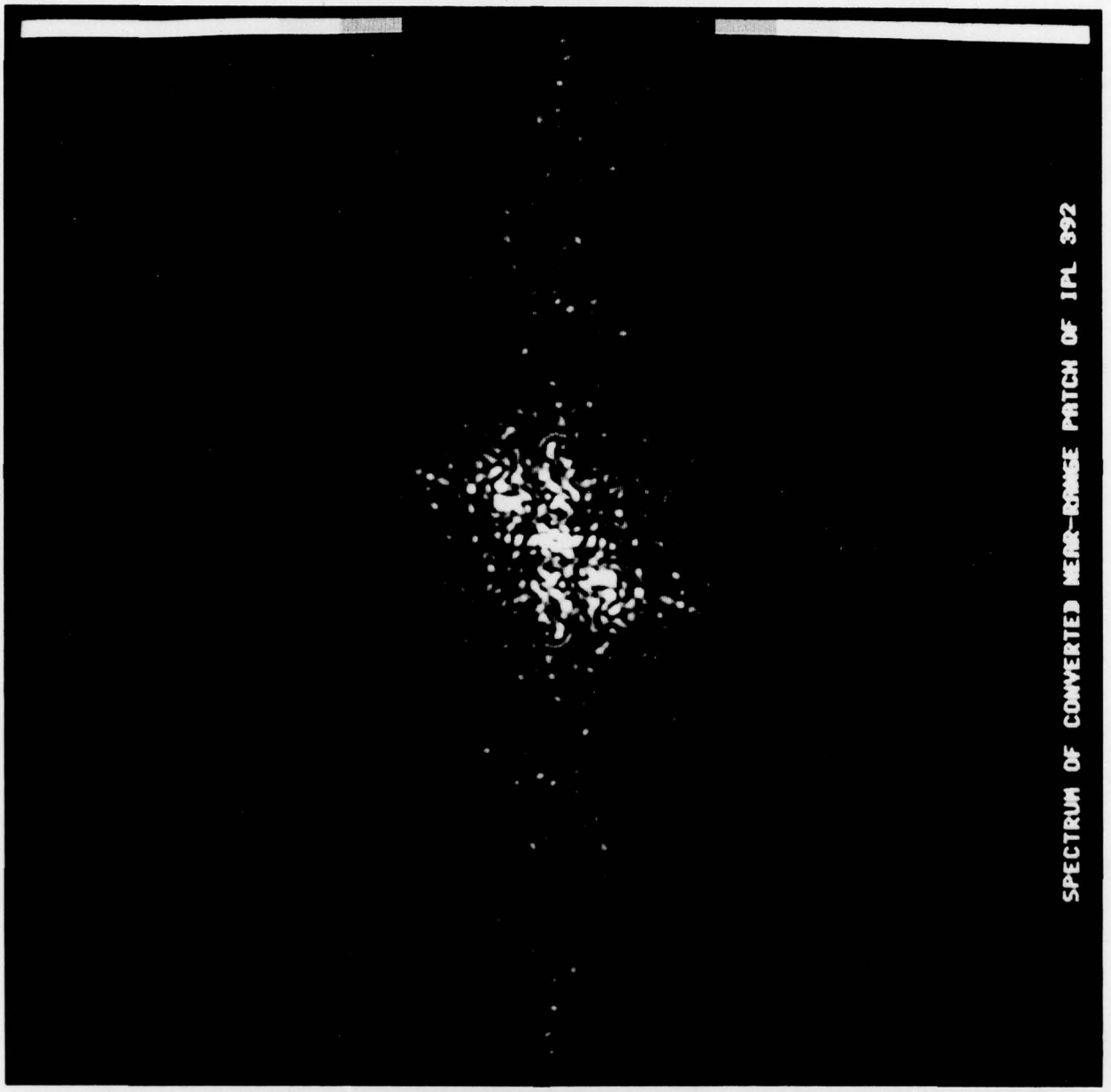

FIGURE 20. Spectrum of Figure 18

6.4 SUMMARY

If SAR is to be a useful tool for imaging ocean waves, the recording procedure should not be allowed to hinder detection of the wave components. In the slant range presentation, the geometry is so non-uniform that comparison of spectra generated from several different regions of the imagery will be difficult or impossible. If, however, the data is first converted to ground range, then a single geometry applies to all regions, and comparison of their spectra will be meaningful. An additional benefit of the conversion is that oceanographers untrained in SAR imagery can visually interpret the ocean imagery without having constantly to mentally correct for the SAR-induced distortion.

7
OPTICAL FOURIER TRANSFORM OPERATIONS TO ANALYZE WAVE CHARACTERISTICS

7.1 INTRODUCTION

The purpose of this particular investigation was to provide a basis for the automatic analysis of wave parameters as an auxiliary output of the SAR optical processor, and to provide a model for a simple optical setup so that the individual scientist can selectively analyze portions of SAR imagery.

Currently, the processing of SAR imagery is primarily an optical and photographic operation. Although digital techniques are more versatile, repeatable, and noise-free than optical techniques, for at least the near future they lack the capability of processing large amounts of SAR data in near real time. Monitoring large areas of ocean, as contemplated by SEASAT, requires an optical approach, or a large digital computer.

Anticipating the necessity of optically processing SEASAT SAR data, we investigated means of optically extracting wave information. The methods that appear to hold the most promise are based on the two-dimensional Fourier transform. Wave parameters which can be inferred from the Fourier transform are wavelength, wave direction, and spatial uniformity (how straight the wavefronts, amount of refraction, number of wave directions, continuity of wavefronts)[17,18]. The optical two-dimensional transform is simply achieved by Fraunhofer diffraction.

---

17. L. J. Cutrona, E. N. Leith, and L. J. Porcello, "Filter Operations Using Coherent Optics", Proceedings of the National Electronics Conference, Volume X, 1959.

18. P. L. Jackson, "Diffractive Processing of Geophysical Data", Applied Optics, Vol. 4, No. 4, April 1965.

Optical experiments included both the direct imaging of the Fourier transform and spatial filtering in the Fourier transform plane while imaging ocean wave patterns.

Results indicate the following: (1) the two-dimensional transform contains information in a form which has the potential for automatic computation, (2) a variety of apodisations (spatial weighting functions) and opaque stop filters can be employed, (3) a very simple optical system can be used, (4) slant-range distortion diffuses energy concentrations (hence, accuracy of wave data) in the Fourier transform plane, and (5) directional filtering operations do not appear to be practicable for ocean wave analysis.

7.2 BACKGROUND

As is well known, a two-dimensional Fourier transform can be obtained with a simple Fraunhofer diffraction setup. As shown in Figure 21, the wave imagery in the form of a variable-density film is placed in a plane wave of monochromatic light. The diffraction patterns formed at the focal plane of the lens are produced by the spatial distribution of the optical transmission of the film. This diffraction pattern is the two-dimensional Fourier transform of the data on the film, and as such, represents information about the wave characteristics recorded on the film.

Figure 22 is a modified form of Figure 21. Here, a diverging wavefront impinges on the film, and a modified Fourier transform is formed at the focal plane on which the pinhole is imaged. The effect of the modification on the accuracy of the Fourier transform is negligible, and for wave analysis purposes can be considered a true Fourier transform. Note that the setup in Figure 22 requires only half the optics of the setup in Figure 21, and that degradation due to lens reflections, noise, and distortions are halved. Note also that the Fourier transform scale can be altered by judicious placement of the lens between the pinhole

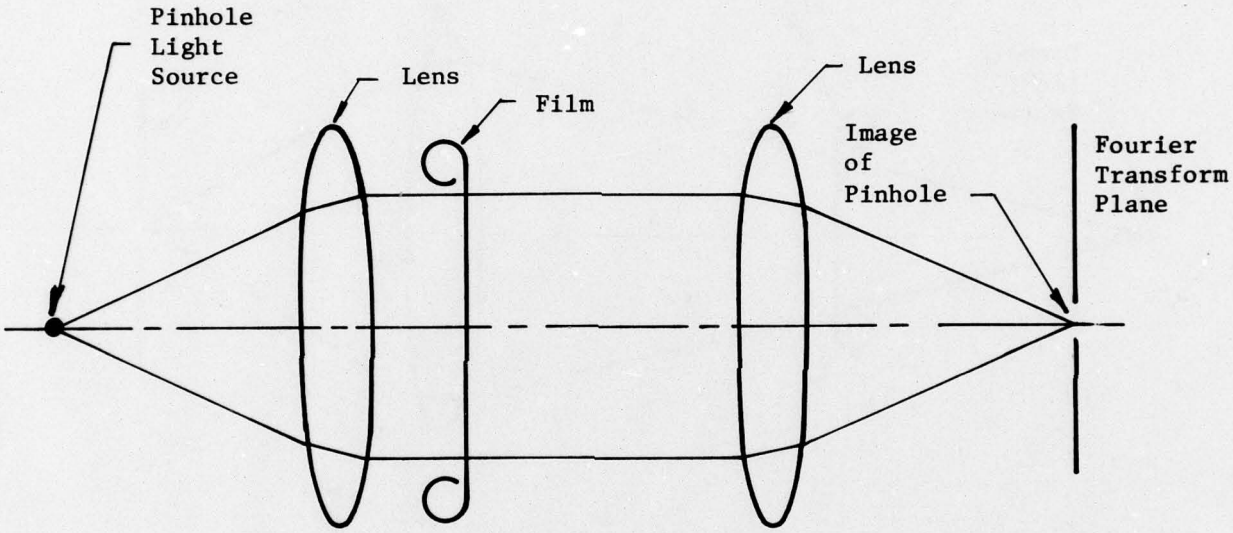

FIGURE 21. Fraunhofer Diffraction Setup to Obtain Two-Dimensional Fourier Transform of Photographic Image. Film Placed in Plane Wave of Monochromatic Light.

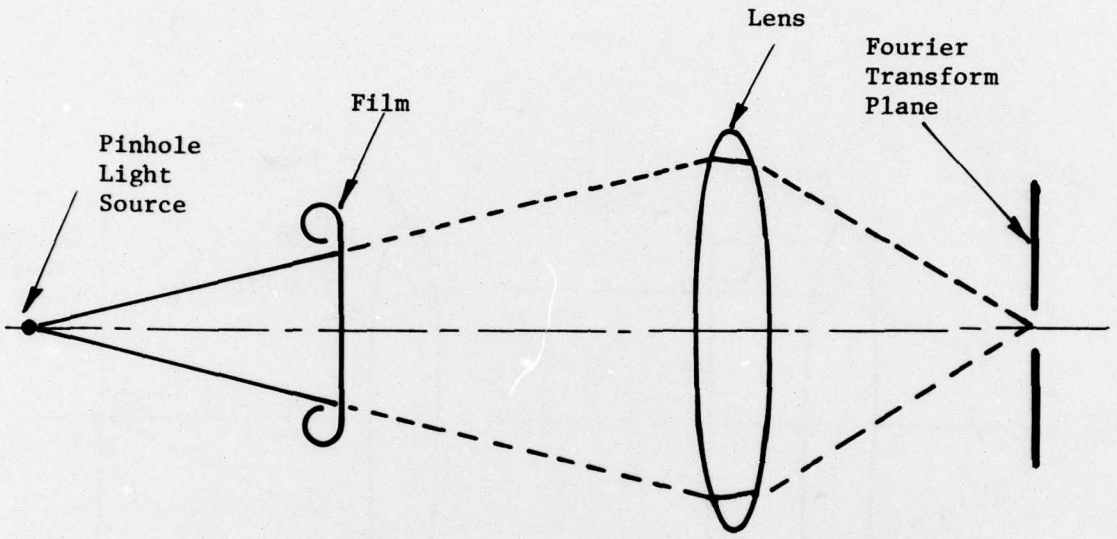

FIGURE 22. Fraunhofer Diffraction Setup to Obtain Two-Dimensional Fourier Transform of Photographic Image. Film Placed in a Diverging Beam of Monochromatic Light. One lens Only Required (Compare with Figure 21)

and its image. This scale alteration is not possible with the plane-wave setup in Figure 21.

The setup in Figure 22 is emphasized here not only because of its superiority for this purpose, but because the more costly, more noisy, and less flexible setup of Figure 21 is often employed, probably because this type of optical operation is described in the literature almost universally with this diagram.

The Fraunhofer diffraction setup and its relationship to the Fourier transform is described elsewhere [17, 18] and has been used for ocean wave analysis [19].

The distribution of light in the Fourier transform plane is principally governed by two of the ocean wave characteristics: the orientation of the wavefronts, and the spatial frequency of the waves. Position within the image does not affect the energy distribution in the transform plane. Translation without rotation of the image leaves the transform plane unchanged.

As illustrated in Figure 23, the diffracted distance of the light energy from the origin is inversely proportional to the wavelength (therefore, directly proportional to the frequency) and the orientation of the energy in the transform is identical to that of the wave propagation of the image. The optical Fourier transform is, then, a concise indicator of the frequency and direction of a SAR image of ocean waves. Also note that the distribution of energy in the transform is an indication of the spatial uniformity of the waves. If the energy is diffused over a relatively large area in the transform plane, one can infer that the waves are diffracted, broken up, have different components, etc.

---

19. W. L. Brown, F. C. Polcyn, A. N. Sellman, and S. R. Stewart, "Water-Depth Measurements by Wave Refraction and Multispectral Techniques," Report No. 31650-31-T, Willow Run Laboratories, Ann Arbor, Michigan, August 1971.

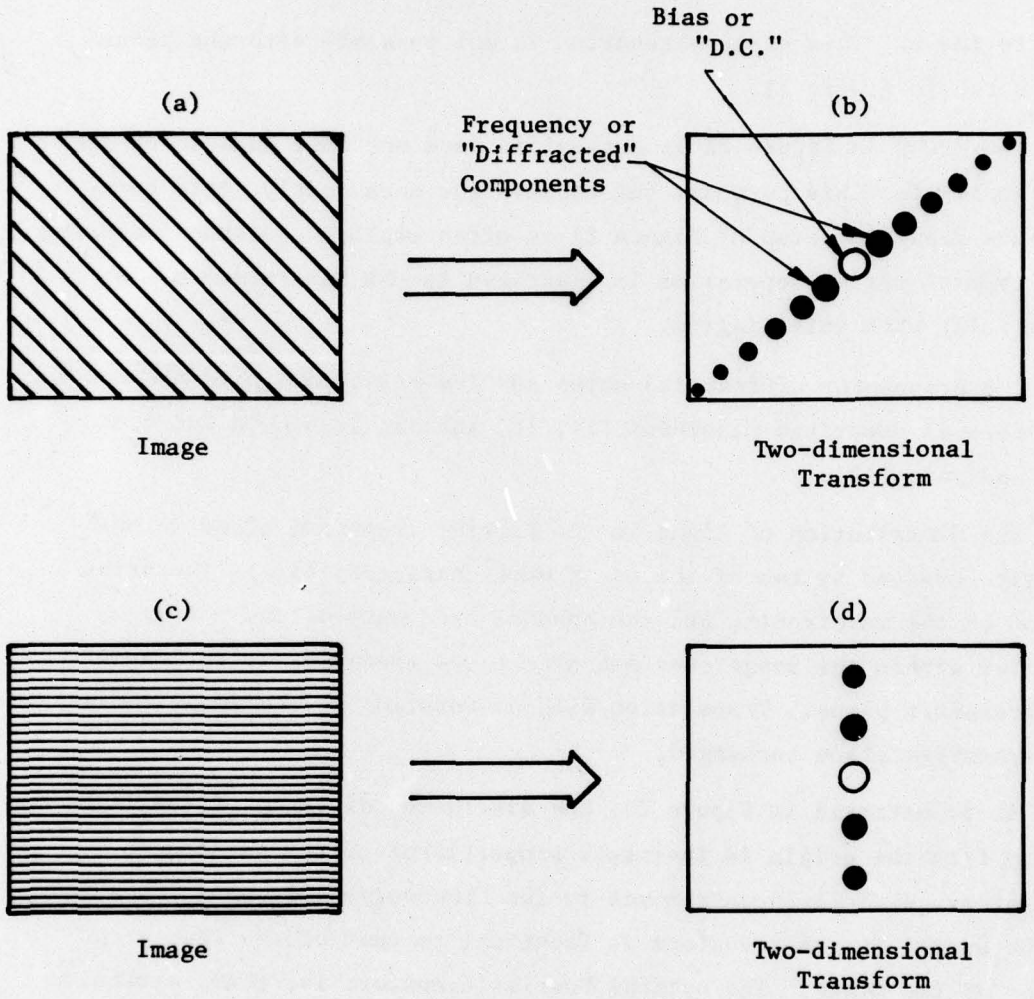

FIGURE 23. Diagrams of Linear Images and Corresponding Two-Dimensional Fourier Transforms. Note that the distribution in the two-dimensional Fourier transform is governed by the frequency and orientation of the spatial distribution of the images. Spacings of components in (b) and (d) are inversely proportional to spacings of lines in the images (a) and (c). The sizes of the dots indicate the amount of energy in the diffracted orders--smaller dots, smaller amount of energy.

If the energy is diffused throughout most of the transform plane, the choppiness or noise might indicate that the sea-state is randomly perturbed--useful information in itself.

The latter indication of diffused energy is caused by the conventional processing of SAR data--a slant range representation of a ground-range phenomenon. Linear wavefronts will be represented in slant range as curved wavefronts, the curvature of which is an inverse function of the slant range. The near range will have a more pronounced curve than the far range. Taken to the extreme--the nadir of the aircraft or spacecraft--wavefronts oblique to the flightline will collapse at the nadir and appear parallel to the flightline (Figure 24).

If a ground-range representation were available, this artificial dispersal of energy in the transform plane could be eliminated, giving a more accurate representation of the actual sea-state. (This applies both to optical and digital representations.)

In addition to obtaining information about waves in the Fourier transform plane, the waves can be imaged through this plane as shown in Figure 25. Filtering can be performed by obstructing or attenuating portions of the Fourier transform. This filtering can be perceived by the fact that the image is a subsequent Fourier transform of the first Fourier transform. The operation is equivalent to taking a digital Fourier transform of data, altering the Fourier transform, and then taking its inverse to obtain a modified version of the data--a commonplace method of digital filtering.

The filtering of interest in ocean wave analysis can be understood by referring to Figure 23. Note that the orientation of the diffracted energy is perpendicular to the lines representing wavefronts, hence is in the direction of ocean wave propagation. A straight line through the origin of the Fourier transform describes the wave directions. A wedge-shaped stop placed in the Fourier transform plane will act as a

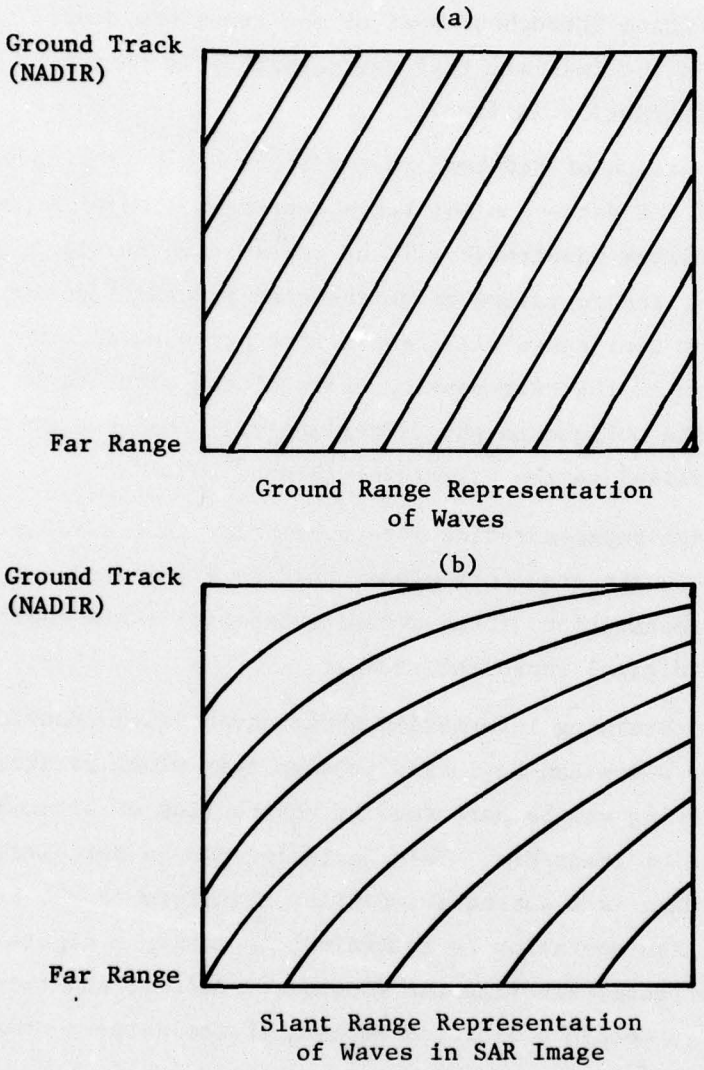

FIGURE 24. Diagram of "Cylindrical" Distortion. Slant range distortion of linear waves oblique to flight path. Each wave asymptotically approaches ground track. (b) appears as if (a) is wrapped around a cylinder. Note that the curvature in (b) will cause radial diffusion of energy in the two-dimensional transform plane, leading to confusion in determining wave direction.

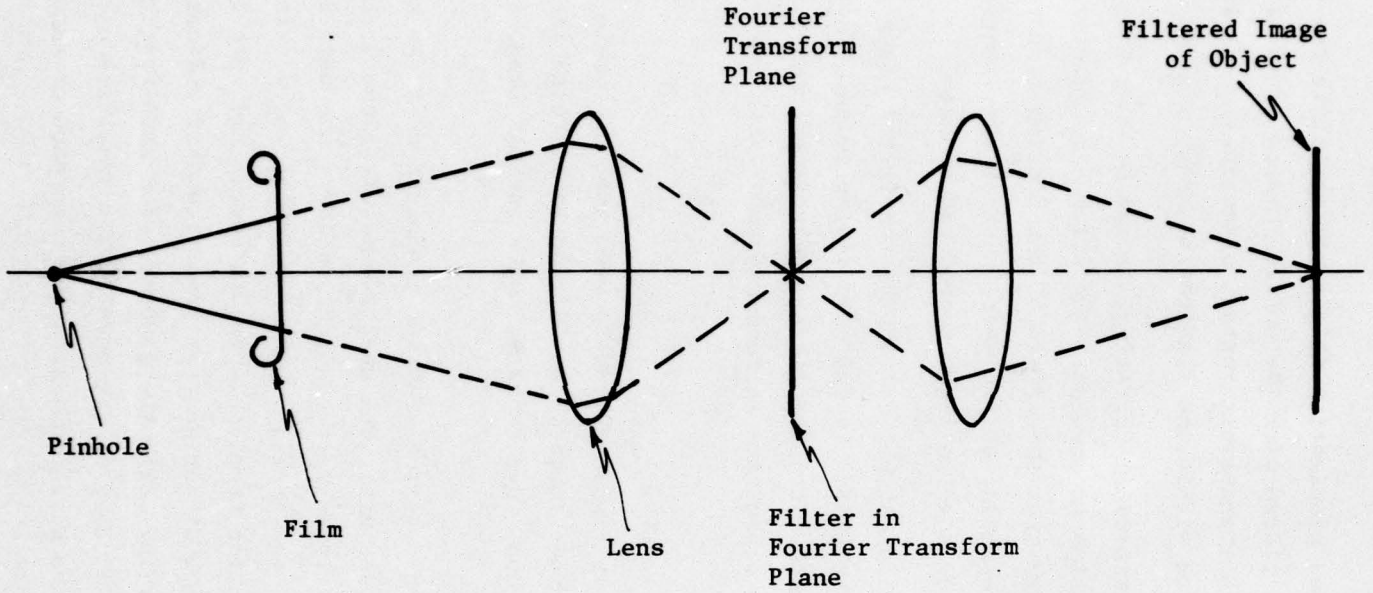

FIGURE 25. Setup for Filtering in the Fourier Transform Plane.

filter to remove the waves propagating in directions within the wedge. Conversely, if a stop is placed over the entire Fourier transform plane, except for a wedge-shaped transparent region, essentially only the waves propagating in a direction within the transparent wedge will be imaged.

For this type of directional filtering, it can be seen that only the direction of diffraction is crucial. The filter is indifferent to the distance of the energy from the origin of the Fourier transform plane, and therefore independent of the wavelength of the light which is diffracted. Therefore, a white light source can be used.

Because the diffraction of white light by the filter edges is smeared, the effect of the filter is softened in the image. This is an advantage over using monochromatic light, where interference fringes occur in the image and extreme care is required for filter placement.

7.3 EXPERIMENTS

The optical setups in Figure 22 and 25 were used to obtain diffraction patterns of wave imagery in addition to filtered images of a radial reference function, wave imagery, and a LANDSAT image for comparison.

Figure 26 is a two-dimensional Fourier transform of a SAR wave image in a rectangular aperture. The energy concentrations in the upper right quadrant and lower left quadrant indicate the wave direction, frequency, and deviation or "spread". The horizontal and vertical bright lines are diffraction from the aperture edges, and zero frequency is at their crossing. The direction from zero frequency indicates the direction of the wave train, while the distance from zero frequency indicates the spatial frequency of the waves. The spreading of the diffracted energy from the waves indicates the coherence or regularity of the wave train.

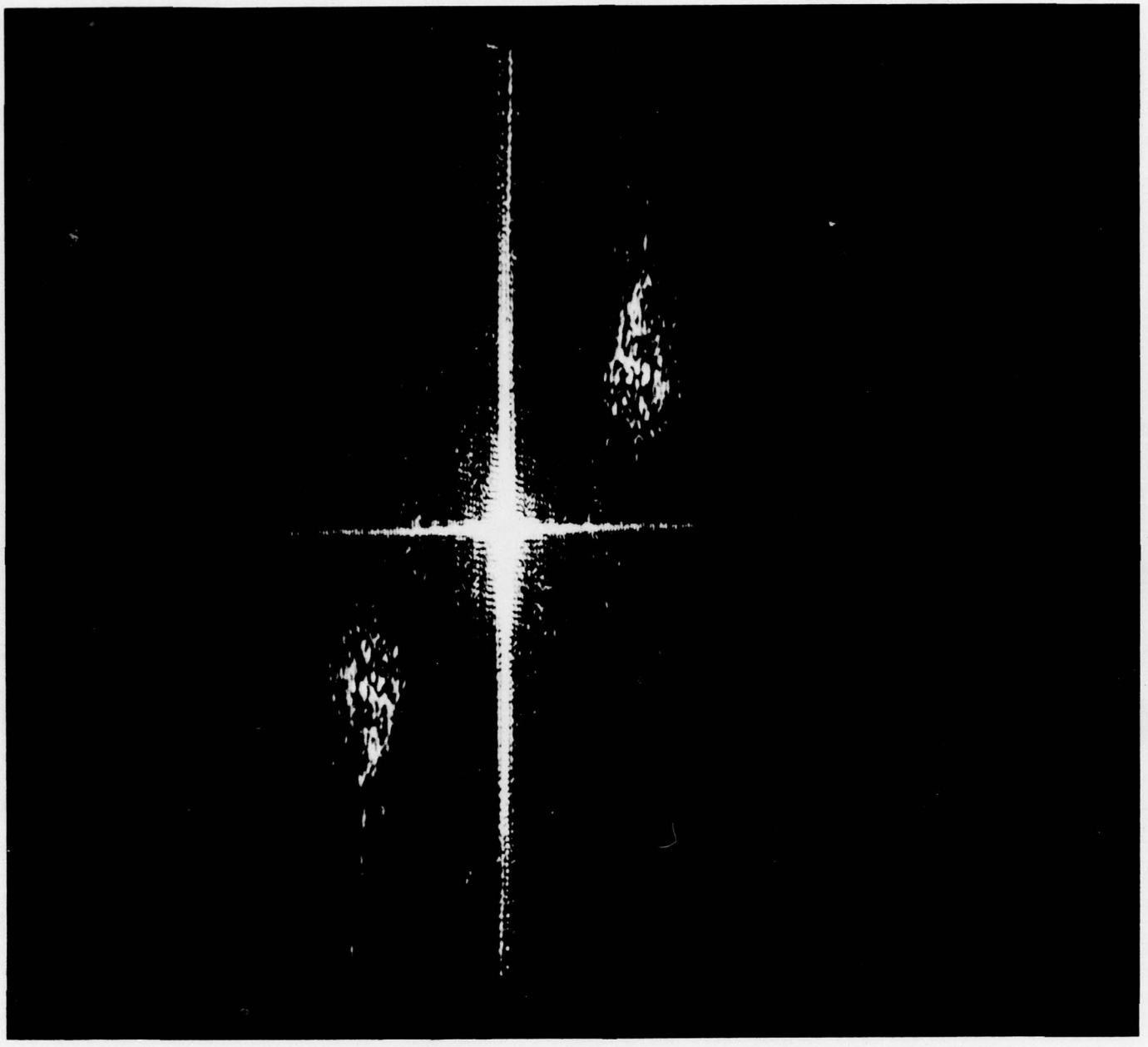

FIGURE 26. Two-dimensional Fourier Transform of a SAR Wave Image in a Rectangular Aperture. Bright Horizontal and Vertical Lines Are Caused By Diffraction from the Aperture Edges

Straight waves of one spatial frequency will cause the diffracted energy to be highly concentrated, while refracted waves will cause the diffracted energy to be dispersed. The distribution of the diffracted energy is therefore diagnostic of the nature of the ocean waves.

The transform shown in Figure 26 was obtained from slant-range imagery and is therefore distorted and diffused in comparison with that which would be obtainable from ground-range imagery.

Figure 27 is a two-dimensional Fourier transform of a wave train with the rectangular aperture diffraction blocked out with opaque strips ("stops").

Blocking out the undiffracted light and the aperture effect enable one to better view the output in a scanning mode. Little change is seen in a photograph because of saturation of the film. However, when the output is viewed directly in a scanning mode, relatively high intensity light overpowers the pertinent wave information.

Figure 28 shows a two-dimensional Fourier transform of a wave train with a truncated circular aperture of the same wave train as shown in Figure 26. The circular aperture produces circular diffraction patterns. The straight edge truncation of the circular aperture produces the vertical line.

SAR ocean wave patterns and a directional reference function of radial lines at 1° angular intervals, both imaged with no filter in the optical system, are shown in Figure 29.

Note the difference in frequency between the bottom (near range) and top (far range) of the SAR image. This difference is caused by slant range distortion. Note also the high frequency wave components aligned about 70° azimuth, and the low frequency components at about 345° azimuth.

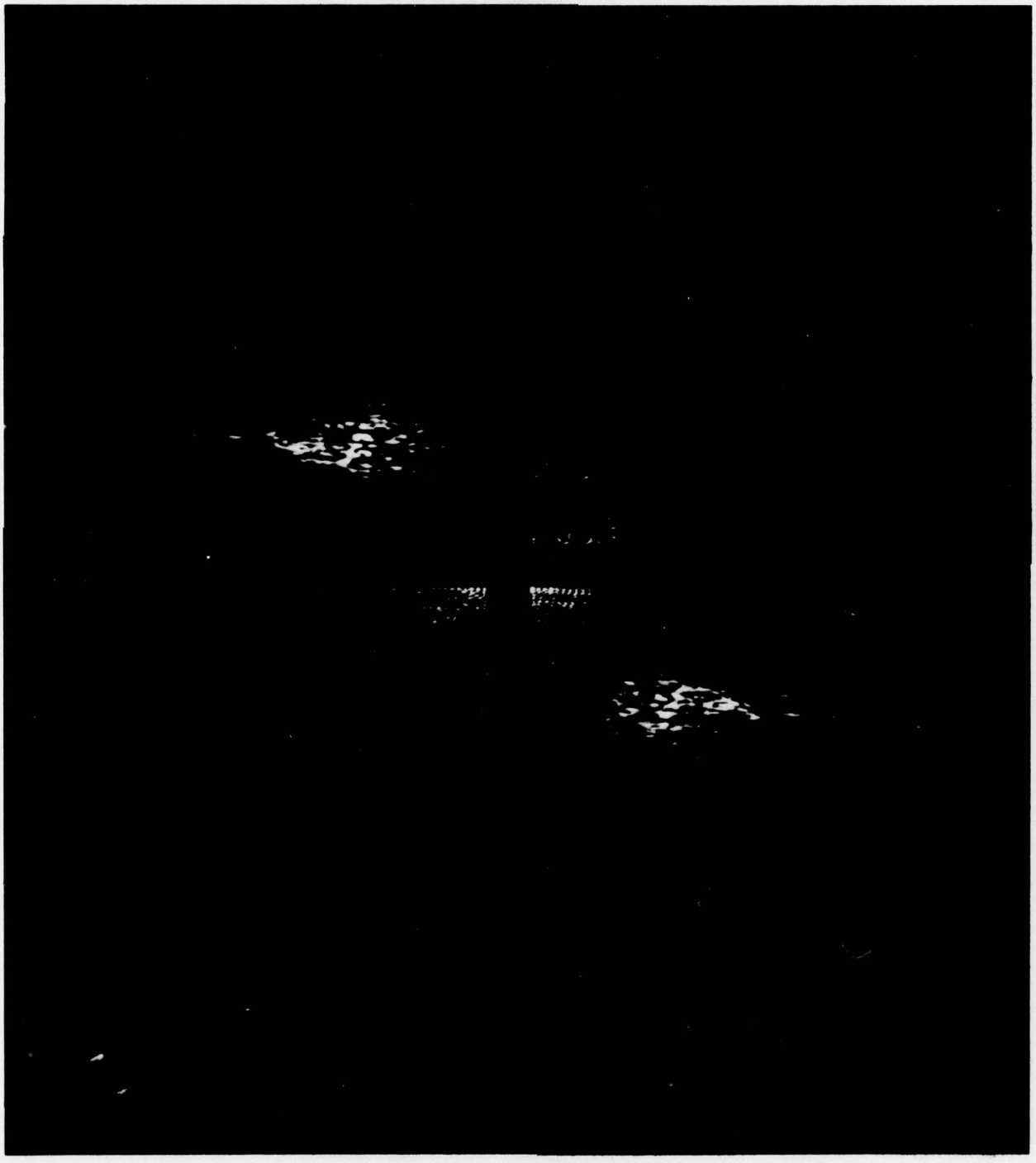

FIGURE 27. Two-dimensional Fourier Transform of a SAR Wave Image with Diffraction From Aperture Blocked Out

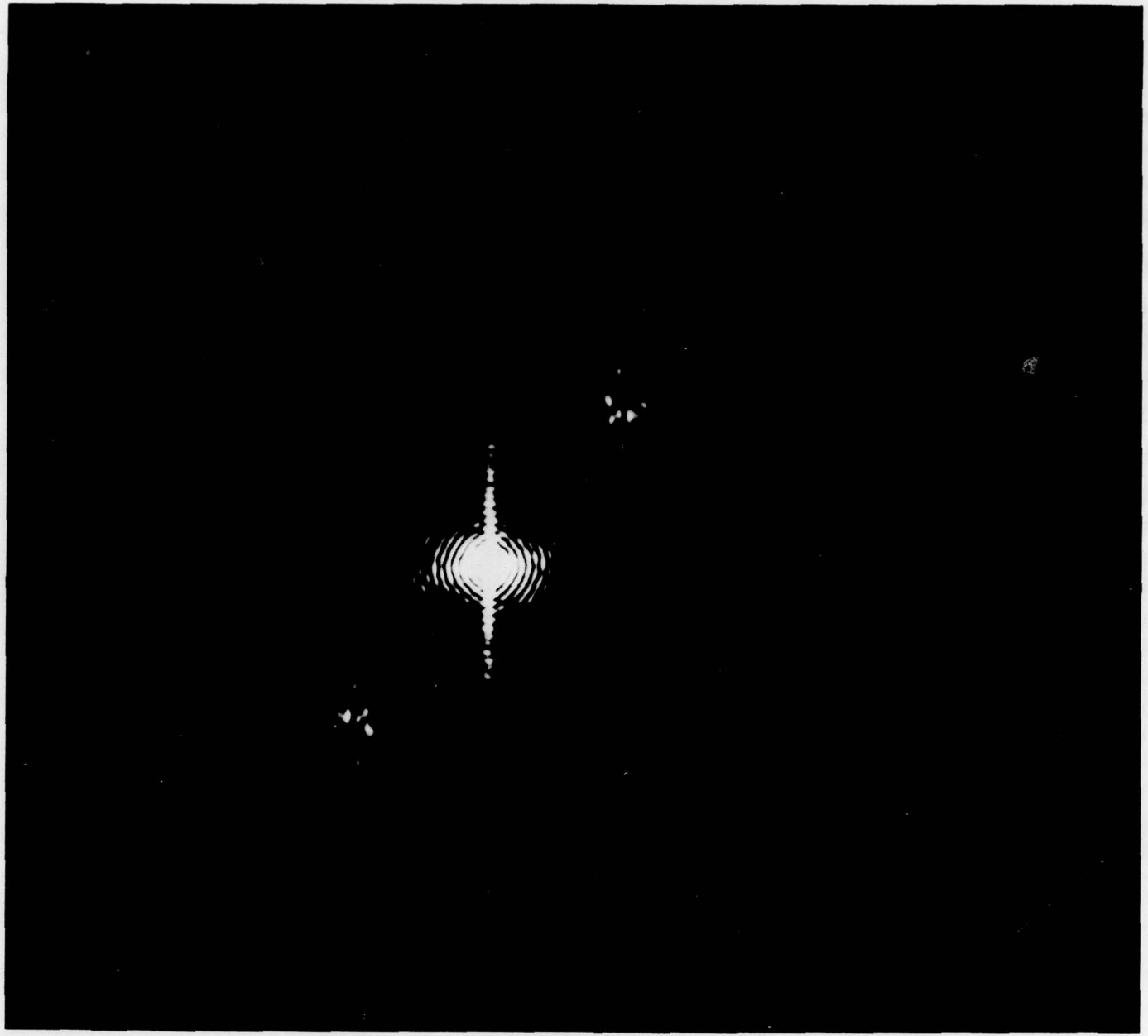

FIGURE 28. Two-dimensional Fourier Transform of a SAR Wave Image With a Truncated Circular Aperture. The Straight Edge Truncation of the Circular Aperture Produces the Vertical Line.

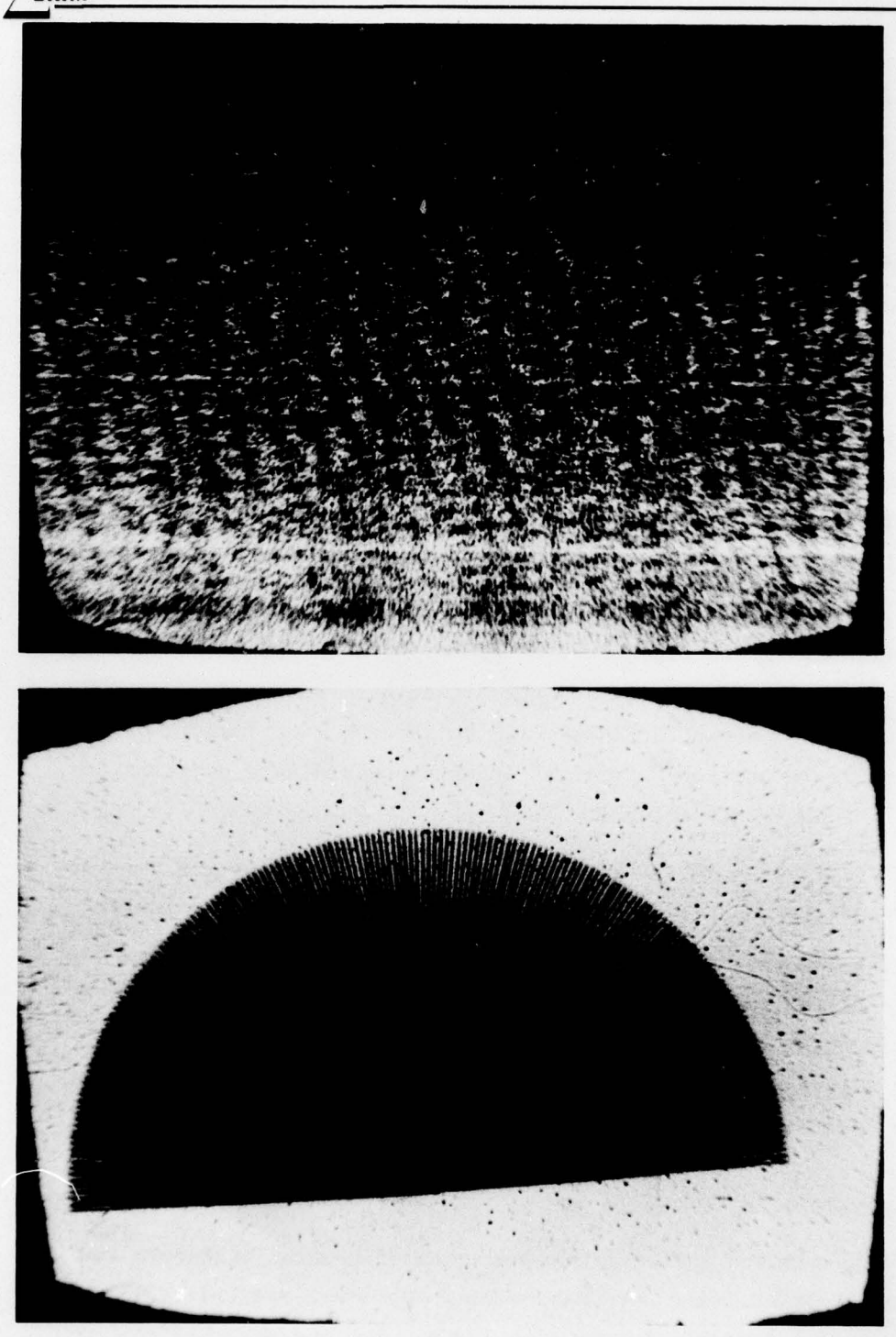

FIGURE 29. SAR Ocean Waves and a Directional Reference Function Both Imaged With No Filter in the Optical System. Lines in Reference Function are Angularly Spaced at 1° Intervals

Figure 30 shows the same SAR wave image as Figure 29, directionally filtered with a center at 60° azimuth. Reference pattern shows width of filter by number of angularly spaced lines which are imaged. Only those lines within the angular width of the filter are imaged. As the lines are at 1° intervals, the number of imaged lines indicate the angular width of the filter.

This picture illustrates a problem in directional filtering of ocean waves. Low frequency components at about 15° azimuth are imaged because the higher frequency components are acting as "carriers". The high frequency components are a series of short waves (in length) which are repetitively truncated by the lower frequency waves. These truncations outline the lower frequency waves. Thus, the lower frequency waves are outlined as "ends" of the higher frequency waves.

To illustrate the dependence of filtering upon the characteristics of the image, a LANDSAT image and the directional reference function were filtered, as shown in Figure 31. Unlike the wave imagery of Figure 29, there are few "carriers" in which subordinate patterns are the basis of dominant patterns.

Figure 31 shows the unfiltered images of the LANDSAT and reference function, while Figure 32 shows the images filtered at 60° azimuth.

Unlike the wave imagery, most of the linears shown are aligned closely with the filter, even though there are a few low frequency trends which are not aligned. This filtered LANDSAT image contrasts with the filtered image of waves shown in Figure 25, which exhibited pervasive patterns "carried" by other patterns.

7.4 DISCUSSION

The experiments indicate that the optical Fourier transform can be useful in determining wave parameters. However, optical filtering does not appear suitable for wave analysis. The character of the wave

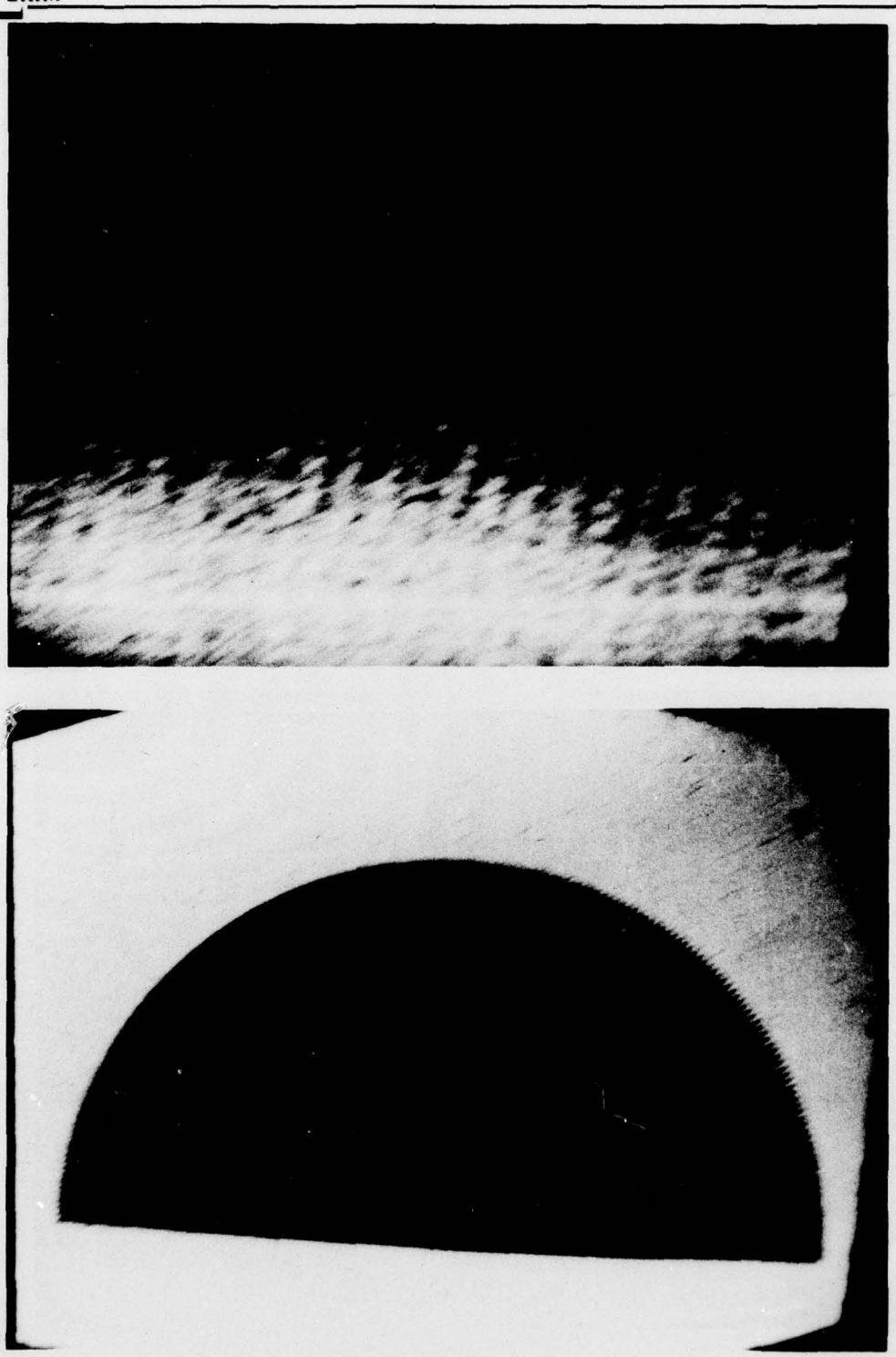

FIGURE 30. SAR Ocean Waves of Figure 29 Directionally Filtered With a Center at 60° Azimuth. Reference Pattern Indicates Angular Width of Filter by Number of 1° Lines Which Are Imaged

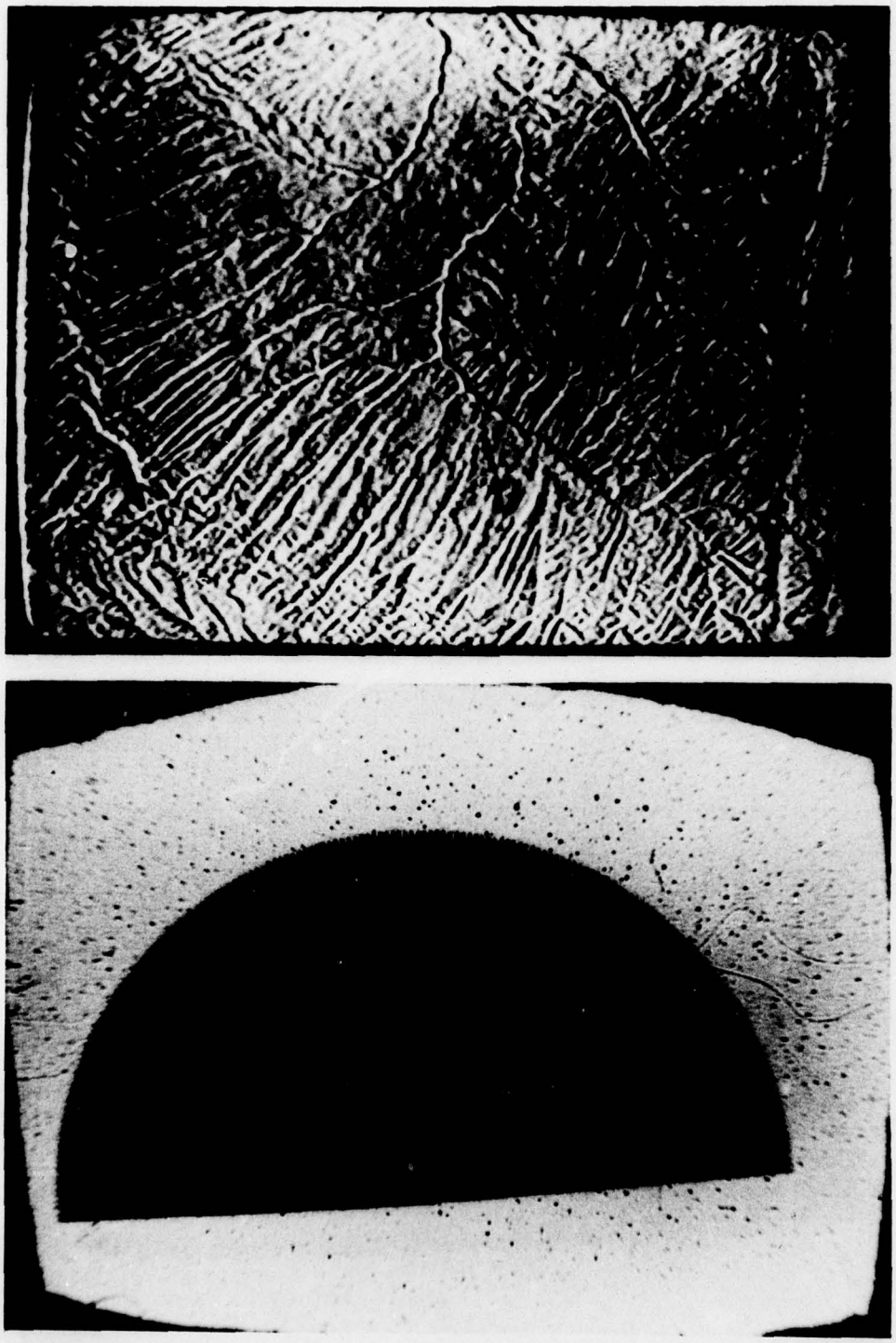

FIGURE 31. LANDSAT Imagery and Directional Reference Function Both Imaged With No Filter in the Optical System

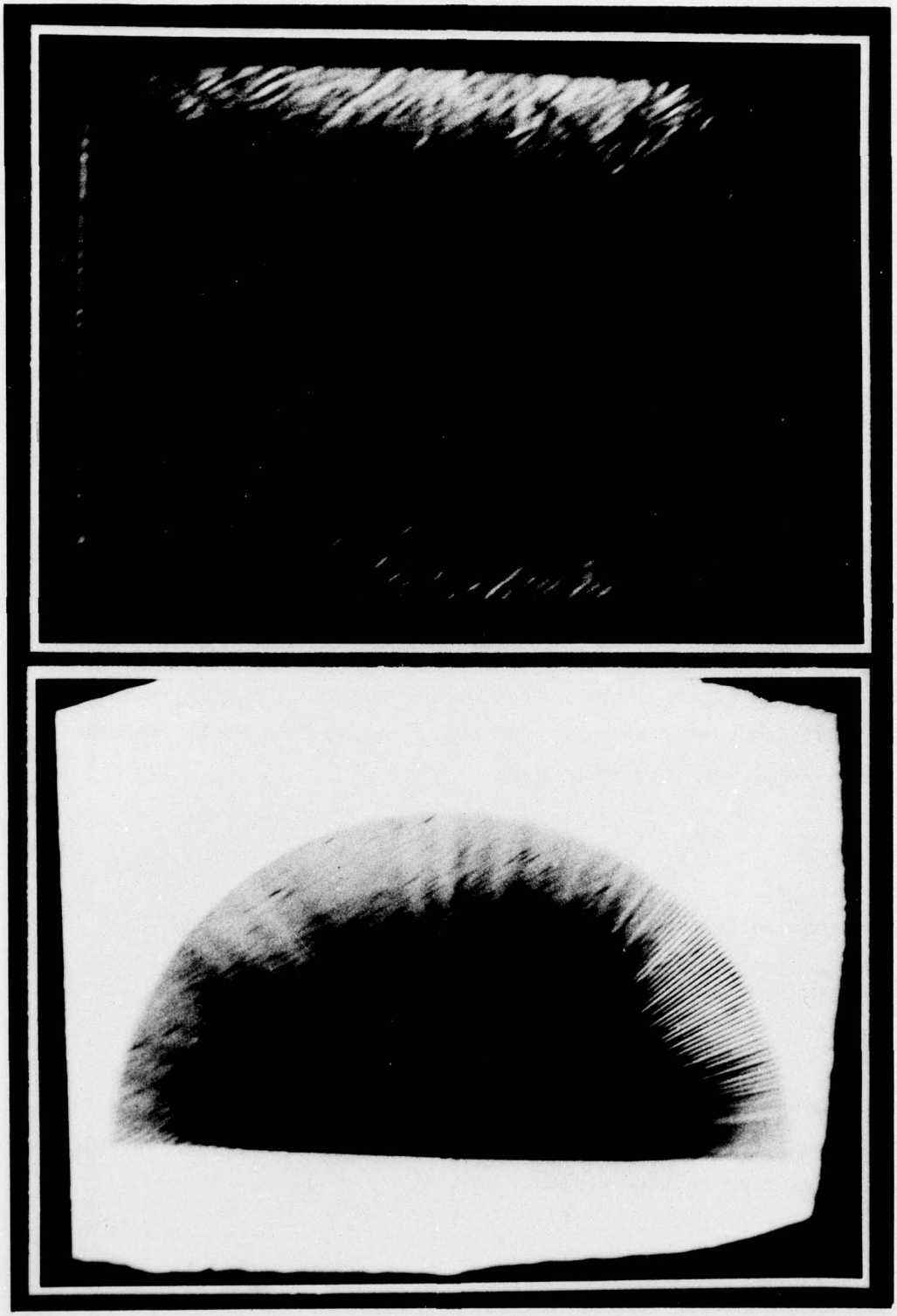

FIGURE 32. LANDSAT Imagery and Directional Reference Function Imaged With Filter Centered at 60° Azimuth

images which were filtered was such that the discontinuities of the wavefronts showed up as enhanced directions. In addition, the filtered image, unlike the Fourier transforms, is not in a form which can be automatically analyzed.

The Fourier transform could be automatically analyzed in the following way:

The optical system for obtaining a two-dimensional transform requires only one lens. A Fraunhofer diffraction system (or modified system) automatically produces a Fourier transform at the plane where the lens images a "point" source such as a pin hole. Figure 22 illustrates a modified Fourier transform setup which could be used for automatic wave parameter determination in the following way.

Transport a transparency of the SAR imagery through the object plane. In the Fourier transform plane, provide a matrix of photo detectors or some type of two-dimensional light-position detector. With suitable integration time, the output of the photocell matrix, with (x, y) coordinates, will then be available. An on-line small computer will provide the wave frequency F_w as

$$F_w = (x^2 + y^2)^{1/2} \tag{36}$$

where x is the horizontal matrix index of the smoothed maximum,
y is the vertical, and the wave direction θ as

$$\theta = \arctan (y/x) \tag{37}$$

The clustering and pattern of energy around x and y could be performed quantitatively in a number of statistical ways, thus giving the wave parameters in some detail.

The operation can also be performed digitally by the fast Fourier transform and the same output obtained. As stated before, the optical versus digital aspect of this problem is worthy of some detailed investigation.

As discussed elsewhere in this report, the objective is to detect wave parameters directly at the output of the optical processor, and a mechanism is described which has this potential. SEASAT, now projected to use optical processing, could then produce near-real time information on wave parameters if the above system were operational. The optical system would require slant-to-ground corrected data.

APPENDIX A

LITERATURE SEARCH PERTAINING TO SYNTHETIC APERTURE RADAR IMAGING OF THE OCEANS

The following print-outs were generated as the result of an on-line search run 12 September 1977 (to update September 1976 search) through Lockheed's DIALOG system. The system allows a researcher to query a bibliographic data base in an interactive mode, and retrieve a set of pertinent citations on a particular subject.

Boolean operators (and, or, not) are used to combine terms and form sets. The following key words were used to construct the search:

remote sensing
remote sensors
remote sensor
radar
ocean wave
ocean waves

Using a Venn diagram, the search can be expressed as:

Remote Sensing or Radar Concepts — Ocean Wave Concepts

with the shaded area representing the desired citations.

A free language approach was taken in order to achieve broad coverage of the literature (i.e., the search did not depend solely on standard indexing terminology).

The data bases searched were: NTIS, COMPENDEX (Engineering Index), and Oceanic Abstracts. The NTIS search, covering government report literature, generated 182 citations which were too many to reprint here, though the results are available by contacting: ERIM Information Center, P. O. Box 8618, Ann Arbor, Michigan 48107, ATTN: E. Turner. An example of a typical NTIS citation follows the DIALOG print-outs.

Permission to reprint the COMPENDEX citations was received from:

Engineering Index, Inc.
Marketing Division
345 East 47th Street
New York, NY 10017
--Mr. John Veyette

Permission to reprint the Oceanic Abstracts citations was received from:

Oceanic Abstracts
A Division of Data Courier, Inc.
620 S. Fifth St.
Louisville, KY 40202
--Ms. Leone Trubkin

The top line of each page of print-out will indicate which of the two data bases the citations come from.

ID NO.- EI770860020 760020
NOTE ON SAR IMAGERY OF THE OCEAN.
Larson, T. R.; Moskowitz, L. I.; Wright, J. W.
Nav Res Lab, Washington, DC
IEEE Trans Antennas Propag v AP-24 n 3 May 1976 p 393-394 CODEN: IETPAK
DESCRIPTORS: (*RADAR, *Imaging Techniques), OCEANOGRAPHY,
CARD ALERT: 716, 471
Synthetic aperture radar (SAR) image formation of the ocean surface including the Gulf Stream Boundary, is discussed. It is pointed out that images in addition to those due to modulation of surface scatterer strength may result from organized scatterer motions such as those due to currents or wave orbital velocities. The modulation of scattering cross section by large waves is expected to depend on the magnitude and direction of the wind, making the relationship between image strengths and wave amplitudes rather complicated. It is suggested that the effect of wave orbital accelerations upon azimuthal focus might provide a more direct measure of wave amplitude. 5 refs.

ID NO.- EI770750807 750807
PHASE AND DOPPLER ERRORS IN A SPACEBORNE SYNTHETIC APERTURE RADAR IMAGING THE OCEAN SURFACE.
Tomiyasu, Kiyo
GE, Valley Forge Space Cent, Philadelphia, Pa
IEEE J Oceanic Eng v OE-2 n 1 Jan 1977 p 68-71 CODEN: IJOEDY
DESCRIPTORS: *OCEANOGRAPHY, RADAR EQUIPMENT, (OCEAN ENGINEERING, Communication Systems),
IDENTIFIERS: SPACEBORNE RADAR
CARD ALERT: 471, 472, 716
Data processing in a spaceborne synthetic aperture radar (SAR) imaging the ocean surface is affected by earth rotation, orbit eccentricity, and wave motion. Without compensation these sources will cause the images to shift in range and in-track positions and also cause defocusing. Ionospheric granularities may degrade image quality. Calculations of the magnitudes of these effects are presented.

ID NO.- EI770428817 728817
PRACTICAL OIL SENSOR.
Rambie, Guy S. Jr.
RAMCO, Irving, Tex
Proc of the Int Symp on Remote Sensing of Environ, 9th, Univ of Mich, Ann Arbor, Apr 15-19 1974 Publ by Environ Res Inst of Mich, Willow Run Lab, Ann Arbor, 1974 v 3 p 1685-1694
DESCRIPTORS: (*WATER POLLUTION, *Oil Spills), INFRARED DETECTORS, REMOTE SENSING,
CARD ALERT: 453, 944, 741
The two wavelength active monostatic infrared sensor detects the anomalous dispersion that occurs in petroleum products as a result of the carbon-hydrogen stretch bands near 3.4 micrometers. By ratioing the reflected power received at the two wavelengths the quotient is a signature proportional to reflectivity only, being independent of common mode effects such as range and time variable surface roughness caused by waves. Field tests were successfully conducted on both inland and ocean waters.

ID NO.- EI770427263 727263
PROBLEMS INHERENT IN USING AIRCRAFT FOR RADIO OCEANOGRAPHY STUDIES.
Walsh, Edward J.
NASA Wallops Flight Cent, Wallops Island, Va
IEEE Trans Antennas Propag v AP-25 n 1 Jan 1977 p 145-149 CODEN: IETPAK
DESCRIPTORS: (*RADIO ALTIMETERS, *Automatic Pilots), (OCEANOGRAPHY, Measurements), (RADAR, Spectrum Analysis),
CARD ALERT: 652, 943, 471, 716
Some of the disadvantages relating to altitude stability and proximity to the ocean are described. The random oscillatory motion introduced by the autopilot in maintaining aircraft altitude requires a more sophisticated range tracker for a radar altimeter than would be required in a satellite application. One-dimensional simulations of the sea surface (long-crested waves) are performed using both the JONSWAP spectrum and the Pierson-Moskowitz spectrum. The results of the simulations indicate that care must be taken in trying to experimentally verify instrument measurement accuracy. Because of the relatively few wavelengths examined from an aircraft due to proximity to the ocean and low velocity compared to a satellite, the random variation in the sea surface parameters being measured can far exceed an instrument's ability to measure them. 9 refs.

ID NO.- EI770427242 727242
DUAL FREQUENCY CORRELATION RADAR MEASUREMENTS OF THE HEIGHT STATISTICS OF OCEAN WAVES.
Weissman, David E.; Johnson, James W.
Hofstra Univ, Hempstead, NY
IEEE Trans Antennas Propag v AP-25 n 1 Jan 1977 p 74-83
CODEN: IETPAK
DESCRIPTORS: (*RADAR, *Measurement Application), (WATER WAVES, Measurements), (AIRCRAFT, Radar Equipment),
CARD ALERT: 716, 471, 631, 652
A radar technique is developed for measuring the statistical height properties of a random rough surface. This method is applied to the problem of measuring the significant wave height and probability density function of ocean waves from an aircraft or spacecraft. Earlier theoretical and laboratory results are extended to define the requirements and performance limitations of flight systems. Some details of the current airborne radar system are discussed and results obtained on several experimental missions are presented and interpreted. 10 refs.

ID NO.- EI770427237 727237
MODELS OF RADAR IMAGING OF THE OCEAN SURFACE WAVES.
Elachi, Charles; Brown, Walter E. Jr.
Calif Inst of Technol, Pasadena
v AP-25 n 1 Jan 1977 p 84-95 IETPAK
DESCRIPTORS: (*RADAR, *Imaging Techniques), SURFACE WAVES, WATER WAVES,
CARD ALERT: 716, 741, 931, 471, 631
A number of models which would explain ocean wave imagery taken with a synthetic aperture imaging radar are analyzed analytically and numerically. Actual radar imagery is used to support some conclusions. The models considered correspond to three sources of radar backscatter cross section modulation: tilt modulation, roughness variation, and the wave orbital velocity. The effect of the temporal changes of the surface structure, parametric interactions, and the resulting distortions are discussed. 30 refs.

ID NO.- EI770426287 726287
OCEAN INTERNAL WAVES OFF THE NORTH AMERICAN AND AFRICAN COASTS FROM ERTS-1.
Apel, John R.; Charnell, Robert L.; Blackwell, Richard J.
Natl Oceanic & Atmos Adm, Miami, Fla
Proc of the Int Symp on Remote Sensing of Environ, 9th, Univ of Mich, Ann Arbor, Apr 15-19 1974 Publ by Environ Res Inst of Mich, Willow Run Lab, Ann Arbor, 1974 v 2 p 1345-1351
DESCRIPTORS: *OCEANOGRAPHY, (WATER WAVES, Remote Sensing),
IDENTIFIERS: ERTS-1
CARD ALERT: 471, 631
Periodic features observed in the ocean portions of certain ERTS-1 images have been identified with reasonable certainty as surface manifestations of oceanic internal gravity waves. A series of images taken over the New York Bight has shown the internal waves to be present when summer solar heating stratifies the water sufficiently well to support such oscillations. When fall and winter wind action mixes the shelf water down to the bottom, the waves no longer appear. In the Bight, the wavelengths range from approximately 400 to 1000 m, with the wave field being most sharply delineated near the edges of the continental shelf.

ID NO.- EI770423723 723723
STUDIES OF THE SEA USING HF RADIO SCATTER.
Teague, Calvin C.; Tyler, G. Leonard; Stewart, Robert H.
Stanford Univ, Cent for Radar Astron, Calif
IEEE Trans Antennas Propag v AP-25 n 1 Jan 1977 p 12-19
CODEN: IETPAK
DESCRIPTORS: (*ELECTROMAGNETIC WAVES, *Scattering), (WATER WAVES, Measurements), DOPPLER EFFECT,
IDENTIFIERS: RADIO WAVES
CARD ALERT: 711, 471, 631, 931
Radio signals of decameter wavelength resonantly scattered from waves on the sea surface are used to measure precisely the wavelength, frequency, and direction of travel of those waves. These measurements are not only important in themselves, but are also used to deduce currents, winds, and perhaps wind stress at the sea surface. Techniques for obtaining these measurements, as well as experiments to evaluate these techniques are discussed. Scatter used to produce the first high-resolution measurements of the directional distribution of large ocean waves, measurements of ocean surface currents at ranges of 20 km, and of surface winds at ranges of 3000 km. 24 refs.

ID NO.- EI770319489 719489
EVOLUTION OF THE SEASAT IMAGING RADAR.
Brown, W. E. Jr.
JPL, Calif Inst of Technol, Pasadena
Proc Natl Telecommun Conf 1975, for Meet, New Orleans, La, Dec 1-3 1975 v 2 Sess 37 p 4-5 CODEN: NTCCAM
DESCRIPTORS: *RADAR SYSTEMS, (SATELLITES, Observatories),
CARD ALERT: 716, 655, 443
An imaging radar is being designed and developed for use on the spacecraft SEASAT-A tentatively scheduled for operation in 1978. In order to maintain a fine angular resolution with a reasonable physical antenna length, the radar will utilize a synthetic aperture. The SEASAT Synthetic Aperture Radar (SEASAR) is designed to operate at altitudes of 800 km and with an orbital inclination of 108 degrees. The nominal resolution is 25 m and swath width about 100 km. The experiments, as planned by the SEASAR Experiment Team, include observations of wave patterns, both open ocean and coastal regions, current patterns, slicks, surface conditions under storms, and the surface effects of internal waves. The discussion presented is principally concerned with the design of the radar system.

ID NO.- EI770105401 705401
LONG-RANGE OCEAN RADAR FOR OCEAN SURFACE STUDIES USING BACKSCATTER VIA THE IONOSPHERE.
Ward, J. F.; Dexter, P. E.
James Cook Univ, North Queensland, Aust
Aust J Phys v 29 n 3 Jun 1976 p 183-194 CODEN: AUJPAS
DESCRIPTORS: (*RADAR, *Measurement Application), OCEANOGRAPHY, METEOROLOGY,
CARD ALERT: 443, 471, 716
An HF Doppler radar, designed for use at long range via an ionospheric propagation model, has been developed primarily for the determination of wave states over large ocean areas. The experimental technique utilizes a well-known resonance interaction mechanism for electromagnetic waves backscattered from a moving sea wave surface to derive sea state parameters in the scattering region for input to oceanographic and meteorological synoptic data networks. An ultimate angular resolution of less than 1 $degree$ of azimuth, coupled with high operational flexibility, suggest possible utilization of the aerial array for tracking and interrogating free-floating ocean buoys, tracking radio noise associated with tropical cyclones and investigating aspects of ionospheric dynamics. 21 refs.

ID NO.- EI760533939 633939
BISTATIC SEA STATE RADAR MONITORING SYSTEM AND APPLICATIONS TO MARINE GEODESY.
Ruck, George T.
Battelle Columbus Lab, Ohio
Appl of Mar Geod, Int Symp, Proc, Columbus, Ohio Jun 3-5 1974 p 237-249. Publ by Mar Technol Soc, Washington, DC, 1974
DESCRIPTORS: (*RADAR, *Measurement Application), RADAR SYSTEMS, (WATER WAVES, Measurement), (SURFACE WAVES, Mathematical Models),
CARD ALERT: 471, 631, 716, 931
Battelle's Columbus Laboratories have developed for NASA-Wallops a bistatic radar system capable of sea state sensing from an orbital or aircraft platform. This system employs a simple low power transmitter in conjunction with a separate receiving unit. Operating in the HF region (3-30 MHz), a vertically polarized pulse or FMCW waveform is transmitted. The transmitted energy is scattered from the sea surface and received at a given time delay after reception of the direct signal from the transmitter. By sweeping or stepping the pulse carrier frequency or FMCW center frequency through the HF band, the heights of the larger ocean waves whose length are equal to the radar wavelength are sampled. Spectral processing of the receiving signal permits the directional component of the ocean-wave spectrum in the sea scattering region to be determined. 9 refs.

ID NO.- EI760426943 626943
RADAR CROSS SECTION OF THE SEA AT 1.95 MHz: COMPARISON OF IN-SITU AND RADAR DETERMINATIONS.
Teague, C. C.; Tyler, G. L.; Stewart, R. H.
Stanford Univ, Calif
Radio Sci v 10 n 10 Oct 1975 p 847-852 CODEN: RASCAD
DESCRIPTORS: (*RADAR, *Cross Sections), (WATER WAVES, Measurement),
CARD ALERT: 716, 471, 631
The rms wave height of seven sec ocean waves determined by remote measurements using high frequency radar is compared with that determined by direct in-situ measurements using an accelerometer buoy. The radar-measured values vary as the buoy-measured values for various sea and wind conditions, but the radar values are systematically low with respect to the buoy values by about 2.8 db. The radar experiment is more straightforward than conventional measurements because the same receiving antenna is used to sample both the illuminating and echo fields. Radar-measured values for ($sigma$ //0) for seven-sec ocean waves under homogeneous sea conditions did not exceed $minus$ 29.7 db. 10 refs.

ID NO.- EI760425963 625963
APPLICATION OF FOURIER TRANSFORMS FOR MICROWAVE RADIOMETRIC INVERSIONS.
Holmes, John J.; Balanis, Constantine A.; Truman, William M.
WVa Univ, Morgantown
IEEE Trans Antennas Propag v AP-23 n 6 Nov 1975 p 797-806 CODEN: IETPAK
DESCRIPTORS: (*OCEANOGRAPHY, *Temperature Measurement), RADIOMETERS, (RADIO RECEIVERS, Microwave Frequencies), (MATHEMATICAL TECHNIQUES, Integral Equations), (MATHEMATICAL TRANSFORMATIONS, Fast Fourier Transforms), REMOTE SENSING,
CARD ALERT: 471, 941, 944, 716, 921, 732
Existing microwave radiometer technology now provides a suitable method for remote determination of the ocean surface's absolute brightness temperature. To extract the brightness temperature of the water from the antenna temperature, an unstable Fredholm integral equation of the first kind is solved. Fourier transform techniques are used to invert the integral after it is placed into a cross correlation form. Application of the methods to a two-dimensional modeling of a laboratory wave tank system are included. The instability of the ill-posed Fredholm equation is examined and a restoration procedure is included which smooths the resulting oscillations. 14 refs.

ID NO.- EI760214163 614163
SHORT PULSE RADAR FOR SENSING OCEAN WAVE STRUCTURE.
LeVine, David M.; Eckerman, Jerome; Kutz, Richard L.; Davisson, Lee D.; Hammond D.
NASA Goddard Space Flight Cent, Greenbelt, Md
IEEE Conf on Eng in the Ocean Environ and Mar Technol Soc, 11th Annu Meet, Proc, San Diego, Calif, Sep 22-25 1975 p 769-774. Publ by IEEE (75 CHO 995-1 OEC), New York, NY, 1975
DESCRIPTORS: (*WATER WAVES, *Spectrum Analysis), (RADAR, Meteorological), PULSE MODULATION,
CARD ALERT: 471, 631, 716, 443
Basic concept of the sensing system and a summary of the research program and results are presented. Graphs illustrate system. 10 refs.

ID NO.- EI760209203 609203
MICROWAVE SCATTERING FROM THE OCEAN SURFACE.
Jones, W. Linwood; Grantham, William L.; Schroeder, Lyle C. ; Johnson, James W.; Swift, Calvin T.; Mitchell, John L.
NASA, Langley Res Cent, Hampton, Va
IEEE Trans Microwave Theory Tech v MTT-23 n 12 Dec 1975 p 1053-1058 CODEN: IETMAB
DESCRIPTORS: (*ELECTROMAGNETIC WAVES, *Scattering), OCEANOGRAPHY, (SATELLITES, Weather),
IDENTIFIERS: SCATTEROMETERS
CARD ALERT: 711, 471, 443
This paper reviews current aircraft and satellite programs which use microwaves to measure ocean wave and surface wind conditions. These particular measurements have been identified by the user community as offering significant economic and technological benefits. Active microwave remote sensing techniques for these applications have been described theoretically and verified experimentally. The results of recent aircraft and satellite experimental programs are presented along with plans for the SeaSat-A satellite scatterometer (SASS). 20 refs.

ID NO.- EI760105284 605284
SPECTRAL CHARACTERISTICS OF REMOTE SENSORS.
Dotsenko, S. V.; Nedovesov, A. N.; Poplavskaya, M. G.
Ukr SSR Acad of Sci, Sevastopol
Colloq Int sur l'Exploit des Oceans, 2nd, Proc. Prepr and Pap, Paris, Fr, Oct 1-4 1974 v 3 Pap 313, 11 p. Publ by Assoc pour l'Organ de Colloq Oceanol a Bordeaux, Paris, Fr, 1974
DESCRIPTORS: (*REMOTE SENSING, *Spectrum Analysis), (OCEANOGRAPHY, Temperature Measurement), (WATER WAVES, Measurement), WATER POLLUTION,
CARD ALERT: 732, 943, 471, 631, 453
Defices for remote sensing, installed in ships and aircraft, have been used recently for the determination of parameters of the physical state of the ocean surface (temperature, waves, contamination). The principle of measuring by such devices is based on sensing them by radiation sensors of a definite wave range. Equations and graphs illustrate characteristics. 3 refs.

ID NO.- EI751283742 583742
MICROWAVE REMOTE SENSING OF THE OCEANS FROM SPACE.
Paul, Charles K.
Lure Ind
Offshore Technol Conf, 7th Annu, Proc, Houston, Tex, May 5-8 1975 v 3, Pap OTC 2422 p 795-804. Publ by Offshore Technol Conf, Dallas, Tex, 1975
DESCRIPTORS: *REMOTE SENSING, (SATELLITES, Telemetering), OCEANOGRAPHY,
CARD ALERT: 732, 655, 471
This paper describes the latest concept designs and flight-proven prototypes of microwave scatterometers, imaging radars, radar altimeters, and radiometers. The numerical reduction processes by which raw sensor data are reduced to meaningful wind, wave, and current parameters are discussed as well as the accuracy limitations of the formats in which ocean information is displayed. 7 refs.

ID NO.- EI751282815 582815
REMOTE SENSING OF OCEANS USING MICROWAVE SENSORS.
Krishen, K.
Lockheed Electron Co, Inc, Houston, Tex
Remote Sensing Appl to Energy-Relat Probl, Symp Course, Proc. Miami, Fla, Dec 2-4 1974 Sess S2 p 25-57. Publ by Univ of Miami, Coral Gables, Fla, 1974
DESCRIPTORS: (*OCEANOGRAPHY, *Measurement), MEASUREMENTS, (AIRCRAFT, RESEARCH, Electronic Equipment), MICROWAVE DEVICES, RADIOMETERS.
IDENTIFIERS: MICROWAVE SENSORS, REMOTE SENSING
CARD ALERT: 941, 471, 942, 652, 715, 714
A review of the results of a study of the ocean surface phenomena is presented. The use of active and passive microwave sensors to detect ocean surface waves, temperature, salinity, storm cells, and oil slicks is demonstrated. The aircraft- and spacecraft-acquired microwave data from the Naval Research Laboratory and the National Aeronautics and Space Administration/Lyndon B. Johnson Space Center are presented. The radar backscattering cross section data shows strong correlation between ocean surface winds/waves, storm regions, and oil slicks. A strong dependence upon these parameters has been shown in the Ku-band at a radar frequency of 13. 9 GHz. The relationship between radiometric brightness temperature and ocean surface temperature, salinity, and sea state are set forth. Evidence of the suitability of microwave sensors in providing data independent of sunlight under almost all weather conditions is provided. Tables and equations show calculations, maps and graphs are appended. 57 refs.

ID NO.- EI751282793 582793
CIVIL ENGINEERING IN THE OCEANS, 3RD CONFERENCE, ABSTRACTS OF PAPERS, 1975.
Resio, Donald T.; Pfafflin, James R.; DeYoung, Raymond K.; Chung, Y. K.; Bomze, H.; Noble, Ronald M.; Borgman, Leon E.; Ross, Duncas; Teleki, Paul; Wiley, James; Machemehl, Jerry L.; French, Thomas J.; Huang, Norden E.
Civ Eng in the Oceans, Conf, 3rd, Abstr of Pap, Univ of Del, Newark, Jun 9-12 1975 Publ by ASCE, New York, NY, 1975, 258 p
DESCRIPTORS: *OCEANOGRAPHY, CIVIL ENGINEERING, (PORT STRUCTURES, Wave Effects), (BEACHES, Erosion), TIDES, WATER WAVES.
CARD ALERT: 407, 471, 631, 901
Proceedings include 80 papers that contribute to civil engineering in the oceans, ocean engineering and oceanography. Following is a list of titles and authors of the papers presented: Extreme Wave Heights for Cleveland Harbor: A Comparison of Different Data and Techniques. By Donald T. Resio. Recurrence Intervals of Abnormally High Tides by Superposition of Storm Surges Over Astronomical Tides. By James R. Pfafflin and Raymond K. DeYoung. Determination of the Maximum Tornado-Induced Wave in a Basin. By Y. K. Chung and H. Bomze. Design Basis Flooding at Offshore Reactor Sites. By Ronald M. Noble. Extremal Statistics in Ocean Engineering. By Leon E. Borgman. Radar in Oceanography. By Duncas Ross, Paul Teleki and James Wiley. New Method for Beach Erosion Control. By Jerry L. Machemehl, Thomas J. French and Norden E. Huang.

ID NO.- EI751178117 578117
REVIEW OF TECHNIQUES FOR DIRECTIONAL WAVE SPECTRA.
Panicker, Narayana N.
Woods Hole Oceanogr Inst, Mass
Inst Symp on Ocean Wave Meas and Anal (WAVES 74), Proc, New Orleans, La, Sep 9-11 1974 p 669-688. Publ by ASCE, New York, NY, 1974
DESCRIPTORS: (*WATER WAVES, *Spectrum Analysis), (MATHEMATICAL TRANSFORMATIONS, Fourier Transforms).
CARD ALERT: 471, 921
Determination of the energy density of ocean surface waves as a function of both frequency and direction is of practical importance. With varying degrees of success several methods of measurement and analysis have been tried for this purpose in the past and their limitations should encourage the development of new techniques. Measurements are of two types: the direct measurements from within the wave field and remote measurements from without using light or radio waves. Direct measurements may be of array type or buoy type. In an array similar quantities are measured at several horizontally separated points. In a buoy type measurement scheme several different quantities are measured at essentially a single point. Remote sensing by use of light or radio waves is done through optical techniques and radio backscatter techniques. Calibration against direct measurements may be necessary for obtaining absolute values of directional spectral density: but the convenience of measurement and analysis by these techniques are becoming evident. Optical techniques may be either photogrammetric or optical analog. The highest directional resolution ever obtained to date for ocean waves appears to have been through the use of a radio backscatter technique. Several methods of analysis are used for estimating directional spectra from measurements. These are the direct Fourier transform, parameterized estimation, amplitude and phase detection technique, discrete wave train analysis, and data adaptive techniques. 91 refs.

ID NO.- EI751175443 575443
PROSPECTS FOR PHYSICAL OCEANOGRAPHY FROM SPACE.
Cartwright, D. E.
Natl Inst of Oceanogr, Wormley, Surrey, Engl
Approaches to Earth Surv Probl Through Use of Space Tech, COSPAR Symp, Proc, Constance, Ger, May 23-25 1973 p 251-256. Publ by Akad-Verlag, Berlin, Ger, 1974
DESCRIPTORS: *OCEANOGRAPHY, (SATELLITES, Telemetering),
CARD ALERT: 471, 655
Apart from applications to marine biology, glaciology and near-shore processes, the principal areas of physical oceanographical research to which remote sensing from space is likely to contribute are: Lagrangian current tracking; global surface temperatures; wave height, roughness and wind parameters; altimetry of static and dynamic features of the ocean surface, including tides. Present and possible future requirements and progress in these topics are reviewed and discussed.

ID NO.- EI750856492 556492
MICROWAVE SCATTERING AND THE DYNAMICS OF SHORT WIND WAVES.
Witting, James; Wright, John W.
NRL, Washington, DC
Rep NRL Prog Feb 1975 p 1-16 CODEN: RNRLAO
DESCRIPTORS: *WATER WAVES,
CARD ALERT: 631
Reports results of measurements of the response of particular components of the water wave spectrum due to changes of wind and surface straining. Microwave radars are used as an accurate and area-averaging wave probe. The growth rates of water waves produced by a suddenly imposed wind in the wavelength range 0. 7 cm $less than$ $lambda$ $less than$ 35 cm are measured over a wide range of wind speeds. The results show that for wind speeds greater than a few knots, most of the momentum input to the ocean is to waves in the wavelength region examined. A linear relaxation theory for the response of a spectral component of a fully developed sea to surface straining is developed. Experiments for the wave component at $lambda$ $equals$ 2. 26 cm agree with theory for weak and moderate winds. There is sudden disagreement for stronger winds, probably indicating the onset of a new phenomenon not considered by the theory. The impact of these results on contemporary understanding of the ocean surface and of applications to forecasting surface conditions is discussed. 21 refs.

ID NO.- EI750533632 533632
FERNERKUNDUNG DER MEERESOBERFLAECHE VON SATELLITEN AUS. $left bracket$ Remote Sensing of Ocean Surfaces by Satellites $right bracket$.
Alpers, Werner; Hasselmann, Klaus; Schieler, Manfred
Univ Hamburg, Ger
Raumfahrtforschung v 19 n 1 Jan-Feb 1975 p 1-7 CODEN: RMFFA7
DESCRIPTORS: (*SATELLITES, *Telemetering), (WATER WAVES, Measurement),
CARD ALERT: 471, 631
Remote sensing techniques for satellite-borne measurements of the sea surface is reviewed briefly. Three methods for determining significant parameters of ocean wave spectra using microwaves are discussed. The two-frequency radar monitoring technique shows most promising results for complete two-dimensional ocean wave spectra. 21 refs. In German with English abstract.

ID NO.- EI750533325 533325
EFFECT OF PULSE WIDTH ON RADAR MEASUREMENT OF OCEAN WAVE HEIGHT.
Young, Tzay Y.
Univ of Miami, Coral Gables, Fla
Int J Electron v 37 n 6 Dec 1974 p 833-848 CODEN: IJELA2
DESCRIPTORS: (*RADAR, *Measurement Application), (WATER WAVES, Measurement),
CARD ALERT: 716, 631, 471
Various factors that affect the accuracy of radar measurement of ocean wave height from space are examined, with particular emphasis on the effect of pulse width. It is shown that at a given signal-to-noise ratio, large or small, there is a pulse width that yields an optimal estimation accuracy. Both optimal and suboptimal estimation schemes are considered, and performance curves are presented. 15 refs.

ID NO.- EI750318514 518514
HF RADIO MEASUREMENTS OF SURFACE CURRENTS.
Stewart, Robert H.; Joy, Joseph W.
Univ of Calif, San Diego, La Jolla, Calif
Deep Sea Res v 21 n 12 Dec 1974 p 1039-1049 CODEN: DROAAK
DESCRIPTORS: (*OCEANOGRAPHY, *Instruments), RADAR,
CARD ALERT: 471, 716
HF radio waves backscattered from the ocean surface can be used to measure ocean surface currents. Measurements of the range-Doppler spectrum of these signals yield the wavenumber and the frequency of an ocean surface wave and its phase velocity relative to the radar. Subtraction of the phase velocity of the wave in still water yields a measure of the average current from the surface to a depth. A measure of the current shear is obtained by observing at more than one radio frequency. To test these ideas, surface currents were measured using both a conventional and the HF technique, and reasonable agreement was found. 9 refs.

AD-A058 617 ENVIRONMENTAL RESEARCH INST OF MICHIGAN ANN ARBOR F/G 17/9
PROBLEMS OF IMAGING OCEAN WAVES WITH SYNTHETIC APERTURE RADAR.(U)
AUG 77 R A SHUCHMAN, P L JACKSON N00014-76-C-1048
UNCLASSIFIED ERIM-124300-1-T NL

2 OF 2
AD
A058817

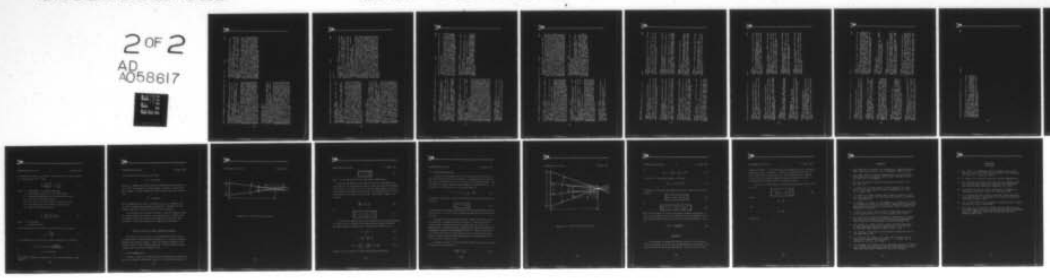

END
DATE
FILMED
11-78
DDC

ID NO.- EI750212330 512330
MEASUREMENTS OF MICROWAVE FORWARD SCATTERING FROM THE OCEAN AT L-BAND.
Beard, Charles I.; Drake, David L.; Morrow, Christopher M.
Nav Res Lab, Washington, DC
IEEE Proc Natl Aerosp Electron Conf 1974, for Meet, Dayton, Ohio, May 13-15 1974, p 269-274 CODEN: NASEA9
DESCRIPTORS: (*RADAR, *Testing), (ELECTROMAGNETIC WAVES, Scattering),
IDENTIFIERS: RADAR SCATTERING
CARD ALERT: 711, 716
Measurements of forward scattering of microwave radiation from the surface of the ocean are in process to extend a scattering model to lower frequencies and higher grazing angles. As a first test of the system, an airborne 1.3 GHz cw transmitter was flown toward a receiver on a cliff overlooking Chesapeake Bay. Horizontal, vertical, and cross polarizations were used. Water-wave recordings were made simultaneously, and aerial photographs of the waves processed for wave spectra by the D. Stilwell method. The depths of the horizontal polarization interference pattern minima vary from 35 db to 15 db. This variation is caused by the incoherent energy scattered from the ocean. A procedure has been developed for separating out the incoherent scattered field so that the coherent field reflection coefficients can be calculated. The receiver is now on a ship at sea for measurements at higher sea states. 13 refs.

ID NO.- EI750211137 511137
PASSIVE RANGING TECHNIQUES.
Heimdal, Per; Bryn, Finn
Norw Def Res Establ, Horten
Signal Process, NATO Adv Study Inst, Proc, Loughborough Univ of Technol, Leicestershire, Engl, Aug 21-Sep 1 1972 p 261-270. Publ by Acad Press Inc, New York, 1973
DESCRIPTORS: *NAVAL WARFARE, (UNDERSEA TECHNOLOGY, Instruments), SONAR, ACOUSTICS, UNDERWATER,
CARD ALERT: 404, 672, 472, 752
High accuracy range measurements are best obtained by using laser, radar or active sonar. However, in some situations, such as underwater warfare, such systems cannot be used since one's own position might be disclosed. It is shown that range may be found by passive acoustic means, by cross bearings. If the target moves nonlinearly, it is difficult to measure range unless simultaneous cross bearings are obtained. This can be obtained by using acoustic sensors (hydrophones) mounted on a submarine, a towed or vertical cable, or the like. Since the baselines are small for such systems, high hydrophone placing accuracy is required. A small error in measured sound wave curvature gives a large error in range estimate. It is concluded that a practical system for passive range measurements has to deal with all undesired phenomena occurring in a real ocean. A man-machine system seems to be the best solution. 4 refs.

ID NO.- EI741065169 465169
RADAR SATELLITE ALTIMETRY AND OCEAN WAVE HEIGHT ESTIMATION.
Dooley, R. P.; Brooks, L. W.
Technol Serv Corp, Silver Spring, Md
IEEE Electron and Aerosp Syst Conv, Rec, Washington, DC, Sep 17-19 1973 p 193-198. Publ by IEEE (73 CHO 783-1 AES), New York, 1973
DESCRIPTORS: *RADIO ALTIMETERS, RADAR, (OCEANOGRAPHY, Equipment), (WATER WAVES, Measurement), (SATELLITES, Observations),
CARD ALERT: 471, 655, 716, 943
The design of a radar satellite altimeter having a $plus$ 10 cm topographic resolution at 20 meter (peak-to-trough) ocean wave heights is described. In addition to altimetry, the resulting design also provides a measurement of significant wave height over the range of 1.0 to 20 meters to within $plus or minus$ 10%. A full deramp pulse compression technique followed by an analog filter bank to separate individual range returns is used in the radar transmitter/receiver design to reduce the analog to digital converter bandwidth from a rather impractical 330 MHz to less than 1 MHz. The altimeter design utilizes an onboard maximum likelihood estimate (MLE) processor to achieve the $plus or minus$ 10 cm topographic resolution. It is shown that an MLE processor provides simultaneous optimum (minimum variance) estimates of satellite altitude, ocean wave height and electromagnetic ocean surface reflectivity.

ID NO.- EI740957918 457918
CURVATURE-CORRECTED KIRCHOFF FORMULATION FOR RADAR SEA-RETURN FROM THE NEAR VERTICAL.
Jackson, Frederick C.
New York Univ, NY
NASA Contract Rep CR-2406 Apr 1974, 75 p CODEN: NSCRAQ
DESCRIPTORS: (*RADAR, *Reflection), (ELECTROMAGNETIC WAVES, Scattering),
CARD ALERT: 711, 716
A new theoretical treatment of the problem of electromagnetic-wave scattering from a randomly-rough surface is given. A high frequency correction to the Kirchoff approximation is derived from a field integral equation for a perfectly conducting surface. The correction, which accounts for the effect of local surface curvature, is seen to be identical with an asymptotic form found by Fock (1945) for diffraction by a paraboloid. The corrected boundary values are substituted into the far-field Stratton-Chu integral, and average backscattered powers are computed assuming the scattering surface is a homogeneous Gaussian process. Preliminary calculations for a K** $minus$ **4 ocean wave spectrum indicate a reasonable modelling of polarization effects near the vertical $theta$ $less than$ 45 $degree$. Correspondence with the results of small perturbation theory is shown. 40 refs.

ID NO.- EI740954429 454429
REMOTE SENSING OF THE TROPOSPHERE.
Hardy, Kenneth R.; Snider, Jack B.; Westwater, Ed R.; Strand, Otto Neall; Taylor, William L.; Hall, Freeman F. Jr.; Little, C. Gordon; Bean, B. R.; Georges, T. M.; Young, J. M.; Hanson, Kirby J.; Strauch, R. G.; Cohen, A.; Schwiesow, R. L.
Remote Sensing of the Tropos Available from Supt of Doc, US Gov Print Off, Washington, DC, 1972
DESCRIPTORS: (*EARTH ATMOSPHERE, *Research), SOUNDING APPARATUS, ATMOSPHERIC STRUCTURE, (RADAR, Meteorological), (RADAR, OPTICAL, Meteorological), OCEANOGRAPHY,
IDENTIFIERS: ACOUSTIC ECHO SOUNDING, ATMOSPHERIC SENSING
CARD ALERT: 481, 657, 443, 716, 752, 471
Following is a continuation of the list of titles and authors: Studies of the Clear Atmosphere Using High Power Radar. By Kenneth R. Hardy. Radiometry. By Jack B. Snider and Ed R. Westwater. Inversion Techniques. By Ed R. Westwater and Otto Neall Strand. Atmospherics and Severe Storms. By William L. Taylor. Temperature and Wind Structure Studies by Acoustic Echo-Sounding. By Freeman F. Hall Jr. Prospects for Acoustic Echo Sounding. By C. Gordon Little. Application of FM-CW Radar and Acoustic Echo-Sounder Techniques to Boundary Layer and Cat Studies. By B. R. Bean. Passive Sensing of Natural Acoustic-Gravity Waves at the Earth's Surface. By T. M. Georges and J. M. Young. Remote Sensing of the Ocean. By Kirby J. Hanson. Atmospheric Remote Sensing with Laser Radar. By R. G. Strauch and A. Cohen. Remote Spectral Sensing of Pollutants. By R. L. Schwiesow.

ID NO.- EI740528515 428515
AMERICAN SOCIETY OF PHOTOGRAMMETRY. FALL CONVENTION. PROCEEDINGS, 1973.
Lippert, Frederick G. III; Hussain, Mushtaq; Veress, Sandor A.; Moffitt, Francis H.; Audirac Padilla, Henri; Moncayo Ruiz, Francisco; McCluney, W. R.; Brown, O. B.; Gordon, H. R.; Ramsey, R. C.; Petri, Kenneth J.; Starry, Robert F.; Szekielda, Karl Heinz
Am Soc of Photogramm, Fall Conv, Proc, Pap, Lake Buena Vista, Fla, Oct 2-5 1973 Available from ASP, Falls Church, Va. 1973, 2 Parts, 1060 p
DESCRIPTORS: *PHOTOGRAMMETRY, AERIAL PHOTOGRAPHY, PHOTOGRAPHY, MAPS AND MAPPING, OCEANOGRAPHY,
IDENTIFIERS: REMOTE SENSING, COASTAL ENGINEERING
CARD ALERT: 405, 471, 742
Following is a continuation of the list of titles and authors of the papers presented: Measurement of Spatial Motion Using Close-Range Analytical Photogrammetric Principles. By Frederick G. Lippert, III, Mushtaq Hussain and Sandor A. Veress. Mapping of Ship Waves Breaking on a Beach. By Francis H. Moffitt. Determacion de Areas por Pesada Analogica. $left bracket$ Determination of Areas by Using Analogy $right bracket$. By Henri Audirac Padilla. Panoramica de la Aplicacion de la fotografia Aerea en Inventarios Forestales de la Republica Mexicana. $left bracket$ Review of the Methods of Application of Aerial Photography for the Forestry Surveys in Mexico $right bracket$. By Francisco Moncayo Ruiz. Satellite Ocean Color Measurements. By W. R. McCluney. Examination of Factors Influencing Ocean Color Using Radiative Transfer Theory. By O. B. Brown and H. R. Gordon. Remote Spectrophotometric Measurements of Portions of the World's Oceans and Lakes. By R. C. Ramsey. Remote Measurements of Sea Surface Wind Velocity. By Kenneth J. Petri and Robert F. Starry. Distribution Pattern of Temperature and Biomass in the Upwelling Area Along the NW Coast of Africa. By Karl Heinz Szekielda.

ID NO.- EI740314491 414491
TEST OF THE RADAR METHOD OF DEFINING OCEAN-WAVE ELEMENTS.
Evmenov, V. F.; Kozhukhov, I. V.; Nichiporenko, N. T.; Khulap, G. D.
S. O. Makarov Leningrad Adv Mar-Eng Sch, USSR
Fluid Mech, Sov Res v 2 n 5 Sep-Oct 1973 p 141-145 CODEN: FMSVAM
DESCRIPTORS: *OCEANOGRAPHY, (RADAR, Measurement Application), (WATER WAVES, Measurement),
CARD ALERT: 471, 716
Experiments to determine some sea-state parameters, using a millimeter radar, are described. Under unfavorable meteorological conditions the radar method is in practice quite accurate, simple and reliable. 3 refs.

ID NO.- EI731260065 360065
TWO FREQUENCY RADAR INTERFEROMETRY APPLIED TO THE MEASUREMENT OF OCEAN WAVE HEIGHT.
Weissman, David E.
Hofstra Univ, Hempstead, NY
IEEE Trans Antennas Propag v AP-21 n 5 Sep 1973 p 649-656 CODEN: IETPAK
DESCRIPTORS: (*WATER WAVES, *Measurement), RADAR, OCEANOGRAPHY,
IDENTIFIERS: RADAR INTERFEROMETRY
CARD ALERT: 471, 631, 716
A technique is developed for measuring the rms wave height averaged over an area of the sea that is much greater than any horizontal scale of the surface waves. The method involves a nadir looking radar which transmit receives two monochromatic signals simultaneously. Signal processing at the receiver involves the computation of the correlation between the two returning signals as a function of their variable frequency separation. The cross correlation between the amplitude and phase functions of the individual returning carries depends on the distribution of discrete scatterers along the direction of the propagation. This information can be used to determine the rms surface elevation (about the mean); it does not depend on the temporal or spatial frequency spectrum of the wave height or slope. Under conditions which are typical for a microwave signal being normally incident and reflected by the sea, the two frequency correlation function R($DELTA$ k) is seen to be equal to the characteristic function of the surface elevation of specular points. 8 refs.

ID NO.- EI730314825 314825
METHOD OF PHASE DETECTION OF THE BEAT SIGNAL IN FM-CW RADAR.
Marukawa, Takeshi; Imai, Isao
Defense Academy, Yokosuka-shi, Jap
Electron Commun Japan v 54 n 4 Apr 1971 p 125-132 CODEN: ECOJAL
DESCRIPTORS: *RADAR CIRCUITS, (WATER WAVES, Measurement), ELECTRONIC CIRCUITS, DETECTOR, (RADAR, Measurement Application),
IDENTIFIERS: PHASE DETECTION
CARD ALERT: 471, 713, 716
When a target moves in the radial direction, the amount and sense of its motion can be found from the phase variation of the beat signal. The measurement accuracy is approximately a half wavelength of the carrier wave. In this paper the authors describe the principle of phase detection, a method of detecting positive or negative change of the range, the circuit construction, and experimental results with FM radar in the X-band. As an application, measurement of the height and period of an ocean wave by this detection method was considered and the experimental work included simulated tests with a pendulum in an anechoic radio chamber. 11 refs.

ID NO.- EI72X022119 222119
Measurement of ocean wave heights with the random- signal radar
CHADWICK RB; COOPER GR
Inst of Telecommunication Sciences, Boulder, Colo
IEEE Trans Geosci Electron v GE-9 n 4 Oct 1971 p 216-21 CODEN: IEGEA
DESCRIPTORS: (*OCEANOGRAPHY, *Instruments), RADAR,
CARD ALERT: 471, 716, 942
The random- signal- radar principle is proposed because of its excellent resolution characteristics. The scatter density function and the random- signal- radar system are discussed, along with the relation between radar cross section and the scatterer density function. A method of estimating wave height is given.

ID NO.- EI72X022118 222118
Bistatic- radar techniques for observing long- wavelength directional ocean- wave spectra
TEAGUE CC
Stanford Electronic Lab, Calif
IEEE Trans Geosci Electron v GE-9 n 4 Oct 1971 p 211-15
CODEN: IEGEA
DESCRIPTORS: (*OCEANOGRAPHY, *Instruments), RADAR,
CARD ALERT: 471, 716, 942
It is shown that bistatic- radar Bragg scattering of medium- to long- wavelength radio waves by ocean waves can be used for observing directional ocean- wave spectra. Only moderate antenna directivity is required; areal and directional resolution are provided by high- resolution delay- Doppler processing of the radar echoes. Directional characteristics of long- wavelength (80 to 200 m) ocean waves have been observed using LORAN A transmission (1. 85 MHz) and a receiver located 280 km from the transmitter. The received signals have been converted into a time- delay Doppler- frequency map and into a plot of normalized radar cross section as a function of directional ocean- wavenumber. 13 refs.

ID NO.- EI72X020052 220052
Instrumentation for measuring the small- scale irregularities of the sea surface and the sea bed
DUNN DJ
Admiralty Underwater Weapons Estab, Portland, Dorset, England
IEEE Int Conf Eng in Ocean Environ, Panama City, Fla, Sept 21-24 1970 Digest of Tech Pap p 25-7
DESCRIPTORS: (*OCEANOGRAPHY, *Instruments), PATTERN RECOGNITION SYSTEMS,
IDENTIFIERS: WATER POLLUTION DETECTION
CARD ALERT: 453
This paper gives details of a wavebuoy which has been devised and used to measure the statistical properties of sea surface waves over a wide range of sea states and of a towed deep submerged echo sounder developed to measure the small scale structure of the sea bed. 20051% 471- 481- 941 EI 72 /GEOPHYSICS, Subaqueous/ WATER POLLUTION Optical (infrared and ultraviolet- visual) remote sensing of pollution of water bodies; M. R. HOLTER (Univ of Michigan, Ann Arbor); IEEE Int Conf Eng in Ocean Environ, Panama City, Fla, Sept 21- 24 1970 Digest of Tech Pap p 45- 50;

ID NO.- EI72X008010 208010
Nanosecond radar observations of the ocean surface from a stable platform
YAPLEE BS; SHAPIRO A; HAMMOND DL; AU BD; ULIANA EA
E.O.Hulburt Cent for Space Res, Washington, DC
IEEE Trans Geosci Electron v GE-9 n 3 July 1971 p 170-4
CODEN: IEGEA
DESCRIPTORS: (*OCEANOGRAPHY, *Sea Level Changes), RADAR,
CARD ALERT: 471, 716
To obtain information on the potential usefulness of a radar altimeter as a remote ocean sensor, an experimental description of the ocean radar reflectivity is needed. This can be derived from an investigation of the electromagnetic impulse response of the sea surface at vertical incidence over a wide range of sea state conditions. For this purpose, a 1- nsec radar was assembled and placed on the Chesapeake Light Tower where, with a moderate antenna size, high spatial resolution is obtained. By recording the return over several minutes, the radar reflection from different portions of the vertical water wave structure is measured. The average radar returns then present the effective impulse response of the ocean. Simultaneously with the radar measurements, wave staff measurements of the water wave structure are obtained so that the relation between geometric and electromagnetic surface distribution can be established. Preliminary results are shown without interpretations to show the effectiveness of a nanosecond radar to measure the ocean surface characteristics.

ID NO.- EI71X048763 148763
Worldwide oceanic wind and wave predictions using a satellite radar- radiometer
MOORE RK; PIERSON JR WJ
Univ of Kansas, Lawrence
J Hydronautics v 5 n 2 Apr 1971 p 52-60 CODEN: JHYDE
DESCRIPTORS: (*SATELLLITES, *Electronic Equipment), (RADAR, Receivers), OCEANOGRAPHY, (RADIO RECEIVERS, Microwave),
CARD ALERT: 471, 655, 716
Data from a combined radar- radiometer in a satellite should permit improved prediction of surface atmosospheric pressure, winds, and ocean wave spectra on a global basis, with consequent advantages to shipping. Radar returns from the sea at 2. 25 cm wavelength have been measured and shown to be proportioned to windspeed. Use of microwave radiometer should permit removing false radar data caused by atmospheric attenuation since the radiometric temperature is highly sensitive to such attentuation. 30 refs.

77-02615
MODELS OF RADAR IMAGING OF THE OCEAN SURFACE WAVES.
BROWN, W.E., JR.; ELACHI, C.
CALIFORNIA INST. OF TECHNOLOGY, JET PROPULSION LAB., SPACE; SCIENCE DIV., PASADENA, CA 91103
Lan: E
IEEE JOURNAL OF OCEANIC ENGINEERING, 2(1): 84-95, JAN. 1977. Publ.Yr: 77
Descriptors: WAVES, OCEAN WAVE IMAGERY, BACKSCATTERING, NUMERICAL ANALYSIS, SURFACE WAVES, RADAR IMAGERY

77-02614
DUAL FREQUENCY CORRELATION RADAR MEASUREMENTS OF THE HEIGHT STATISTICS OF OCEAN WAVES.
WEISSMAN, D.E.; JOHNSON, J.W.
HOFSTRA UNIV., DEPT. OF ENGINEERING AND COMPUTER SCIENCES,; HEMPSTEAD, NY 11550
Lan: E
IEEE JOURNAL OF OCEANIC ENGINEERING, 2(1): 74-83, JAN. 1977. Publ.Yr: 77
Descriptors: WAVE HEIGHTS, MEASURING METHODS, RADAR, AIRBORNE INSTRUMENTS, REMOTE SENSING, SURFACE ROUGHNESS, DUAL FREQUENCY CORRELATION

77-00455
WAVE PATTERNS ACROSS THE NORTH ATLANTIC ON SEPTEMBER 28, 1974, FROM AIRBORNE RADAR IMAGERY.
ELACHI, C.
CALIFORNIA INST. OF TECHNOLOGY, SPACE SCIENCES DIV.,; JET PROPULSION LAB., PASADENA, CA 91103
Lan: E
JOURNAL OF GEOPHYSICAL RESEARCH, 81(15): 2655-2656, MAY 20, 1976. Publ.Yr: 76
Descriptors: RADAR IMAGERY, ATLANTIC OCEAN NORTH, WAVE PATTERNS, AERIAL SURVEYS, ATMOSPHERIC PRESSURE, STORMS, SURFACE ROUGHNESS, SEPT. 28, 1974, LOW PRESSURE AREAS

76-05521
FUTURE POSSIBILITY OF INVESTIGATING THE OCEAN USING ARTIFICIAL SATELLITES.
FEDOROV, K.N.; SKLYAROV, V. YE.
Lan: E
SCIENTIFIC AND TECHNICAL AEROSPACE REPORTS, 14(2): 199, JAN. 23, 1976. Publ.Yr: 76
Descriptors: SURFACE WATERS, OCEAN SURVEYING, SATELLITES, ICE COVER, OCEAN FLOOR, BUOYS, COASTAL ZONES, LASERS, RADAR, SUMMARY ONLY, TEMPERATURE FIELDS, REMOTE SENSORS, WAVE MEASUREMENTS, MEASURING INSTRUMENTS, MEASURING METHODS, SEA LEVELS

76-03515
OCEAN WAVE CROSS-RADIAL IMAGE ERROR IN SYNTHETIC APERTURE RADAR DUE TO RADIAL VELOCITY.
TOMIYASU, K.
GEC, VALLEY FORGE SPACE CENTER, PHILADELPHIA, PA 19101
Lan: E
JOURNAL OF GEOPHYSICAL RESEARCH, 80(33): 4555, NOV. 20, 1975. Publ.Yr: 75
Descriptors: RADIAL VELOCITY, SYNTHETIC APERTURE RADAR, WAVE IMAGE ERROR, RADAR IMAGERY, WAVE VELOCITY

76-02529
MEASUREMENT OF SEA SCATTER AND BUOY TRACKS AT LONG RANGES BY HIGH-RESOLUTION OTH-B RADAR.
BARNUM, J.R.; MARSHALL, W.F.
STANFORD RESEARCH INST., 333 RAVENSWOOD AVE., MENLO PARK,; CA 94025
Lan: E
SCIENTIFIC AND TECHNICAL AEROSPACE REPORTS, 14(1): 90, JAN. 8, 1976. Publ.Yr: 76
Descriptors: SUMMARY ONLY, BACKSCATTERING, BUOYS, CALIFORNIA, HAWAII, MONITORING SYSTEMS, PACIFIC OCEAN NORTH, POSITIONING, RADAR, RESEARCH VESSELS, TRACKING INSTRUMENTATION, WAVE HEIGHTS, WIND DATA

76-01566
MICROWAVE REMOTE SENSING OF THE OCEANS FROM SPACE.
PAUL, C.K.
LURE INDUSTRIES
OFFSHORE TECHNOLOGY CONFERENCE: SEVENTH ANNUAL: PROCEEDINGS: VOL. III. (N.P.): OFFSHORE TECHNOLOGY CONFERENCE, 1975. PP. 795-804. Publ.Yr: 75
Descriptors: MICROWAVE RADIOMETRY, OCEAN SURVEYING, OFFSHORE OPERATIONS, RADAR IMAGERY, RADIOMETERS, REMOTE SENSING, SCATTEROMETRY, WAVE DATA

75-03697
A SIMULATION OF SYNTHETIC APERTURE RADAR IMAGING OF OCEAN WAVES.
SWIFT, C.T.
NASA, LANGLEY RESEARCH CENTER, HAMPTON, VA 23365
SCIENTIFIC AND TECHNICAL AEROSPACE REPORTS, 13(3): 284, FEB. 8, 1975. Publ.Yr: 75
Descriptors: ABSTRACT ONLY, DOPPLER SPECTRA, RADAR IMAGERY, SIMULATION, WAVES

75-02662
A NOTE ON SPECULAR OCEAN SURFACE RADAR CROSS SECTION.
TOMIYASU, K.
GEC, VALLEY FORGE SPACE CENTER, PHILADELPHIA, PA 19101
JOURNAL OF GEOPHYSICAL RESEARCH, 79(21): 3101, JULY 20, 1974. Publ.Yr: 74
Descriptors: OCEAN SURFACE, ELECTROMAGNETIC RADIATION, RADAR, WAVE REFLECTION

75-00354
OCEAN WAVE SENSORS. A BIBLIOGRAPHY WITH ABSTRACTS.
RINGE, A.C.
USDC, NATIONAL TECHNICAL INFORMATION SERVICE,; SPRINGFIELD, VA 22151
GOVERNMENT REPORTS ANNOUNCEMENTS, 74(5): 72, MAR. 8, 1974. Publ.Yr: 74
Descriptors: ABSTRACT ONLY, ABSTRACT COLLECTIONS, BIBLIOGRAPHIES, MEASURING INSTRUMENTS, REMOTE SENSING, SURFACE ROUGHNESS, WAVE SPECTRA, WAVES

74-03672
SKYWAVE RADAR.
ANONYMOUS
FISH BOAT, 18(8): 31, AUG. 1973. Publ.Yr: 73
Descriptors: OCEAN SURVEYING, RADAR, WEATHER CONDITIONS, SHIP TRACKING, WAVE DATA, IONOSPHERE, SKYWAVE RADAR TECHNIQUE

74-02666
RADAR SEA RETURN-JOSS II.
DAVIS, W.T.; RANSOME, J.T., JR.; DALEY, J.C.
NRL, 455 OVERLOOK AVE. SW, WASH., DC 20390
GOVERNMENT REPORTS ANNOUNCEMENTS, 73(9): 62, MAY 10, 1973. Publ.Yr: 73
Descriptors: WAVES, RADAR, WIND, POLARIZATION, JOINT OCEAN SURFACE STUDY, SEA STATES, ABSTRACT ONLY, ATLANTIC OCEAN

73-20892
RADAR PULSE SHAPE VERSUS OCEAN WAVE HEIGHT.
YAPLEE, B.S.; ULIANA, E.A.; SHAPIRO, A.
NRL, E.O. HULBURT CENTER FOR SPACE RESEARCH, WASH., DC NRL, E.O. HULBURT CENTER FOR SPACE RESEARCH, WASH., DC NRL, E.O. HULBURT CENTER FOR SPACE RESEARCH, WASH., DC
SEE CITATION NO. 73-5B-00885, 29 PAGES, FEB. 1972. Publ.Yr: 72
Descriptors: WAVE HEIGHT, SATELLITE GEODESY, SURFACE WATERS, RADAR

73-20245
MEASUREMENT OF OCEAN WAVE HEIGHTS WITH THE RANDOM-SIGNAL RADAR.
COOPER, GEORGE R.; CHADWICK, RUSSELL B.
INST. OF TELECOMMUNICATION SCIENCES, BOULDER, CO PURDUE UNIV., DEPT. OF ELECTRICAL ENGINEERING, LAFAYETTE,; IN
IEEE TRANSACTIONS ON GEOSCIENCE ELECTRONICS, NEW YORK, GE-9(4): 216-221, OCT. 1971. Publ.Yr: 71
Descriptors: WAVE HEIGHT, RANDOM-SIGNAL., REMOTE SENSING, RADAR PLOTTING

73-20244
BISTATIC-RADAR TECHNIQUES FOR OBSERVING LONG-WAVELENGTH DIRECTIONAL OCEAN-WAVE SPECTRA.
TEAGUE, CALVIN C.
STANFORD UNIV., STANFORD ELECTRONICS LABS., CENTER FOR: RADAR ASTRONOMY, CA
IEEE TRANSACTIONS ON GEOSCIENCE ELECTRONICS, NEW YORK, GE-9(4): 211-215, OCT. 1971. Publ.Yr: 71
Descriptors: BISTATIC TECHNIQUES., REMOTE SENSING, WAVE SPECTRA, RADAR PLOTTING, CALIFORNIA, WAVE SCATTERING

71-30326
OCEAN SPECTRA FOR THE HIGH-FREQUENCY WAVES AS DETERMINED FROM AIRBORNE RADAR MEASUREMENTS.
VALENZUELA, G. R.; LAING, M. B.; DALEY, J. C.
JOURNAL OF MARINE RESEARCH, 29(2): 69-84, MAY 15, 1971. Publ.Yr: 71
Descriptors: RADAR, WAVE SPECTRA, SCATTERING, GRAVITY WAVES, MATHEMATICAL MODELS, AIRBORNE MEASUREMENTS

71-22247
CORRELATION OF RADAR BACKSCATTERING CROSS SECTIONS WITH OCEAN WAVE HEIGHT AND WIND VELOCITY.
KRISHEN, K.
JOURNAL OF GEOPHYSICAL RESEARCH, 76(27): 6528-6539, SEPT. 20, 1971. Publ.Yr: 71
Descriptors: WIND VELOCITY, WAVE HEIGHT, CORRELATIONS, BACKSCATTERING, RADAR

71-22244
REMOTE SENSING OF OCEAN EFFECTS WITH RADAR.
GUINARD, N. W.
U.S. NAVAL RESEARCH LABORATORY. WASH., D.C. PROGRESS REPORT: 1-11, AUG. 1971. Publ.Yr: 71
Descriptors: REMOTE SENSING, RADAR, OCEAN SURFACE EFFECTS, RADAR SEA RETURN, WIND FIELDS, WAVE SPECTRA, OIL SPILLS

71-20290
BISTATIC-RADAR OBSERVATION OF LONG-PERIOD, DIRECTIONAL OCEAN-WAVE SPECTRA WITH LORAN A.
PETERSON, ALLEN M.; TEAGUE, CALVIN C.; TYLER, G. LEONARD
SCIENCE, 170(3954) :158-161, OCT. 9, 1970. Publ.Yr: 70
Descriptors: CALIFORNIA COAST, LORAN A, RADAR OBSERVATION, RESONANCE, WAVE SPECTRA

69-07225
OBSERVING OCEAN SURFACE WAVES WITH A HELIUM-NEON LASER.
ROSS, DUNCAN B., JR.; PELOQUIN, ROBERT A.; SHELL, RICHARD J.
MILITARY OCEANOGRAPHY. U.S. NAVY. FIFTH SYMPOSIUM. PROCEEDINGS. VOL. I. HELD IN PANAMA CITY, FLA., MAY 1-3, 1968. SPONSORED BY THE OCEANOGRAPHER OF THE NAVY, ALEXANDRIA, VA. PP.291-308. 1968. ABS., 12 FIGS., 9 REFS., *AA. Publ.Yr: 68
Descriptors: AIRBORNE INSTRUMENTS, LASERS, REMOTE SENSING, WAVE MEASUREMENTS

69-00897
RADAR DETERMINATION OF SOME OCEAN-WAVE ELEMENTS.
OREMLYUG, V. V.
APL LIBRARY BULLETIN. TRANSLATIONS SERIES, TG 230-T551, 7 PAGES, MARCH 13,1968. SUM., 1 FIG., 2 REFS., AS. CONTRACT-NAVAL ORDNANCE SYSTEMS COMMAND NOW 62-0604-C. TRANS OF-LENINGRAD. ARKTICH. I ANTARKTICH. NAUCHNO- ISSLED. INST., TRUDY. LENINGRAD ARCTIC AND ANTARCTIC SCIENTIFIC RES. INST., TRANS., NO. 210, P.135-138, 1960. Publ.Yr: 68
Descriptors: SEA WAVE ELEMENTS, RADAR

68-00677
ON THE GENERATION OF OCEAN WIND WAVES AS INFERRED FROM AIRBORNE RADAR MEASUREMENTS OF FETCH-LIMITED SPECTRA.
BARNETT, T. P.; WILKERSON, J. C.
JOURNAL OF MARINE RESEARCH, VOL. 25, NO. 3, P.292-328, SEPT.15,1967. ABS., 13 FIGS., 2 TABLES, 27 REFS. 1 IN GER., 1 APP., AA. Publ.Yr: 67
Descriptors: FETCH-LIMITED WAVE SPECTRA, WIND WAVES, RESONANCE, AIRBORNE RADIOMETRY, INSTABILITY MECHANISM

67-05499
OCEAN SURFACE ENVIRONMENT DEFINITION UTILIZING LASER TECHNIQUES.
KIRK, RONALD L.
IEEE INTERNATIONAL CONVENTION RECORD. 1967. ANNUAL. PART 8. INSTITUTE OF ELECTRICAL AND ELECTRONIC ENGINEERS. CONVENTION HELD AT NEW YORK, N.Y. MARCH 20-23.1967. ALSO AS- IEEE INTERNATIONAL CONVENTION. 1967. INSTITUTE OF ELECTRICAL AND ELECTRONICS ENGINEERS. SYMPOSIUM. HELD AT NEW YORK, N.Y. MARCH 20-23,1967. ANNUAL RECORD. P.84-93. SUM., FIGS., 1 TABLE. 31 REFS., MF, SA. CONTRACT- U.S. NAVAL AIR SYSTEMS COMMAND. NOW 66-0509-C. Publ.Yr: 67
Descriptors: SYMPOSIA, REMOTE SENSING, LASER INSTRUMENTATION, AIRBORNE PLATFORMS, ELECTRO-OPTICAL INSTRUMENTATION

67-04017
AN OCEANOGRAPHIC AIRCRAFT.
SCHULE, JOHN J., JR.
U.S. NAVAL OCEANOGRAPHIC OFFICE. WASH., D.C. INFORMAL REPORT. NO. IR 66-26. JAN.1967. REPRINTED APRIL 1967. 16 PAGES, ABS., FIGS., 1 REFS., MF, AA. Publ.Yr: 67
Descriptors: AIRCRAFT, AIRBORNE MEASUREMENTS

67-03871
SURFACE EVALUATION AND DEFINITION SUEDE PROGRAM.
KIRK, R. L.
ELECTRO-OPTICAL SYSTEMS, INC. PASADENA, CALIF. FINAL REPORT. NO. 7067. DEC.13.1966. 123 PAGES. NO ABS., FIGS., TABLES. 50 REFS., MF, SA. CONTRACT- USN NOW 66-0509-C. REF. ORDER NO. AC 646 828. Publ.Yr: 66
Descriptors: ELECTRO-OPTICAL INSTRUMENTATION, LASER INSTRUMENTATION, SEA STATE PARAMETERS, AIRBORNE LASER TECHNIQUES, REMOTE SENSING, SUEDE, WIND EFFECTS

67-03004
RECENT DEVELOPMENTS IN REMOTE SENSING OF DEEP OCEAN WAVES.
ROSS, DUNCAN B.
NEW THRUST SEAWARD. TRANSACTIONS OF THE THIRD ANNLAL MTS CONFERENCE & EXHIBIT, 5-7 JUNE 1967, SAN DIEGO, CALIFORNIA. MARINE TECHNOLOGY SOCIETY, WASHINGTON, D.C. 1967. ALSO AS-MARINE TECHNOLOGY SOCIETY. WASH., D.C. TRANSACTIONS OF THE THIRD ANNUAL MTS CONFERENCE & EXHIBIT. 5-7 JUNE 1967. SAN DIEGO, CALIFORNIA. 1967. P.371-393. ABS., 17 FIGS., 13 REFS., MF, AA. Publ.Yr: 67
Descriptors: INFRARED HEIGHT SENSORS, INSTRUMENTS, WAVE HEIGHT MEASUREMENT, SURFACE WAVES, REMOTE SENSING, REAL TIME

67-00313
THE GROWTH OF OCEAN WIND WAVES AS OBSERVED WITH AN AIRBORNE WAVE PROFILING RADAR.
BARNETT, TIM P.; WILKERSON, J. C.
REMOTE SENSING OF ENVIRONMENT. PROCEEDINGS OF THE FOURTH SYMPOSIUM HELD APRIL 12-14,1966. AT THE INFRARED PHYSICS LABORATORY, WILLOW RUN LABORATORIES, INSTITUTE OF SCIENCE AND TECHNOLOGY, UNIVERSITY OF MICHIGAN. SPONSORED BY ONR, AFCRL, AND NAS-NRC, JUNE 1966. P.243-258 ABS., 8 FIGS., 1 TABLE, 9 REFS. Publ.Yr: 66
Descriptors: AIRBORNE SENSORS, INSTRUMENTATION, WIND WAVES, REMOTE SENSING, WAVE PROFILING RADAR

AN EXAMPLE OF A TYPICAL NTIS CITATION PAGE

Remote Sensing of Oil Pollution at the Sea Surface 2. Damping of Water Waves by an Oil Layer as a Possible Indicator for SLAR Observations

Netherlands Interdepartmental Working Group on the Application of Remote Sensing, Delft.

Ph.D. Thesis - Univ. of Technol.
AUTHOR: Pronk, A. C.
D2985J4 Fld: 13B, 8J, 68D, 47B STAR1514
Jul 75 12p
Rept No: NIWARS-PUBL-22
Monitor: 18

Abstract: The damping action of oil pollution on sea waves is discussed in view of observation from the air. It is found that oil layers of all thicknesses damp a part of the wave spectrum. Only in the case of thicker layers is the damping related to the nature of the oil. The distance over which the sea waves damp out after an oil slick has entered seems a useful indicator for the oil properties.

Descriptors: *Damping, *Oil pollution, *Water waves, Layers, Ocean surface, Properties, Thickness, Viscosity

Identifiers: *Remote sensing, *Water pollution detection, Netherlands, Theses, NTISNASAE

N77-23583/6ST NTIS Prices: PC A02/MF A01

Analysis of Synthetic Aperture Radar Ocean Wave Data Collected at Marineland and Georges Bank

Environmental Research Inst. of Michigan, Ann Arbor. Radar and Optics Div.*National Environmental Satellite Service, Washington, D.C. (408 392)

Final rept.
AUTHOR: Shuchman, Robert A.; Rawson, Robert F.; Kasischke, Eric S.
D2991B4 Fld: 8C, 47B, 86P GRAI7718
Apr 77 171p
Rept No: 123000-11-F
Grant: NOAA-04-6-158-44078
Monitor: NOAA-77052503

Abstract: A program involving the processing and analysis of SAR data collected by the ERIM X-L Imaging Radar at Georges Bank and Marineland has been carried out. The purpose of this work was to extract useful information about ocean waves. A focusing algorithm was developed and backscatter measurements were made using an optical processor. A number of interesting conclusions have been made, including (1) the 180 degrees wave-direction ambiguity can be resolved by a study of defocusing in the processor, (2) non-linear wave refraction does not occur across the Gulf Stream boundary, (3) the modulation depth is greater for X-band than for L-band and greater for range-direction waves than for azimuth-direction waves, and (4) X-band (HH), L-band (HH), and L-band (HV) produce significant backscatter and discernible images while X-band (HV) produces little backscatter.

Descriptors: *Ocean waves, *Radar cross sections, Synthetic aperture radar, Sea state, Backscattering, Remote sensing, Algorithms

Identifiers: Gulf Stream, Georges Bank, NTISCOMNOA

PB-268 675/6ST NTIS Prices: PC A08/MF A01

Remote Sensing of the Ocean. Part 2. Dynamics (A Bibliography with Abstracts)

National Technical Information Service, Springfield, Va. 391 812)

Rept. for 1970-Jun 77
AUTHOR: Brown, Robena J.
D2874H4 Fld: 8C, 47B*, 86W GRAI7717
Jun 77 119p*
Monitor: 18
Supersedes NTIS/PS-76/0469, NTIS/PS-75/447, and Updates COM-73-11676.

Abstract: The studies include remote sensing methods as they are applied to ocean currents, wind sediment transport, ocean waves, sea states, and air water interactions. The various techniques of measurement using radiometers, lasers, radar, and microwave and infrared equipment are described. (This updated bibliography contains 114 abstracts, 13 of which are new entries to the previous edition.)

Descriptors: *Bibliographies, *Ocean waves, *Air water interactions, *Remote sensing, Ocean currents, Sediment transport, Ocean surface, Sea states, Wind(Meteorology), Internal waves, Spaceborne photography, Radiometers, Infrared photography, Lasers, Radar reflections, Surface roughness

Identifiers: NTISNTIS

NTIS/PS-77/0533/8ST NTIS Prices: PC N01/MF N01

APPENDIX B

EFFECT OF MIXED INTEGRATION ON DEPTH OF FOCUS

EM-77-1203

ELECTROMAGNETIC MEASUREMENTS
DEPARTMENT

17 August 1977

MEMORANDUM TO: SEASAT and Marineland Teams

FROM: R.A. Shuchman and J.S. Zelenka* RAS

SUBJECT: Effect of Mixed Integration on Depth of Focus

1
INTRODUCTION

This memorandum discusses the effect of using mixed integration during SAR data processing and the subsequent depth of focus that results. It will be demonstrated that the depth of focus for a mixed integrator processor, such as that proposed for SEASAT-A, is equal to the geometric mean of the depth of focus corresponding to the full aperture and the depth of focus for the partial aperture. In the case of SEASAT-A this would be 6.25 and 25 meters, respectively.

This depth of focus question is important when one considers whether focus adjustment for moving ocean waves is necessary during SEASAT-A SAR data processing. Recall from previous ERIM work [1,2] that a simple expression was derived for those wave velocities requiring processor compensation (i.e., refocusing). The expression was obtained

*Present Affiliation: Science Applications Inc., Tuscon, Arizona

1. R.A. Shuchman, R.F. Rawson and E.S. Kasischke, Analysis of Synthetic Aperture Ocean Wave Data Collected at Marineland and Georges Bank, Report No. 123000-11-F, Environmental Research Institute of Michigan, Ann Arbor, 1977.

2. R.A. Shuchman and J.S. Zelenka, Processing of SAR Ocean Wave Data, Boundary Layer Meteorology, 1976, (In Press).

by setting the depth of focus (DF) < the shift in focal length produced by a moving target (δF). Thus,

$$2/\lambda_\ell \left(\frac{V_f \rho}{M V_{AC}}\right)^2 < 2F_o \frac{V_T}{V_{AC}} \quad * \tag{1}$$

where λ_ℓ = wavelength of the optical processor

ρ = the azimuth resolution of the radar system

M = azimuthal demagnification of the optical processor

V_{AC} = the along track speed of radar

F_o = the along track focal length of stationary target

V_T = the target speed in the along track direction

V_f = speed of the recording film

If

$$F_o = \frac{R\lambda}{2M^2\lambda_\ell} \left(V_f/V_{AC}\right)^2 \tag{2}$$

where R = slant range

λ = radar wavelength

Then substituting Eq. 2 into Eq. 1 and solving for V_T we obtain

$$V_T > \frac{2\rho^2 V_{AC}}{\lambda R} \tag{3}$$

If the SEASAT case of one-look 6.25 meter resolution is considered

$$V_T > (2)\ (6.25)^2\ \frac{(7,868)}{.235\ (845,000)} \tag{4}$$

or

$$V_T > 3.10 \text{ m/sec}$$

*The reader is referred to References 1 and 2 for derivation of (DF) and (δF).

If the resolution is 25 meters (one-look)

$$V_T > 49.53 \text{ m/sec}$$

However, if SEASAT uses mixed integration during data processing (i.e., use of four non-coherently averaged images to produce a four-look 25 meter image), a smaller minimum V_T results than for the fully coherent case

$$V_T > 12.38 \text{ m/sec}$$

Thus if SEASAT-A uses either a resolution of 6.25 m or employs four-look mixed integration processing, refocusing to compensate for the azimuth component of the wave velocity will be necessary.

The discussion that follows in Section 2, entitled "Depth of Focus for a Mixed Integrator Processor", was written by J.S. Zelenka after R. Shuchman raised the question upon examination of empirical data. References 1 and 2 show examples that support this discussion.

2 DEPTH OF FOCUS FOR A MIXED INTEGRATOR PROCESSOR

The purpose of this section is to determine the depth of focus associated with a mixed integrator processor (i.e., one which combines multiple-look coherent images). First, we review the depth of focus associated with a fully coherent processor. Then we extend the fully coherent case to the mixed integrator case.

2.1 FULLY COHERENT CASE

Consider a lens L_1 of diameter D, which is diffraction limited and has a focal length F as shown in Figure 1. The resolution is given by

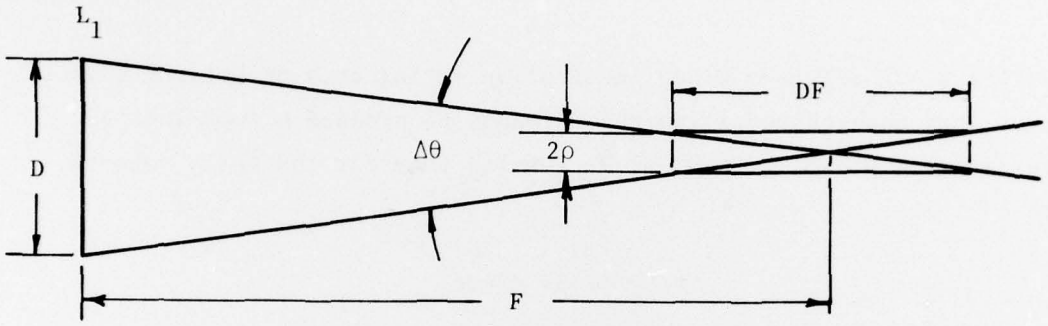

Figure B-1. A Fully Coherent Processor

$$\boxed{\rho = \frac{\lambda}{\Delta\theta} = \frac{\lambda D}{F}} \tag{5}$$

where λ is the wavelength of the light under consideration.

We define the depth of focus (DF) by the total longitudinal distance that one can move about the plane of best focus and still maintain a resolution of at least 2ρ (i.e., we say the image remains in focus if the resolution is no worse than twice the ideal resolution which can be realized only in the plane of best focus). According to Figure 1, we can write

$$\frac{DF/2}{2\rho} = \frac{F}{D} = \frac{1}{\Delta\theta} \tag{6}$$

or

$$\boxed{DF = \frac{4\rho}{\Delta\theta} = \frac{4\lambda}{(\Delta\theta)^2} = \frac{4\rho^2}{\lambda}} \tag{7}$$

For the fully coherent case if the resolution is increased (spoiled) by a factor of N, we obtain the following results wherein the primes designate parameters obtained after spoiling the resolution by N.

$$\Delta\theta' = \frac{1}{N}\,\Delta\theta \tag{8}$$

$$\rho' = \frac{\lambda}{\Delta\theta'} = \frac{\lambda N}{\Delta\theta} = N\lambda \tag{9}$$

$$DF' = \frac{4\lambda}{(\Delta\theta')^2} = \frac{4\lambda N^2}{(\Delta\theta)^2} = N^2\ (DF) \tag{10}$$

Now we turn our attention to the mixed-integration processor.

2.2 MIXED INTEGRATION CASE

In Figure 2, we subdivide the cone of light which is focusing to a point into equal one-thirds as indicated. We assume that one-third of the light is allowed to focus at a time in a fully coherent manner. The resulting three point images are then combined as intensities (i.e., incoherently). The resolution for the system shown is

$$\rho'' = \rho' = 3\rho = 3\,\frac{\lambda}{\Delta\theta} = 3\,\frac{\lambda D}{F} \tag{11}$$

In general, we have that resolution achievable with a mixed-integration processor

$$\boxed{\rho'' = \rho' = N\rho} \tag{12}$$

In other words, resolution associated with the mixed integration process is the same as it is for a fully coherent process taken over the partial aperture.

The depth of focus associated with the central one-third of the input processor is designated as DF' in Figure 2. Note that the light from the upper and lower thirds of the input aperture do not pass through the $2\rho'$ longitudinal tube centered at the point focus except for longitudinal distances corresponding to $\pm$ DF''/2. Thus, it there is to be no additional smearing (defocusing) of the final mixed integration image, we require that the superimposed images be formed within DF''/2 from the plane of optimum focus.

According to Figure 2, we have that the depth of focus for the mixed integration processor shown is

$$\frac{\frac{1}{2}\,DF''}{F} = \frac{2\rho'}{D} \tag{13}$$

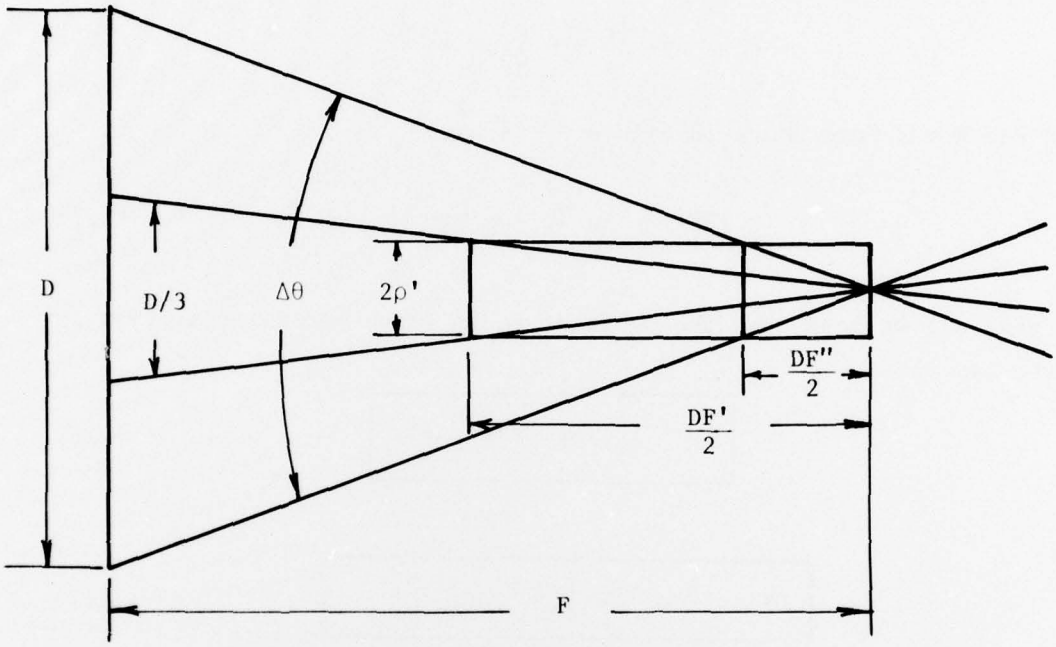

Figure B-2. A Mixed-Integrator Processor

or

$$DF'' = 4\frac{\rho' F}{D} = 4\frac{\rho'}{\Delta\theta} = 4\frac{\rho\rho'}{\lambda} \tag{14}$$

For the N = 3 case shown in Figure 2, we have

$$DF'' = 12\frac{\rho^2}{\lambda} = \frac{4}{3}\frac{\rho'^2}{\lambda} \tag{15}$$

In general, we have that the depth of focus for a mixed integration is given by

$$\boxed{DF'' = N(DF) = \frac{1}{N}(DF')} \tag{16}$$

or

$$\boxed{DF'' = \frac{4}{\lambda}\rho\rho' = \frac{4N}{\lambda}\rho^2 = \frac{4}{\lambda N}\rho'^2} \tag{17}$$

Note that the depth of focus for the mixed integration processor is equal to the geometric mean of the depth of focus corresponding to the full aperture and the depth of focus for the partial aperture. That is

$$DF'' = \sqrt{(DF)(DF')} \tag{18}$$

3
CONCLUSION

In conclusion, we should note that the depth of focus has been arbitrarily defined to be the total displacement from the optimal focal plane for which the resolution degraded by a factor of two over the

diffraction limit. If this definition is inappropriate for a particular application, one can introduce a constant of proportionality into the above expressions for depth of focus. This proportionality constant could be up to an order of magnitude larger or smaller than unity depending upon the application of the imaging process.

A more exact rule-of-thumb for system resolution than used in this note is

$$\boxed{\rho = \left[(\rho_g)^2 + (\rho_D)^2\right]^{\frac{1}{2}}} \tag{19}$$

where

$$\rho_g = \frac{\lambda F}{D}$$

and

$$\rho_D = \frac{\lambda}{2\Delta\theta}$$

RAS:JSZ:as

REFERENCES

1. W.M. Brown and L.J. Porcello, An Introduction to Synthetic Aperture Radar, IEEE Spectrum, Vol. 6, No. 9, September 1968, pp 52-66.

2. R.K. Raney, Synthetic Aperture Imaging Radar and Moving Targets, IEEE Transactions on Aerospace and Electronic Systems, May 1971, Vol. AES-7, No. 3, pp 499-505.

3. R.O. Harger, Synthetic Aperture Radar Systems, Academic Press, New York, 1970.

4. C. Elachi and W.E. Brown, Models of Radar Imaging of the Ocean Surface Waves, IEEE Journal of Oceanic Engineering, Vol. OE-2, No. 1, January 1977.

5. J.C. Daley, W.T. Davis, and N.R. Mills, Radar Sea Return in High Sea States, Report No. 7142, Naval Research Laboratory, Washington, D.C., September 1970.

6. O. Shemdin, W.E. Brown, F.G. Standhammer, R.A. Shuchman, R.F. Rawson, J.S. Zelenka, D.B. Ross, and R.A. Berles, Comparison of In Situ and Remotely Sensed Ocean Waves off Marineland, Florida, Boundary Layer Meteorology (In Press).

7. A. Kozma, E.N. Leith, and N.G. Massey, Tilted Plane Optical Processor, Applied Optics, Vol. 11, No. 8, August 1972, p 1766.

8. F.L. Smith and R.F. Rawson, Four-Channel Simultaneous X-L Imaging SLAR Radar, Proceedings of the Ninth International Symposium on Remote Sensing of the Environment, Ann Arbor, Michigan, 1974.

9. R.F. Rawson, F.L. Smith, and R.W. Larson, The ERIM Simultaneous X- and L-Band Dual-Polarization Radar, Report of the IEEE 1975 International Radar Conference, New York City, p 505.

10. J.W. Goodman, Introduction to Fourier Optics, McGraw-Hill Book Co., New York, 1968, p 192.

11. L.J. Porcello, N.G. Massey, R.B. Innes, and J.M. Marks, Speckle Reduction in Synthetic Aperture Radars, J. of the Opt. Soc. of America, Vol. 66, No. 11, p 1305.

12. R.A. Shuchman, R.F. Rawson, and E.S. Kasischke, Analysis of Synthetic Aperture Radar Ocean Wave Data Collected at Marineland and Georges Bank, ERIM Final Report 123000-11-F, Ann Arbor, Michigan.

REFERENCES
(Concluded)

13. T.R. Larson, L.I. Moskowitz, and J.W. Wright, A Note on SAR Imagery of the Oceans, IEEE Trans. on Antennas and Propagation, Vol. AP-24, No. 3, 1976, pp 393-394.

14. O. Shemdin, Jet Propulsion Laboratory, Personal Communication.

15. D.A. Ausherman, W.D. Hall, J.N. Latta, and J.S. Zelenka, Radar Data Processing and Exploitation Facility, Proceedings IEEE International Radar Conference, Washington, D.C., 1976.

16. J.M. Wozencraft and I.M. Jacobs, Principles of Communication Engineering, John Wiley & Sons, Inc., New York, 1967.

17. L.J. Cutrona, E.N. Leith, and L.J. Porcello, Filter Operations Using Coherent Optics, Proceedings of the National Electronics Conference, Volume X, 1959.

18. P.L. Jackson, Diffractive Processing of Geophysical Data, Applied Optics, Vol. 4, No. 4, April 1965.

19. W.L. Brown, F.C. Polcyn, A.N. Sellman, and S.R. Stewart, Water-Depth Measurements by Wave Refraction and Multispectral Techniques, Report No. 31650-31-T, Willow Run Laboratories, Ann Arbor, Michigan, August 1971.